Visualizing APP trafficking and processing reveals its functional relationship with neuronal membrane cholesterol

By

Claire Elise DelBove

Dissertation

Submitted to the Faculty of the
Graduate School of Vanderbilt University
in partial fulfillment of the requirements
for the degree of

DOCTOR OF PHILOSOPHY

in

Pharmacology

August 10, 2018

Nashville, Tennessee

Approved:

Christine Konradi, Ph.D.

Qi Zhang, Ph.D.

Randy Blakely, Ph.D.

Kevin Currie, Ph.D.

Charles Sanders, Ph.D.

ACKNOWLEDGMENTS

First, I would like to thank all of the members of the Zhang lab and my mentor, Qi Zhang. I appreciated his support through the difficult times. I would like to thank Roman Lazarenko and Haigang Gu for teaching me and helping me survive my first conference. I would also like to thank Inga Kristaponyte for her hard work maintaining our animals and keeping the lab running, Danielle Bailey for helping me access equipment I needed, and Kristina Kitko for helping me become a better presenter. I am grateful to Linda Xu, Claire Strothman, and Xian-zhen Deng for the opportunity to learn how to teach and mentor, and for all of their hard work.

I would not have made it this far without my committee. Thanks to my committee chair, Christine Konradi, for going above and beyond. I thank Randy Blakely and Kevin Currie for providing excellent advice and continuing to offer support. Thanks to Chuck Sanders for the opportunity to collaborate on my paper.

I am very grateful to Hui Huang, who generated the cholesterol binding-deficient mutants so efficiently. I also thank the current and former members of the Hamm lab for helping me, especially Karren Hyde and my fiancé, Zack Zurawski.

I am so grateful for the love and support of my family. My parents, Ralph and Helen, always had time for me no matter what else was going on. They have supported my dreams all my life. Thanks to my siblings, Catherine and Steven, for our wonderful childhoods together, and for always being understanding.

This work would not have been possible without funding from the NIH and Vanderbilt University.

TABLE OF CONTENTS

Page

LIST OF TABLES

Table Page

LIST OF FIGURES

Figure Page

LIST OF ABBREVIATIONS

ABCA7	ATP-binding cassette sub-family A member 7
AChE	acetylcholinesterase
AD	Alzheimer's disease
ADAM10	A Disintegrin and metalloproteinase domain-containing protein 10
ADAM17	A Disintegrin and metalloproteinase domain-containing protein 17
ADAS-Cog	Alzheimer's Disease Assessment Scale-cognitive subscale
AEP	Asparagine endopeptidase
AICD	APP intracellular C-terminal fragment
AMPA	α-amino-3-hydroxy-5-methyl-4-isoxazolepropionic acid
APLP1 and APLP2	amyloid precursor-like protein 1 and 2
APP	Amyloid Precursor Protein
APPSwe	KM670/671NL APP; APP with the Swedish FAD mutation
Aβ	β-amyloid
BACE1	beta-site APP cleaving enzyme 1
cAMP	Cyclic adenosine monophosphate (cyclic AMP)
C83	the membrane bound CTF produced by α-cleavage of APP
C99	the membrane bound CTF produced by β-cleavage of APP
CME	clathrin-mediated endocytosis
CNS	central nervous system
CREB	cAMP response element-binding protein
CTF	C-terminal fragment
df	degrees of freedom
DIV	days in vitro
FAD	Familial Alzheimer's disease
holo-APP	Full length, uncleaved APP
hpSynI	human Synapsin 1 promoter
LRP1	low density lipoprotein receptor-related protein 1
LTP	long-term potentiation
MCI	mild cognitive impairment
MMSE	Mini–Mental State Examination

MT5-MMP	membrane-type 5-matrix metalloproteinase
MβCD	methyl-β-cyclodextrin
NFTs	neurofibrillary tangles
NMDA	N-methyl-D-aspartate
NMDAR	N-methyl-D-aspartate receptor
NSAID	nonsteroidal anti-inflammatory drug
ORF	open reading frame
PLCG2	Phospholipase C Gamma 2
ROI	Region of interest
SAD	Sporadic Alzheimer's disease
sAPPα	soluble amyloid precursor protein α
sAPPβ	soluble amyloid precursor protein β
SEM	Standard error of the mean
SP	signaling peptide
SREBP	sterol regulatory element binding protein
SypHTm	Synaptophysin-pHTomato
SytI	Synaptotagmin I
TREM2	Triggering receptor expressed on myeloid cells 2
α-cleavage	cleavage by α-secretase
α-SI	α-secretase inhibitor
β-cleavage	cleavage by β-secretase
β-SI	β-secretase inhibitor
γ-cleavage	cleavage by γ-secretase
γ-SI	γ-secretase inhibitor

Chapter I

INTRODUCTION

Alzheimer's Disease

AD characteristics and prognosis

Alzheimer's disease (AD) is thought to be responsible for 60 to 80% of cases of dementia, a generic term for a decline in cognitive capacities typically but not exclusively seen in the elderly. The loss of synapses and the death of neurons results in atrophy of several critical brain regions in AD patients. As the neurodegeneration progresses, Alzheimer's patients suffer a decline in quality of life, require extensive care, and eventually die of the disease or associated comorbidities. AD is now a leading cause of death in America [1] and in much of the developed world. The prevalence of AD doubles every 5.5 years [2]. As the population ages due to advances in other areas of medicine, incidence of Alzheimer's disease increases [1]. This is very notable in Japan, which has a very high percentage of elderly people and a high life expectancy [3-5]. In the US, the population of AD patients is expected to double by 2050[1].

The most recent recommendations divide AD into three stages [6]. Early stage symptoms include difficulty driving and other familiar tasks, changes in personality, forgetting names, losing things, and poor judgment. Middle-stage Alzheimer's disease

is usually the longest stage. During this stage, AD patients begin to have difficulty functioning in society and may require care [1]. Other symptoms include wandering, confusion, disrupted sleep, and noticeable personality changes. During late stage Alzheimer's disease, patients typically need 24-hour care [1] and eventually lose the ability to communicate, understand what's going on around them, and walk unassisted. Eventually AD patients even lose the ability to swallow, and the disease is ultimately fatal.

AD patients may have a wide variety of other symptoms in addition to memory and cognition failures. For example, many AD patients with no history of epilepsy start having seizures [7, 8]. Depression is also a common comorbidity[9-11]. As the disease advances, some patients present with psychosis[9, 12]. Due to the variety of symptoms, differentiating Alzheimer's disease from other dementias in living patients is not trivial. The emergence of symptoms at certain times often follow a pattern that is characteristic of each disease. The inability to form new memories, or anterograde amnesia, starts first during early stage AD and is followed by the failure to retrieve older personal memories, or retrograde amnesia [13]. By contrast, patients with Lewy body dementia often have visual hallucinations and motor dysfunctions in the early stages [14], while patients with vascular dementia typically present with impaired decision-making, planning, or motor function depending on the affected areas of the brain [1]. It is common to present with multiple forms of dementia; vascular dementia after a stroke may mask the early to mid-stage symptoms of Alzheimer's disease. Any

other form of dementia is no longer used to exclude a diagnosis of Alzheimer's disease [1]. AD is the most common type of dementia to occur in mixed dementia [15, 16].

There are two types of Alzheimer's disease based on genetics: sporadic and familial. The exact cause(s) of sporadic Alzheimer's disease (SAD) are not understood, but age is the highest risk factor. Familial Alzheimer's disease (FAD), like Huntington's disease, is caused by autosomal dominant mutations. Although only a small percentage of AD patients have FAD, it is disproportionately studied because people with these mutations can be identified before they become symptomatic by genetically testing the family members of known FAD patients. Early intervention and prevention trials are facilitated by the predictable nature of FAD, although no cure has been found so far. Furthermore, most animal models of AD utilize known AD mutations. However, this research relies on the unproven assumption that preventative or disease modifying therapies for FAD would also be efficacious for SAD, which is more common by far.

Alzheimer's disease may also be classified as early onset or late onset, which simply means the disease was diagnosed before or after the age of 65. Typically FAD is early onset and SAD is late onset, but FAD is so rare (1-3% of all cases[17-19]) that the majority of cases of early onset AD are sporadic[1]. However, most cases diagnosed before the age of 50 are FAD. Preclinical AD begins before the symptoms that typically prompt diagnosis, perhaps by decades, which complicates early and late onset classification. In fact, Alzheimer's disease is often not diagnosed until an individual's family notices differences in their day to day function[1]. Nevertheless, separating early and late onset

patients helps to identify SAD risk factors besides age. Some people with preclinical AD may be identified with mild cognitive impairment (MCI), a very useful classification for studies, although some MCI patients eventually develop other forms of dementia [1].

In clinical practice, symptoms typically determine the diagnosis of AD, although recent advances in biomarker analysis have started to change this [6, 20]. However, sporadic Alzheimer's disease is only definitively diagnosed postmortem. AD brains have characteristic amyloid plaques and tau tangles composed of extracellular beta amyloid peptides and intracellular neurofibrillary tau, respectively. Amyloid plaques are primarily comprised of β-amyloid (Aβ) peptides. Aβs are proteolytic products of APP, an integral membrane protein with a single transmembrane domain [21, 22]. These Aβ plaques have been causatively linked to AD, which is strongly supported by the genetics of FAD. All known FAD mutations are found in one of three genes: amyloid precursor protein (APP), presenilin 1, and presenilin 2. Presenilin is the catalytic subunit of γ-secretase, one of the enzymes that produces Aβ from APP. Aβ can be 40 or 42 amino acids long, and the length depends on γ-secretase. FAD mutations in the presenilins typically cause an increase in the ratio of Aβ42 to Aβ40[23] and FAD mutations in APP may cause an increase in production of Aβ overall, increased Aβ42 to Aβ40, or both[19]. Aβ42 tends to form insoluble aggregates, and is thought to be the more pathogenic variant of Aβ.

AD researchers have investigated APP and its proteolytic processing since the early 1980s in hope of a cure[24]. The original amyloid cascade hypothesis states that

Alzheimer's disease is primarily caused by the aberrant deposition of Aβ in plaques, which precedes and causes tau neurofibrillary tangles (NFTs) and all other events in the progression of AD pathology [24, 25]. Many variations on this hypothesis have been proposed. For example, some authors suggest that soluble oligomeric Aβ is the critical pathogenic form [26-31], meaning that the insoluble plaques themselves may be protective[32]. Although the intensive research on APP and Aβ so far has not led to any effective treatments for AD [33, 34], the amyloid hypothesis retains dominance in the field for now.

Amyloid precursor protein and the secretases

It has been well documented that APP is usually subject to one of two routes of proteolytic processing, amyloidogenic and nonamyloidogenic, catalyzed by three proteases known as the α-, β- and γ-secretases [35]. These pathways are summarized in **Figure 1**. In the amyloidogenic pathway, APP is first cleaved by β-secretase in its membrane-proximal ectodomain to generate a large soluble protein (sAPPβ) and a membrane-bound C-terminal fragment (CTF) of 99 amino acid residues (C99). Subsequently, C99 is cleaved by γ-secretase within the transmembrane domain, yielding Aβ-secretase and a short intracellular C-terminal fragment (AICD). The rate-limiting step in Aβ production is β-cleavage[35]. In the nonamyloidogenic pathway, APP is first cleaved by α-secretase at an extracellular site just before the transmembrane domain to generate a longer soluble ectodomain (sAPPα) and a membrane-bound 83-

residue CTF (C83). C83 is also cleaved by γ-secretase within the transmembrane domain, generating a shorter 30mer peptide (P3) and an identical AICD [36].

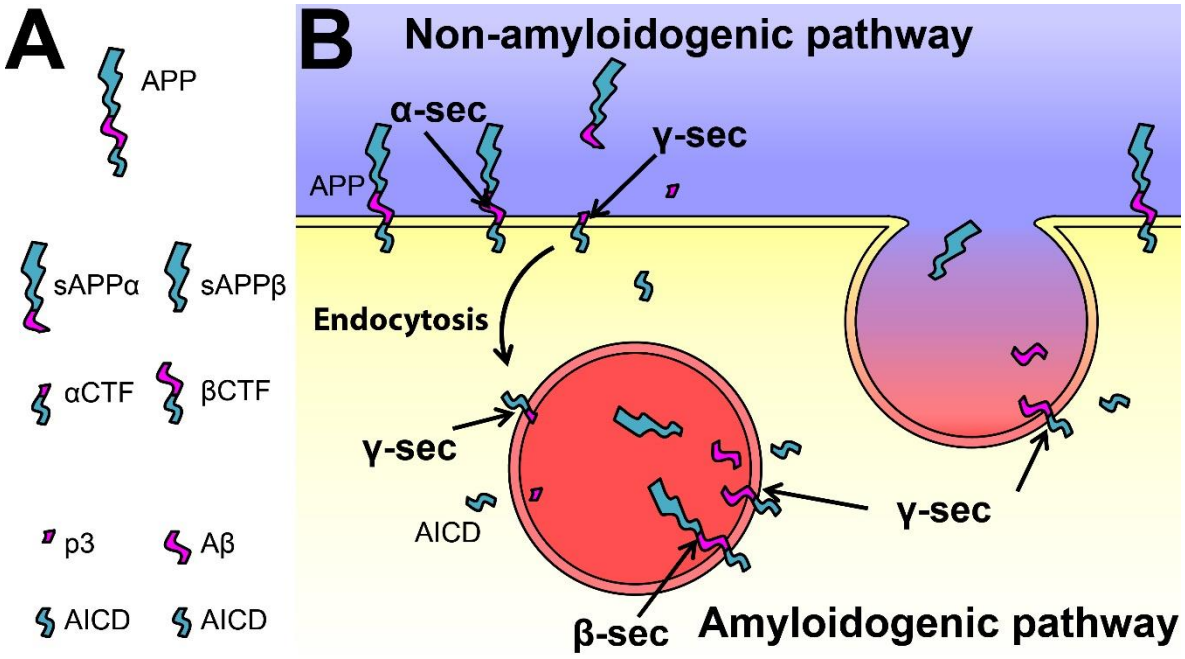

Figure 1: Amyloid precursor protein processing. A, Labeled graphical representations of APP and its cleavage products. **B,** Illustration of APP processing. The non-amyloidogenic pathway predominates on the plasma membrane, where α-secretase is thought to be located. The pH-dependent β-secretase cleavage occurs in acidic organelles, producing Aβ.

ADAM10 (A Disintegrin and metalloproteinase domain-containing protein 10) is the major α-secretase that cleaves APP[37], although some other members of the ADAM family, ADAM17 most notably, are also capable of APP cleavage[38]. BACE1 (beta-site APP cleaving enzyme 1) is thought to be the most physiologically relevant β-secretase to Aβ production[39]. The enzyme complex known as γ-secretase is composed of four subunits[40]: presenilin[41], Pen-2[42], Aph-1[43], and nicastrin[44]. Most γ-secretase contains presenilin-1, but either presenilin can act as catalytic subunits for γ-secretase.

Alternate cleavage of APP has also been described, as well as additional cleavage products [45]. Asparagine endopeptidase (AEP), already known for cleaving tau, has been recently discovered to cleave APP and linked to AD pathogenesis [45, 46]. AEP may be referred to as δ-secretase in the context of APP cleavage, and this cleavage is referred to as δ-cleavage. Membrane-type 5-matrix metalloproteinase (MT5-MMP) also cleaves APP and is referred to as η-secretase in this context [47, 48]. The CTF product of η-cleavage, CTFη, may be cleaved by α- or β-secretase. CTFη may be predisposed to beta cleavage, as MT5-MMP deficiency reduces Aβ production [47, 49]. Furthermore, alternate β-cleavage by Cathepsin B[50] and Meprin β[51] creates different species of Aβ that may be pathogenically important. There have also been reports of APP-derived peptides of unknown origins with respect to cleavage[45]. Future studies will determine the relevance of noncanonical APP cleavage to APP's endogenous and pathological functions.

APOE and the cholesterol connection

Apolipoprotein E is the major cholesterol transport protein in the brain [52]. Like other apolipoproteins, it is a structural component of lipoprotein particles and the receptor ligand that allows uptake into cells. Although neurons are capable of producing cholesterol, the majority of the cholesterol utilized in the neurons is produced by the astrocytes and transported into the neurons via APOE[53, 54]. Due to its role in cholesterol delivery to the neurons, APOE is very important to synapse formation[55].

There are three major alleles of APOE, each with different properties[56]. APOE4 is by far the strongest genetic risk factor for late-onset Alzheimer's disease [57], while APOE2 is protective[58], and APOE3 is the most common allele[59, 60]. Furthermore, APOE colocalizes with amyloid plaques[61] and APOE4 gene dosage is reported to be highly correlated with the severity of amyloid plaques in both AD brains[62] and in cognitively normal aging brains [63].

Because APOE4 is such a strong risk factor, cholesterol trafficking and regulation is widely studied in the context of Alzheimer's research[52, 64]. In addition to APOE, a variety of other genes involved in cholesterol transport and metabolism have been implicated as risk factors in sporadic Alzheimer's disease such *as* CLU, SORL1, PICALM, *and* BIN1[65]. A disruption in cholesterol homeostasis, cholesterol trafficking, or cholesterol metabolism must be a critical factor in the development of SAD, at least in a sizable subset of individuals. One clue is in the basic function of APOE: APOE4 does not deliver cholesterol as efficiently as the other isoforms[65].

APOE is involved in Aβ clearance[52, 64] through multiple mechanisms. Studies have shown that APOE is involved in transporting Aβ across the blood brain barrier [66, 67]. Some 25% of secreted Aβ is cleared through the blood brain barrier, particularly during sleep, making it the most important Aβ clearance route. Compared to the other isoforms APOE4 travels through the blood brain barrier less efficiently due to its poor affinity for LRP1[56], essentially the same reason it is an inferior cholesterol carrier to the other isoforms. Furthermore, recent work in mouse models has shown

that the level of APOE expression in addition to the isoform positively correlates with Aβ plaque deposition[68, 69]. Similar results have been observed in humans[62, 70]. Furthermore, APOE4 mice have a higher level of soluble Aβ in the interstitial fluid and a lower Aβ clearance rate [71]. Aβ itself can also find lipoprotein receptors and APOE may in fact be competing with it in some cases, therefore decreasing clearance.

APOE is also important for Aβ uptake into astrocytes and microglia[72], another important clearance route of Aβ, and specifically has been implicated in Aβ degradation in the microglia by neprilysin [73]. TREM2 is also important for this process [74], and it is an AD risk gene[75, 76] as well as a binding partner of APOE [77].

APOE4 has recently been implicated in the seeding stage, or the initial formation of amyloid plaques, of Alzheimer's disease[78, 79]. This stage is thought to occur extremely early during the amyloid cascade and may indeed be the critical event, at least in some cases of SAD. This suggests that APOE targeted therapies may be most useful as a preventative measure, particularly for APOE4 carriers [80].

There are many other potential factors that may determine the susceptibility of APOE4 carriers to AD. For example, APOE4 and promotes inflammation[81], a well-established component of AD[81-83]. Although nonsteroidal anti-inflammatory drugs (NSAIDs) are controversial as AD treatments[84], it has been reported that NSAIDs decrease the risk of Alzheimer's disease only and APOE4 carriers, which explains the poor and inconsistent results in other studies[84].

APP and the secretases are also linked to cholesterol regulation. Reportedly, γ-secretase regulates cholesterol[85-87]. APP[88-94] and γ-secretase both bind cholesterol[95].

In turn, cholesterol modulates APP and the secretases. Cholesterol has been reported by many to regulate APP trafficking in some way [96-100]. Cholesterol has been linked to the regulation of α-secretase[101-104], β-secretase[100, 105-108] and γ-secretase [105, 109-111]. Cholesterol bridges the gap between the amyloid cascade hypothesis and the risk factors that are actually associated with sporadic Alzheimer's disease.

Available treatments for AD and rationale

Currently there are no successful disease modifying therapies available at all, and the available treatments of Alzheimer's disease are focused on ameliorating the symptoms, improving quality of life for the patients, reducing caregiver burden, and delaying nursing home placement. A variety of drugs, including antipsychotics and antidepressants, are prescribed to manage behavioral symptoms or comorbidities, which will not be discussed here. The first drugs to be approved specifically for Alzheimer's disease were acetylcholinesterase (AChE) inhibitors in the mid-1990s [112]. Although memantine was marketed in Germany for dementia as early as 1989, it was not specifically approved for Alzheimer's disease until the early 2000s in Europe and the US [113, 114]. In addition, nonpharmacological therapies are frequently utilized by caregivers and therapists to manage symptoms [115].

AChE inhibitors have been used to treat Alzheimer's disease symptoms for many years. Initially, these drugs were hoped to be disease-modifying because of the now-antiquated cholinergic hypothesis of Alzheimer's disease, which predates the amyloid cascade hypothesis[34, 116, 117]. It is true that the nucleus basalis of Meynert undergoes

severe neurodegeneration in AD patients [118, 119]. In fact, the cholinergic neurons in the NBM start to break down quite early in Alzheimer's disease[116, 119]. These neurons project to the cerebral cortex, the hippocampus, and the amygdala, which are affected in AD. According to the cholinergic hypothesis, the loss of these cholinergic inputs leads to neurodegeneration [120].

The degradation of the cholinergic system appears to occur after deposition of beta-amyloid and tau, one of the reasons why the amyloid cascade hypothesis largely replaced the cholinergic hypothesis. Studies in AD patient's brains strongly suggests that the loss of cholinergic innervation in the NBM is caused by neurofibrillary tangles [121, 122]. Furthermore, cholinergic abnormalities and amyloid plaque deposition are correlated in AD brains, and even in patients that were not demented at time of death, although not as strongly correlated as tau NFTs [123, 124].

Cholinergic function in other parts of the brain, for example in the thalamus, appears to be preserved in AD brains. The NBM is in the basal forebrain and is near the hippocampus, the amygdala, and the entorhinal cortex. Unsurprisingly amyloid deposition and tau pathology is typically high in this region [124, 125]. This suggests that the cholinergic pathology is linked to the specific brain region, the NBM, rather than cholinergic neurons are just more sensitive to Alzheimer's pathology. There is evidence of cholinergic dysfunction in preclinical Alzheimer's disease as well. It is typically thought that the cholinergic dysfunction is a result of the amyloid and tau pathology, rather than the other way around, which means the well-established cholinergic pathology is considered to be a downstream component of the amyloid

cascade, along with inflammation and disrupted cholesterol. Cholinergic denervation is a critical event in Alzheimer's disease pathogenesis and there is some evidence that treatments with AChE inhibitors delay the course of the disease [126], though none that it increases lifespan. For example, some studies indicate that AChE inhibitors promote nonamyloidogenic cleavage [127, 128]. However there is no evidence to suggest that acetylcholinesterase inhibitors are curative. In fact, AChE inhibitors have only been shown to be moderately efficacious [129], with some studies citing no benefit at all [130]. However, the benefits are most pronounced when patients are treated very quickly upon diagnosis. Multiple studies have demonstrated that individuals placed on cholinergic inhibitors later, in mild to moderate stages, receive less benefits [120, 126].

Acetylcholinesterase inhibitors are prescribed to patients a day to improve the ability to perform daily tasks, improve the cognitive capacity, and decrease behavioral irregularities consistent with Alzheimer's disease. Cholinergic therapy for preclinical AD patients may preserve function for much longer when they do develop Alzheimer's. In support of this idea, it has been shown that AChE inhibitors reduce nursing home placement by approximately 30% each year of treatment in one study[131] and delay it for approximately 17-21 months in another study [126]. AChE inhibitors also reduce caregiver burden, including time with the patient and stress [126].

Donezepil was approved specifically for Alzheimer's disease in 1996. However, studies have shown that less than half of AD patients take AChE inhibitors, citing distrust of the drugs by primary care physicians in particular [132]. Compliance in patients who

have actually been prescribed the drug is also poor, although highly variable[133, 134]. These studies illustrate the difficulties in treating AD patients in reality.

The only drug approved for Alzheimer's disease that is not an AChE inhibitor is memantine, a noncompetitive N-methyl-D-aspartate (NMDA) receptor antagonist. Memantine has also been prescribed for other kinds of dementia [114]. The rationale behind memantine treatment of Alzheimer's disease is not as well developed as that of AChE inhibitors. However, glutamate synaptic terminal dysfunction is found in Alzheimer's disease, particularly in the most affected brain regions [8, 135-137].

Synaptic dysfunction in AD occurs much earlier than the symptoms can be clinically diagnosed[138]. Aberrant Aβ production and processing are likely involved in synaptic dysfunction, which has the strongest correlation to AD severity[139]. Memantine reportedly reduces the production of amyloid-β peptides through modulation of amyloid precursor protein trafficking[140]. Interestingly, memantine has also been shown to prevent some of the defects in axonal transport trafficking caused by Aβ [141]. There has even been some suggestion that NMDA receptors (NMDARs) also mediate tau toxicity. However, human studies on these topics are scant.

Because memantine preferentially binds open channel NMDARs, it may have positive effects due to selective inhibition of overactive NMDARs [114]. Extra synaptic NMDARs have been implicated in excitotoxicity, which may be treated by memantine[142]. In general, NMDA receptors in the synapses promote cell survival, whereas the extra synaptic pool inactivates cAMP response element-binding protein (CREB) and promotes apoptosis [142]. However there have been conflicting results about the roles of

NMDARs in cell survival. NMDA-mediated dysfunction may also be underlying mitochondrial dysfunction and damage. Mitochondrial damage contributes to synaptic dysfunction in AD [141, 143, 144] and evidence suggests that the mitochondria localized to the synapses are specifically targeted. NMDARs and especially GluN2B subunit-containing NMDARs have been linked to Aβ induced neurotoxicity and calcium homeostasis dysfunction in many studies[141, 145, 146].

There is no evidence that memantine has an effect on brain atrophy, but some suggest that memantine delays nursing home placement, slows the apparent progression of symptoms, and improves language, memory, and daily life functioning [147-149]. However, results have been mixed [113, 150].

A recent and thorough meta-analysis[129] showed that only donepezil, donepezil in combination with memantine, and transdermal rivastigmine were efficacious over placebo in in terms of Mini–Mental State Examination (MMSE) score and overall in terms of behavior improvement, although only donezepil and galantamine improved Alzheimer's Disease Assessment Scale-cognitive subscale (ADAS-Cog) score. Overall most likely donepezil in combination with memantine is the most effective therapy.

Non-pharmacological therapies are another option that is frequently utilized by caregivers and healthcare professionals. This can include talk therapy, exercise, brain training, massage, and a variety of other treatments intended to improve quality of life for patients. A meta-analysis in 2010 sought to determine the efficacy of nonpharmacological intervention.[115] The authors divided a wide variety of treatments into various categories. For example, cognitive training, behavioral intervention,

physical exercise, use of music, and psychotherapy. In specific studies, by the end of the study was found that 10.6% in the treatment groups compared to 14.9% w were placed in nursing homes. The study strongly recommended that these interventions should be added to a two treatment plan that includes medication. They concluded that it is difficult to determine which interventions are most helpful because so many studies included multiple components or had poor controls. Individually, they found little evidence for the efficacy of many popular interventions including physical exercise, massage, touch, and recreation therapy, citing poor study design. However, in combination with each other, nonpharmacological interventions decrease caregiver burden and increase quality of life and may delay nursing home placement. There is no evidence to suggest that these treatments are disease modifying, nor are they intended to be. Nonpharmacological therapies are a cost-effective option to improve the day to day lives of AD patients and their caregivers, and no more.

Outside of ongoing clinical trials, AChE inhibitors, memantine, and pharmacological and nonpharmacological symptom management are the only treatments for Alzheimer's disease. Most current drug development is based around Aβ. By comparison, anti-tau therapies are understudied[151], even though combination therapy is perhaps the most feasible option to halt already established Alzheimer's disease [152, 153]. A better understanding of how APP and Aβ contribute to early AD pathogenesis is sorely needed to guide future treatment discovery and development.

APP and the secretases as therapeutic targets

Anti-amyloid therapies, and specifically β- and γ-secretase inhibitors, have proven to be problematic in clinical trials. Because α-secretase cleavage (α-cleavage) prevents Aβ production, it is also a proposed drug target[154]. Positive modulators of α-secretase have not made it to clinical trials yet. Many secretase inhibitor trials were conducted on symptomatic Alzheimer's patients unlikely to respond to therapy even according to the amyloid hypothesis, due to the irreversible damage and tau pathology that has already occurred. However, some trials made patients worse or had other intolerable side effects. A more in-depth look at secretase cleavage is useful background to explain difficult to target the secretases, especially while sparing their other very important targets.

Compartmentalization and environmental sensitivity of secretases

Since APP's expression is ubiquitous, most studies on APP processing have been conducted in non-neuronal cells or cell lines [155, 156] for reasons of technical practicality. Investigations using those cells revealed that α-secretase cleaves APP in the plasma membrane, whereas β-secretase cleaves APP in acidic compartments [157, 158], suggesting that APP's subcellular membrane localization determines its proteolytic fate. However, γ-secretase cleavage is less straightforward. Unlike β-secretase, γ-secretase activity is not pH dependent[159], but like β-secretase, γ-secretase has been shown to be associated with lipid rafts[160-162]. Both sides of the synapse harbor γ-secretase in neurons[163, 164]. In fact, γ-secretase has been found [163-170] and demonstrated to be

active[48, 161, 167, 171, 172] at the plasma membrane and in several different internal compartments. Furthermore, γ-cleavage of APP specifically has been observed in different locations[173-178]. It has been recently reported that α- and γ-secretase form complexes with each other, and is suspected that β- and γ-secretases do also[155]. In fact, association of BACE1 with γ-secretase subunit nicastrin[179] was reported much earlier and other studies corroborate the association [155, 180]. This suggests that γ-cleavage may occur in the same locations as both α- and β-secretase, likely in concert with them. This explanation reconciles many other seemingly contradictory reports.

Challenges in drug development

Anti-amyloid therapies have long been the focus of Alzheimer's disease treatment. It is generally agreed that the best chance for anti-amyloid therapies is prevention, but until recently is been difficult to arrange such clinical trials. There are a number of different options including secretase inhibitors and active and passive immunotherapy targeting Aβ plaques, oligomers, and monomers. Because it is not known which aspects of Aβ are the most toxic, it is difficult to predict which treatments will be effective. For example, breaking down the plaques with immunotherapy is very likely to increase soluble Aβ levels in the brain, at least acutely, which could in theory worsen the disease [28]. By contrast, decreased amyloid production with secretase inhibitors is likely to have very little effect on already existing amyloid plaques, for example. Despite this uncertainty, secretase inhibitors

have been a high priority drug target for Alzheimer's disease for many years now and were aggressively pushed, perhaps prematurely[181], into clinical trials.

Semagacestat, a γ-secretase inhibitor, performed disastrously in a Phase 3 clinical trial[182]. The inhibitor causes a variety of different side effects, including alopecia, gastrointestinal symptoms, and the development of skin cancer. More deaths occurred in the treatment group than in the control group, although it is difficult to directly attribute these deaths to the inhibitor. The most shocking result, however, was that patients taking the inhibitor had decreased cognitive capacity compared to patients taking placebo[182]. After the trial, many reasons for its failure were put forth. Rather than continuous and prolonged low dose use, patients were given high doses only once a day. Perhaps the constant fluctuation in secretase activity doomed the trial, not secretase inhibition per se[181]. However, many suggested that a critical γ-secretase substrate was responsible [183].

Although all of the secretases have important substrates besides APP, it is not surprising that γ-secretase inhibitors in particular are dangerous. Perhaps the most notable of these substrates is Notch, which is cleaved by α-secretase then sequentially by γ-secretase in the same manner as APP [184-186]. The Notch pathway is extremely important to a variety of different cellular functions including but not limited to cell proliferation and survival. Semagacestat's failure was considered to be partially due to Notch[183].

Avagacestat was developed as a possible solution. This γ-secretase inhibitor is purportedly Notch sparing. The drug made it to phase 2 clinical trials [187] before being

discontinued due to the severity of the side effects. One possible explanation is that the inhibitor actually does not spare Notch, which was demonstrated in vitro after the trial [188]. However, Notch is not necessarily responsible for all of the side effects. There are many pathways affected by γ-secretase. It has been demonstrated to regulate synaptic vesicles and neurotransmission[189-194]. APP trafficking is also regulated by γ-secretase[195-200], reportedly both indirectly[201, 202] and via direct binding[203, 204]. Additionally through this regulation as well as cleavage of APP, γ-secretase regulates additional cellular processes [86, 205, 206]. Reportedly, γ-secretase also regulates trafficking of other proteins [207-209] and has even been shown to regulate the other secretases[155, 185, 210, 211].

Proposed roles for APP and its cleavage products

There are a number of different potential roles that amyloid precursor protein and its numerous cleavage products may play[212, 213]. For many years, APP has been reported to play a role in development and survival of neurons. APP has been shown to contribute to neurite outgrowth[214, 215] and is also important for neuron survival in the adult brain[216]. It is now widely accepted that secreted soluble APP, specifically sAPPα, mediates many of these processes [217-219]. These processes have been shown to be critical to survival and normal neuronal development. There is partial redundancy with amyloid precursor-like proteins 1 and 2 (APLP1 and APLP2), APP family members that lack the Aβ domain, but triple knockout is lethal[220].

APP plays a role in axonal transport, and there are indications that disruption of this role may contribute to amyloidogenesis. Overexpression of APP was shown to disrupt axonal transport in a tau-dependent fashion in Drosophila [221]. Furthermore, APP mutations also disrupted axonal transport and by so doing caused neuronal damage and death in Drosophila[222]. A more recent study investigated APP-dependent disruption of the endocytic pathway in mouse neurons. This particular study demonstrated that full-length APP and C99/β-CTF, not Aβ, promoted endosomal swelling, axonal dysfunction, and neuronal death[223].

Much like Notch, the APP intracellular C-terminal fragment (AICD) acts as a transcription factor[224, 225]. Like any transcription factor, the AICD has been linked to a variety of interconnected and opposing cellular processes. For example, the AICD promotes neurite outgrowth [226] and neuroprotection [227], but also apoptosis [225, 228]. In addition to its proposed functions in normal cells, the AICD may play a role in Alzheimer's disease pathogenesis[229]. The extent of its involvement is yet to be determined.

APP in synaptic activity

Synaptic plasticity, the ability of synapses to adjust their connectivity in response to their own activity, is central to learning and memory. Rapid firing of presynaptic action potentials induces long-term potentiation (LTP), which is thought to encode memories in neural networks. APP knockout mice have impaired LTP and reduced synaptic proteins, which suggests an intrinsic, nonpathological role for Aβ in synaptic

plasticity[230]. In fact, Aβ[231, 232] as well as sAPPα[219] have been shown in some studies to be important for LTP induction. APPsα helps with spine growth, axon length, and many other structural correlates of synaptic activity[219].

Notably, studies have shown that soluble oligomeric Aβ inhibits LTP[233] and induces synaptic depression in hippocampal neurons[234]. Although many such studies have not been performed at physiological levels of Aβ, it has nevertheless been widely speculated that abnormally high soluble Aβ levels may cause the memory failure that occurs in preclinical AD prior to structural damage and Aβ aggregation[233, 235].

Somewhat confusingly, unprovoked seizures are more prevalent in AD patients even though Aβ mediates depression and synapse loss[236]. Furthermore, mice that overexpress human APP have seizures and other spontaneous epileptiform activity[237, 238]. Because of these and other studies, many suggest excitotoxicity contributes to the cognitive failure in AD[236]. However, it is difficult to reconcile the hypothesis that Aβ itself is causing hyperexcitability with the well-established Aβ-induced depression. There is another seemingly contradictory observation made about Aβ and synaptic activity: AMPA (α-amino-3-hydroxy-5-methyl-4-isoxazolepropionic acid) receptor agonism and induction of LTP both suppress Aβ mediated depression, but not Aβ production[239, 240].

However, Aβ-mediated synaptic depression can also be conceived as part of the regulation of synaptic activity in the healthy brain. APP or Aβ may depress synaptic transmission and inhibit synaptic potentiation in order to counteract excessive elevation of neural network activity. Aβ's synaptic targets, like glutamate receptors or

Ca^{2+}-signaling, are also involved in mechanisms reported to govern homeostatic plasticity[135]. Homeostatic plasticity, the ability of individual neurons or networks of neurons to adjust all of their synapses in order to compensate for network-level activity changes, prevents unconstrained synaptic potentiation or depression and thus helps to maintain network stability[241]. This global regulation is achieved by both pre- and postsynaptic mechanisms including adjusting postsynaptic receptors and synaptic vesicle release probability[242]. These mechanisms scale all synapses of a neuron or a neural network down or up to create room for individual synapses or neurons to go up or down[241]. Intriguingly, Aβ is altered by pharmacologically induced network activity changes *in vitro*[233] and has been shown to be present in and secreted by synaptic vesicles[243]. The AICD has also been implicated in synaptic homeostasis via ryanodine receptors.

Sleep itself may be a major regulator of homeostatic plasticity [244-246], although this is controversial [247]) and several lines of evidence show that sleep links to APP and Aβ in AD. The sleep hypothesis of synaptic homeostasis states that neural circuits are scaled up during wakefulness and scaled down during sleep in order to maintain the capacity for synaptic plasticity[244]. Aβ release may be part of the homeostatic mechanism during sleep. Notably, Aβ levels fluctuate diurnally in coordination with the sleep-wake cycle in both humans and mice. Aβ level is the highest at night and the lowest in the morning in human subjects[248], which echoes the idea that Aβ facilitates synaptic depression[249]. Diurnal fluctuation of Aβ is significantly decreased in a mouse model of AD and correlates with the animals' disrupted sleep-wake cycle[250]. These

studies also suggest that Aβ and sleep may be linked in AD pathogenesis. Clearance of Aβ through the blood brain barrier is greatly facilitated by sleep[251], and sleep disorders are a confirmed risk factor for AD[248].

APP in cholesterol

There are many reports of regulation between APP, the secretases, and cholesterol concentration and trafficking. APP reportedly regulates cholesterol[252-255]. Aβ itself has been implicated in cholesterol regulation [86, 256, 257]. APP also regulates γ-secretase[258, 259], which as we discussed previously, regulates cholesterol concentration and trafficking.

While some report that γ-cleavage is cholesterol dependent[260], it is more typically thought that while the cleavage itself is independent[95, 261], APP's association with γ-secretase is increased by higher cholesterol concentrations[262]. Interestingly, while membrane cholesterol enhances β-secretase [100, 105] and γ-secretase [105, 110, 111] cleavage, it has been reported to suppress α-secretase activity [101, 102].

Irregularities in lipid homeostasis have been overlooked for a very long time in Alzheimer's disease research. In fact, Alois Alzheimer actually describes a third irregular structure in his original case report [263]– "large fatty sacks", according to a very careful relatively recent translation[264]. The Swedish mutation was identified in 1995 in a landmark paper[265]. Haas et al. reported that the localization of APPSwe was irregular. Specifically, that the localization of APPSwe was shifted radically away from the cell surface and towards internal vesicular compartments. The field focused on

the cleavage and production of Aβ, perhaps wrongly, not the implications of the redistribution of full-length APP. It has also been reported that the same cells with tau NFTs have extremely high levels of cholesterol [266]. This is in fact extremely similar to what Alzheimer's original patient had – cells forming the fibrils at the same time times as the lipid structures [264]. There have been many reports since of irregular cholesterol trafficking in AD, including swollen endosomes [266]. The buildup of APP in internal acidic compartments with BACE1 does lead to increased Aβ production, but it is only one consequence. Using live cell imaging, we have investigated the trafficking of full-length APP itself, and our data suggests that APP is involved in lipid trafficking between the plasma membrane and internal compartments, and plays an important role distinct from the production of Aβ that may be relevant Alzheimer's disease pathogenesis.

Dissertation Aims

The contributions of full length APP and its cleavage products, particularly Aβ, to Alzheimer's disease pathogenesis are still controversial, and the amyloid hypothesis has failed to yield clinical results for decades. We sought to increase our understanding of APP itself, including its trafficking, cleavage, and response to neuronal activity. Ultimately, we proposed a functional role for APP based on our results in the regulation of plasma membrane cholesterol concentration.

Our first goal was to create and characterize our 3-color probe and live cell imaging assay. Next, we wanted to determine if the trafficking of newly synthesized APP in primary neurons was consistent with many other reports in cell lines that indicate a large fraction of APP is transported to the cell surface before being either cleaved by α-secretase or endocytosed. We performed time lapse imaging on newly transfected cells without foreknowledge of fluorescent protein expression. Finally, due to the reported association between Aβ production and synaptic activity, we wanted to determine if APP trafficking and exocytosis is correlated to synaptic activity. Our results in Chapter I paint a fuller picture of APP production and fate in living neurons.

The aims of Chapter IV were to determine how the localization of APP is related to its cleavage. We discovered that the surface trafficking of APP changed in response to secretase inhibitor treatment, separately and in combinations. It has been reported using techniques with little spatial resolution that γ-secretase regulates APP trafficking independently of cleavage. We wanted to confirm this in neurons using

our live cell imaging assay and determine if the other secretases also alter APP trafficking. Furthermore, by comparison with a synaptic vesicle protein (SypHTm), we wanted to determine if the alterations were specific to APP.

Based on our results, we proposed that APP's response to synaptic activity may be indirect, and that surface APP level is tightly regulated by an endocytosis-dependent mechanism in addition to cleavage. The aims of Chapter V were to determine if cholesterol concentration and direct binding of APP and cholesterol affects APP surface trafficking. Next, we looked for evidence that APP in turn affects cholesterol at the plasma membrane by filipin staining cells expressing mutant APP deficient in cholesterol binding. We also wanted to determine whether these effects are related to γ-secretase-inducted surface presentation. Finally, we want to determine if APP's direct cholesterol binding is important to maintaining the integrity of the plasma membrane at the synapses.

Chapter II

MATERIALS AND METHODS

Materials

Buffers and media

Tyrode's saline contains (in mM): 150 NaCl, 4 KCl, 2 $MgCl_2$, 2 $CaCl_2$, 10 N-2 hydroxyethyl piperazine-n-2 ethanesulphonic acid (HEPES), 10 glucose, pH 7.35 or pH 5.5. The 50 mM NH_4Cl solutions was made by substituting for NaCl equimolarly, pH 7.35. Plating media consists of Minimal Essential Medium (MEM, Life Technologies) and (in mM) 27 glucose, 2.4 NaHCO3, 0.00125 transferrin, 2 L-glutamine, 0.0043 insulin and 10%/vol fetal bovine serum (FBS, Gibco) Ara-C media consists of MEM and (in mM) 27 glucose, 2.4 $NaHCO_3$, 0.00125 transferrin, 0.5 L-glutamine, 2 Ara-C, 1 %/vol B27 supplement (Life Technologies) and 5 %/vol FBS. Transfection media is serum free and consists of MEM and (in mM) 27 glucose, 2.4 $NaHCO_3$, 0.00125 transferrin, 0.5 L-glutamine, and 1 %/vol B27 supplement.

Primers and plasmids

The pHluorin-APP plasmid, which contains a human synapsin1 promoter, was a gift from Dr. Jürgen Klingauf [243]. The Synaptophysin-pHTomato plasmid (pTGW-UAS-SypHTm-T2A-BFP2) was a gift from Dr. Yulong Li [267]. The SypHTm fragment was amplified from the Synaptophysin-pHTomato plasmid and inserted into a

mammalian expression vector (pCDNA3.1) containing human synapsin1 promoter using Gibson Assembly Cloning Kit (NEB) [268]. SypHTm along with the T2A linker was amplified from the pTGW-UAS-SypHTm-2ABFP2 with Phusion kit (NEB) and using 5'-CGTGCCTGAGAGCGCAGTCGAATTAGCTTGGTACCATGGACGTGGTGAATCAGCTGGTGG -3' (forward primer) and 5'-CCAGGCTGGGCAGCATGGTGGCGGCGGATCCAGGGCCGGGATTCTCCTCCACGTCAC-3' (reverse primer). SypHTm:T2A:pH-APP was verified by sequencing. Next, BFP2 was amplified from pTGW-UAS-SypHTm-T2A-BFP2 using 5'-CAAGTTCTTTGAGCAGATGCAGAACGCAGCGGCCGCAATGGTGAGCAAGGGCGAGGAGC -3' (forward primer) and 5'-CATTTAGGTGACACTATAGAATAGGGCCCTCTAGATTACTTGTACAGCTCGTCCATGCCG -3' (reverse primer), and was inserted to the C-terminal of pHluorin-APP before the stop codon using the Gibson Assembly Cloning Kit (NEB). The resulting plasmid, SypHTm:T2A:pH-APP-BFP2 was verified by DNA sequencing. Mutagenesis was performed by Hui Huang.

Equipment

Most samples were imaged on a Nikon Eclipse Ti inverted microscope with a 100X Plan Apo VC objective (N.A. 1.40) and an EMCCD camera (Andor). For Alexa 488, 568, and 647 fluorescence, we used the following filter sets (Semrock) respectively:

Ex 405/20X, DiC 425LP and Em 460/50; Ex 460/50, DiC 495LP and Em 535/25; Ex 565/25, DiC 585LP and Em 644/90; Ex 644/10 DiC 660LP and Em 710/50. All imaging conditions including the intensity of input light source, exposure time and EM gain were kept the same among different treatment groups.

The live cell soma imaging experiments (**Figure 8A-B**) were performed in a similar manner using a spinning disk confocal microscope equipped with the same perfusion system as the Eclipse Ti and a LUMPlanFl 40x/0.80w objective. 405, 480 and 561nm lasers paired with the emission filters Et460/50m, Et525/50m and Et605/52m were used to image BFP2, pHluorin, and pHTomato, respectively.

For long-term time-lapse imaging, we used an Olympus IX-81 microscope equipped with ASI motorized xy stage, Mightex LED light source, an Olympus 10X Ph1/Fl (N.A. 0.10) objective and a Flash 4.0 sCMOS camera (Hamamatsu) was used for long-term time-lapse imaging.

Cell culture, transfection and DNA constructs

All animal protocols were approved by the Vanderbilt University Animal Care and Use Committee. Rat postnatal hippocampal cultures were prepared according to an established protocol [269] with slight modifications. Briefly, rat hippocampi (CA1-CA3) dissected from P0 or P1 Sprague-Dawley rats were dissociated via an 11-min incubation in Trypsin-EDTA (Life Technologies) followed by gentle trituration using three glass pipettes of different diameters (~1 mm, 0.5 mm, and 0.2 mm), sequentially.

Dissociated cells in suspension were recovered by centrifugation (x 200 **G,** 5 minutes) at 4°C and re-suspended in plating media. 100 µl of resuspended cells were plated onto single round 12mm-ø glass coverslip (~200,000 cells/mL) pre-coated with Matrigel (Life Technologies) and all coverslips were placed in 24-well plates (ThermoScientific). Cells were allowed to adhere to the coverslips for 30-60 minutes before the addition of 1 mL plating media per well. After 1-2 days in culture, an additional 1 mL of AraC media was added into every well. Ara-C in the culture media efficiently prevented the overgrowth of astroglia. Calcium phosphate transfection was performed at 8-9 days and most experiments were performed at 14-17 days after the full maturation of neuronal synapses. In all time lapse imaging experiments, dissociated cells were plated onto glass bottom, 4-compartment 35/10 mm cell culture dishes (Greiner Bio-one) and were transfected at 11-16 days at the start of the experiment.

APP antibodies and immunofluorescence imaging

Standard Immunocytochemistry

After treatments or imaging, coverslips were fixed in PBS containing 4% paraformaldehyde for 20 minutes, permeabilized with 0.25% Triton X-100 for 10 minutes and blocked for at least one hour with goat serum and BSA solution all at room temperature (substituting horse serum if a goat primary was used). Next, they were incubated with diluted primary antibodies (**Table 1**) overnight at 4 ºC or at room

temperature for at least one hour. After incubation with primary antibodies, cells were thoroughly washed and then incubated with specific secondary antibodies labeled by distinct fluorophores (see Table 1, 1: 1000 dilution for all, Life Technologies or Biotium) at room temperature for at least one hour before mounting.

Primary Antibodies	Dilution	Supplier	Catalog No.
Rabbit anti-APP (Y188)	1:250	Epitomics, Abcam	1655-1, ab32136
Chicken anti-GFP	1:1000	Life Technologies	A10262
Mouse anti-MAP2	1:200	Millipore	MAB3418
Guinea pig anti-Synapsin 1/2	1:1000	Synaptic Systems	106 004
Mouse anti-APP (22C11)	1:200	Millipore	MAB348
Guinea pig anti-Synaptophysin 1	1:1000	Synaptic Systems	101 004
Goat anti-mCherry	1:250	Sicgen Antibodies	AB0040-20
Mouse anti-Synaptotagmin 1	1:500	Synaptic Systems	105 311BT
Secondary Antibodies	**Dilution**	**Supplier**	**Catalog No.**
488 goat anti-Chicken	1:1000	Life Technologies	A-11039
488 goat anti-Rabbit	1:1000	Life Technologies	A-11034
647 goat anti-Mouse	1:1000	Life Technologies	A-21236
568 donkey anti-Guinea pig	1:1000	Biotium	20377
568 goat anti-Mouse	1:1000	Biotium	20101
405 donkey anti-Guinea pig	1:1000	Biotium	20376
568 donkey anti-Goat	1:1000	Life Technologies	A-11057

Table 1: Antibodies.

Surface isolation technique

In order to isolate different populations of APP using immunocytochemistry, three separate APP antibodies were applied to the same samples. Two different N-terminal APP antibodies with no overlapping epitopes were selected for surface and total N-terminal labeling. After treatments, coverslips were fixed using 4% paraformaldehyde

in PBS for 30 minutes and blocked with horse serum and BSA in PBS for at least one hour in the absence of detergents. Then, the coverslips were treated with goat anti-APP-N overnight at 4°C, washed, and treated with an anti-goat secondary antibody for one hour at room temperature. After at least 5 washes to eliminate the anti-goat secondary entirely, the cells were permeabilized with 0.25% Triton X-100 for 10 minutes. The coverslips were blocked for one additional hour in goat serum, BSA, and Triton X-100 solution at room temperature. Next, they were incubated with the two other APP antibodies (22C11 and Y188) and guinea pig anti-Synaptophysin at room temperature for at least one hour, washed, and treated with three fluorophore-labeled goat secondary antibodies (see **Table 1**, 1: 1000 dilution for all, Life Technologies or Biotium) at room temperature for one hour before mounting.

Filipin staining

Coverslips were removed from their incubator and washed briefly in pre-warmed (37°C) 4K Tyrode. AM1-43 was diluted in 90K solution and applied to the cells for 1 minute at room temperature. After at least 2 gentle washes with room temperature PBS, the cells were fixed for 30 minutes in 4% paraformaldehyde. The paraformaldehyde was quenched with 1.5 mg/mL glycine in PBS for 10 minutes at room temperature before washing in PBS. Filipin solution (0.05 mg/mL in PBS) was applied to the cells. In order to minimize filipin's permeabilization of the cells, the

staining was performed at 4°C for 30 minutes only. The coverslips were then washed and mounted.

Filipin imaging was performed using AM1-43 to select FOV to minimize photobleaching in the filipin channel. Due to the lack of synaptic markers, region of interest (ROI) selection was focused on the processes. Rather than hand drawing all processes as in quantifications that feature transfected cells only, the images were thresholded as a base, additional processes of lower intensity were added by hand, and the somas and debris were excluded. The processes were divided into ROIs of relatively uniform size. Areas with a lower density of astrocytes were intentionally selected but astrocytes could not be completely separated from the neurons.

For **Figure 27**, AM1-43 was once again used to define processes. No hand-drawing was used for this figure. We found that the pHTm signal was too punctated to define the processes using thresholding. Although pHluorin was present in the transfected neurons, we found that it has a negligible effect on the apparent AM1-43 signal. So, it was not possible to automatically define transfected processes using thresholding. Instead, transfected and untransfected process segments were selected manually by visual comparison of the somas, where the SypHTm signal was most easily detectable. Any processes originating outside the field of view or that are ambiguous with respect to their somas of origin were excluded from the analysis. After this determination was made, the process segments themselves were not sorted or excluded based on the signal in any channel; even negative values after background subtraction were included.

The control sample from **Figure 28** was prepared with the same 90K incubation, but without AM1-43. In the absence of AM1-43, the same channel was still used to isolate individual processes using a much lower threshold due to the combination of pHluorin signal and natural autofluorescence. Transfected processes were still selected based on pHTm signal.

Time lapse live cell imaging

For long-term time-lapse imaging, we used an Olympus IX-81 microscope equipped with ASI motorized xy stage, Mightex LED light source, an Olympus 10X PH1/FI (N.A. 0.10) objective and a Flash 4.0 sCMOS camera (Hamamatsu) was used for long-term time-lapse imaging. Cells were grown in 4 compartment glass bottom 35/10 mm dishes (Greiner Bio-one), transfected and treated immediately prior to the experiment. The dish was placed in a sealed microscope stage chamber. A customized weather station enclosure maintained a constant temperature of 37°C. 5% CO_2 air was supplied to the sealed stage after bubbling through a H_2O tank inside the weather station in order to maintain 5% CO_2 and saturated humidity in the sealed imaging chamber. The image acquisition started approximately 1 hour after replacement of regular media after transfection and addition of the drugs. 4-5 fields of view were chosen per quadrant in areas of high neuronal density without the knowledge of the fluorescent protein expression. Image acquisition was controlled via Micro-

Manager[270] (UCSF). Phase contrast images as well as blue, green and red fluorescence images for every field of view were taken every 30 minutes.

Fiji [271], a distribution of ImageJ [272], was used for quantification. For immunofluorescence and live-cell imaging, soma ROIs were hand drawn in areas with a relatively low background based on APP. Nearby regions, either relatively cell free or on top of glia as appropriate for each individual soma were selected as background regions. Mean values were exported from Fiji and background subtraction was performed using Microsoft Excel. Prism 7.03 was used to generate all plots and perform all statistical analysis. For long-term time-lapse imaging, image stacks were corrected for stage drift using FIJI plugins called StackReg[273] and Somas. Whenever possible, processes (divided into 100uM segments) were quantified. For **Figure 12**, one soma with three processes with very few morphology changes was chosen, and the same ROIs were used for every frame. Using the MultiStackRegistration plug-in, pHTm images were used to align all stacks for the same field of view. For **Figure 13**, only soma ROIs were hand-drawn frame by frame based on phase-contrast images because morphology changes to the soma shape and size was too common to be a basis for exclusion. For these experiments, the background was defined by a single ROI near the cell to account for uneven illumination and, in some cases, auto fluorescence from untransfected glia. Due to the high variability in background and fluorescence interference by Dyngo4a, the pHluorin images were corrected before being quantified ("Float the stack" macro, Kenton Arkill).

Acute live cell imaging

Live cell imaging was performed with a Nikon Eclipse Ti inverted microscope, a 20X or 100X Plan Apo VC objective and an Andor iXon+ 887 EMCCD camera or a Hamamatsu Flash4 (**Figure 1D**). 12 mm coverslips were mounted in an RC-26G imaging chamber (Warner Instruments) bottom-sealed with a 24x40 mm size 0 cover glass (Fisher Scientific). The chamber was fixed to a PH-1 platform (Warner Instruments) placed on the microscope stage. Gravity perfusion-powered solution exchange was controlled by a VC-6 valve control system and a 6-channel manifold (Warner Instruments) with a constant rate of ~50 µL/sec which allowed a complete bath solution turnover in the recording chamber in under 30 s. Image acquisition and synchronized perfusion were controlled via Micro-manager software. For every fluorophore, the acquisition settings including excitation power, fluorescence filter set (excitation, dichroic and emission filters), exposure time, camera gain and frame rate were all kept the same among different samples on all experiments. The optical filter sets (Chroma and Semrock) for Alexa 405/BFP2, pHluorin and pHTomato were, respectively: Ex 405/20X, DiC 425LP and Em 460/50; Ex 480/20X, DiC 495LP and Em 535/40; Ex 560/40M, DiC 585LP and Em 610/20nm BP. Samples were exposed to normal Tyrode's saline at pH 7.35, a 50mM NH_4Cl solution and normal Tyrode's solution adjusted to pH5.5 sequentially. Some of the older data sets in **Figure 16** and **Figure 10** were collected using NH_4Cl before 4K. Tyrode's saline contains (in mM): 150 NaCl, 4 KCl, 2 $MgCl_2$, 2 $CaCl_2$, 10 N-2 hydroxyethyl piperazine-n-2

ethanesulphonic acid (HEPES), 10 glucose, pH 7.35 or pH 5.5. The 50 mM NH_4Cl solutions was made by substituting for NaCl equimolarly, pH 7.35. All solutions contained 10 μM NBQX and 20 μM D-AP5 except in the experiment in **Figure 7 F-H**, which was meant to replicate the experiment in **Figure 7 A-E** during which MβCD was applied to the home media as a pretreatment in the absence of such activity altering drugs. StackReg [273] was used to correct for state drift. MultiStackRegistration (Brad Busse) was used to align the pHluorin stacks using the pHTm stacks as reference, with individual frames adjusted as needed manually. For the purposes of quantification, the 3 most representative frames (5 for **Figure 16** and **Figure 10**) were chosen in each solution and averaged together in ImageJ. For example, as NH4Cl is applied, fluorescence increases to a peak and then begins to decrease. Three consecutive frames with the highest fluorescence signal are used to represent of the maximum fluorescence. Because BFP2 signal is not pH-dependent, all BFP2 frames were averaged together for quantification. Using averaged frames rather than taking the beginning, maximum and minimum from each trace reduces the error caused by actively moving puncta passing by a synapse. Average frames were used for most analyses except **Figure 15**, which is intended to detail acute responses to activity rather than to determine the surface and internal fractions of the fluorophores at a steady state as in the other figures. For live cell imaging analysis, synapses were defined based on the SypHTm signal; specifically, all static puncta. ROIs for synapses and neurites were manually selected in ImageJ. In addition, multiple cell-free areas were selected as background ROIs. Separate background ROIs were selected for BFP2

because astrocytes and untransfected neurons produced a high background in that channel; some ROIs chosen based on SypHTm were excluded due to the background in the blue channel in order to avoid individually defining the background for each ROI. Nonsynaptic ROIs were defined by manually drawing processes as seen on all 3 channels, subtracting out any regions suspected to be synapses, and dividing the remainder into similarly sized ROIs. Additionally, only ROIs with a detectable SypHTm signal in normal Tyrode's solution were included because puncta that are only visible in NH4Cl are not necessarily synapses. For the purposes of defining nonsynaptic regions for quantification, all stationary SypHTm puncta were subtracted out. The somatodendritic regions were excluded, usually by choosing an imaging field without a transfected soma, due to high background and low prevalence of probable synapses compared to puncta visible only in NH4Cl. The values of all ROIs, including background, for each image (average NH4Cl, 4K, pH5.5 for SypHTm and pHluorin and stack average for BFP2) were exported to Microsoft Excel. The background was then subtracted, and then NH4Cl – 4K was used to calculate the internal protein and 4K – 5.5 was used to calculate the surface protein. For the purposes of quantification of APP in the synapses, only ROIs with a positive value for Total, Internal and Surface in the pHluorin and pHTm channels were included in the analysis. If the BFP2 signal was not higher than background, the ROI was also excluded. To avoid bias towards any field of view, an equal number of ROIs from each FOV was randomly selected and pooled. The n for each condition is the total number of pooled ROIs.

Kymographs were generated by manually tracing the processes using the Segmented Line tool in Fiji based on an averaged image of the BFP2 channel, using the "Reslice" command (Output Spacing = 1 pixel, Avoid interpolation). Paths of the moving puncta were traced by hand using the Segmented Line tool and saved to the ROI Manager. These selections were exported as XY coordinates with interpolation of 1 pixel. In order to be as accurate as possible, the actual time each image was taken was extracted and used to convert vertical pixel distances to time because the timing did not sync perfectly to the frame number across different fields of view. Because puncta sometimes split, appeared and disappeared, the n was determined separately at each time point for the purpose of calculating the mean and SEM. Puncta that disappeared were not counted as a zero but as a blank, while puncta that were still present but were not moving were included in the analysis. Synapses were determined using SypHTm puncta that did not move across the smaller number of frames collected of the channel. For each kymograph, the position of all synapses along the processes was listed on each spreadsheet page. Using Microsoft Excel's array functions, the closest synapse to the puncta at any given time point was selected from the list. When a punctum moving between two synapses A and B became closer to B than **A,** it was then considered to be moving in the positive direction towards the nearest synapse. The position of the puncta with respect to the soma was not considered for the purpose of this calculation because the experimental question was whether lateral movement toward or away from the synapse. There was no marker used in any live cell imaging that can separate axons from dendrites, so no claim is made about the

identity of the processes quantified. However, due to the distance from the soma needed to get lower backgrounds, the narrow and consistent width of the selected processes, and the expression pattern of SypHTm, they are most likely axons.

The analysis of **Figure 29** was performed differently because the size was the most important feature to be quantified, and hand drawn ROIs were therefore unsuitable. The images were also collected differently (detailed below). First, Convoluted Background Subtraction from the BioVoxxel Toolbox (http://imagej.net/BioVoxxel_Toolbox) was used, followed by Non-local Means Denoising [274, 275], bandpass filter, auto-local threshold using the Bernsen method, Adjustable Watershed (Michael Schmid) with a tolerance of 0.1. Using a macro, the same procedure was applied to all images and then debris were manually removed, non-static ROIs were excluded, and compounded ROIs that escaped the watershed were manually separated. The measure tool was then used to collect the data. All of the intensity values were taken from the original, unaltered images. During the collection of this data, multiple fields of view were observed from the same coverslip between solution changes using the Position List feature on Micro-Manager to return to the locations. 10 frames were collected from each channel at each field of view in each solution, aligned and averaged. To correct for cumulative photobleaching, values for NH4Cl and pH 5.5 were multiplied by arbitrary factors so that the quantification can still be performed. Furthermore, due to morphology changes over time during this extended imaging, the ROIs were manually moved as the processes moved based on the pHTm channel, which the other channels were aligned to. Additionally, due

to the high signal to noise ratio each ROI had its own background ROI defined by shifting all ROIs in the manager about 10 pixels over in the x and y directions and manually moving the background ROIs from there to the most suitable area with a similar background (for example, a transfected cell-free area on the same auto fluorescing flat glial cell as the synapse). After the background subtraction and arbitrary photobleach correction was equally applied to all conditions, ROIs were excluded as before for having below background signal in any of the channels. Because of this, it is difficult to compare the fluorescence results from this figure to other experiments in the paper directly. For this experiment, it was very important to select FOV without consideration to factors such as the size of the synapses, process health and morphology. Because fields of view were not chosen based on the quantity of synapses but rather on the presence of transfected punctated structures at all, ROIs were not randomly selected from each field of view and instead all were included and pooled.

ELISA

The Mouse/Rat sAPPα (highly sensitive) Assay Kit (IBL #27419) was used to measure the sAPPα concentration in the undiluted media. Serum-containing culture media was removed and replaced with 1mL of serum-free NeuroBasal media supplemented with 2 mM L-glutamine, 2% B27-supplement and 100 ng/mL BDNF. Treatments were applied during the media exchange. After 24-hour incubation, the media was

collected. Aβ40 was measured using SensoLyte® β-Amyloid (1-40) ELISA kits (AnaSpec). To achieve greater sensitivity for Aβ40 measurement, only 0.5 mL of media was added at time of treatment. Once collected, a protease inhibitor cocktail (Roche) was added to the samples to protect them while they were concentrated to 300 µL using an evaporator. All samples were aliquoted and frozen at -80°C if not used fresh and were only thawed once. After following the instructions provided with each kit, the plates were scanned using a GloMax Discover (Promega). A sigmoidal dose-response curve (constrained to bottom=0 because of subtraction of media-only blanks) was fit to the standards using Graphpad Prism 7.03 for Windows (Graphpad Software, La Jolla California USA, www.graphpad.com) and the curve was used to calculate the concentration of the samples. 2 technical replicates (2 wells) per biological replicate (media sample) were normalized to the vehicle (DMSO) control and averaged together before the three biological replicates were averaged for an n of 3. Samples slightly below background with a technical replicate slightly above background were treated as 0 rather than excluded.

Characterization of α-SI

We chose GI 254023X as our α-SI. Because it is selective for ADAM10 over ADAM17, we expected that alpha cleavage would still be possible but decreased [276, 277], but this approach is advantageous over broad-spectrum protease inhibitors because of minimal interference with other cellular processes. To our knowledge, this inhibitor has not been characterized before for efficacy in inhibiting the cleavage of APP, as it

is typically used in Notch research [276, 277], so we used ELISA to test 4 concentrations of inhibitor (**Figure 2**). We selected 1 μM for our experiments.

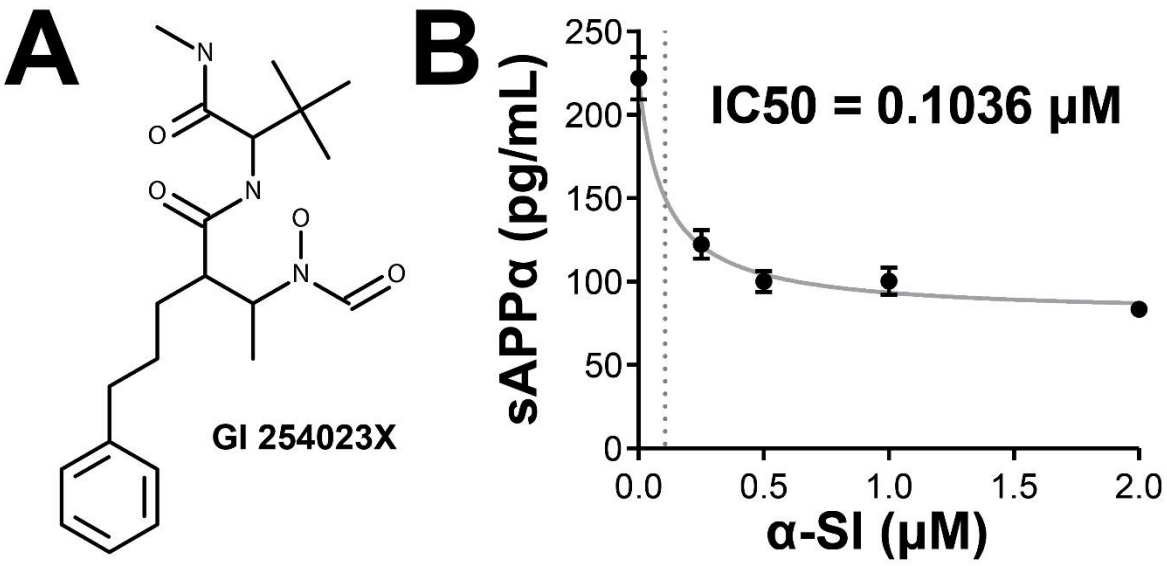

Figure 2: Characterization of a specific ADAM10 inhibitor (α-SI). A, Chemical structure of GI 254023X (generated by PubChem). **B,** dose response curve for α-secretase inhibitor (α-SI, i.e. GI 254023X), a highly specific ADAM10 inhibitor, based on sAPPα ELISA measurement. ADAM10 is thought to be the most relevant α-secretase (Kuhn et al., 2010). The nonlinear-fit was generated by Prism 7.03 with the constraint that IC50 > 0. Pearson's R^2 = 0.9127, IC50 = 0.1036 μM. 1 μM was chosen as the application concentration in all subsequent experiments. n = 4, 2 biological replicates with 2 technical replicates for each.

Confirmation of SI treatments

Based on selectivity, potency and usage reported in the literature, we selected β-secretase inhibitor II (i.e. CAS 263563-09-3) and Compound E (i.e. CAS 209986-17-4) to block β-secretase and γ-secretase respectively. Using ELISA assays for sAPPα and Aβ40, we determined that 24-hour incubation was sufficient for all three inhibitors, including the α-SI, inhibitors to take effect (**Figure 3**).

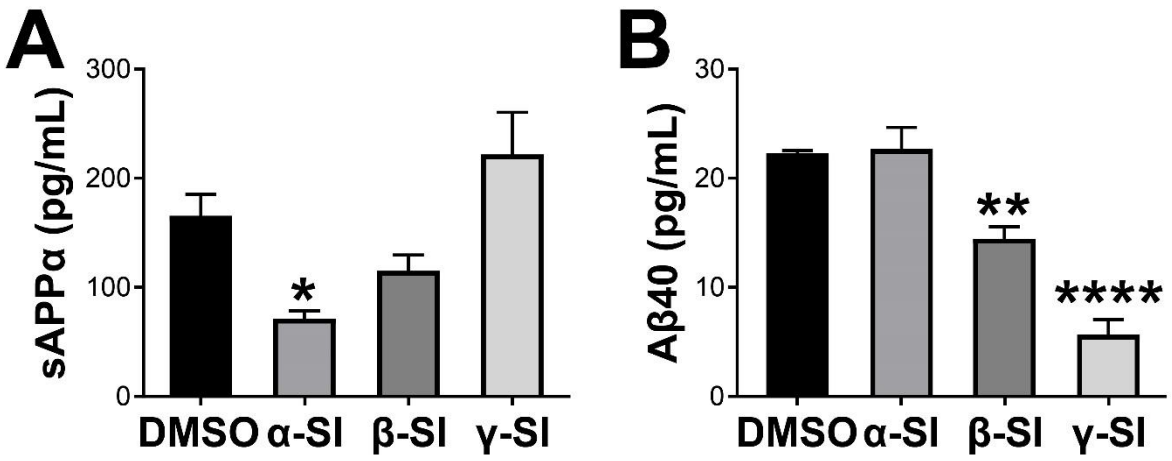

Figure 3: Secretase inhibitors significantly impair the cleavage of endogenous APP. **A,** the effect of α/β/γ-secretase inhibitors (α/β/γ-SIs) on sAPPα secretion according to its concentration in the culture media (one-way ANOVA: F (3, 20) = 7.8821, p = 0.0012). Dunnett's multiple comparisons test shows that only α-SI significantly decreases the secretion of sAPPα in comparison to DMSO control. For all four groups, N = 4, 2 biological replicates with 2 technical replicates for each; for α-SIs, *, p = 0.0241; for β-SI, p = 0.3086, for γ-SI, p = 0.2341. **B,** Aβ40 secretion is decreased by β-SI and γ-SI, while α-SI has no effect. One-way ANOVA detects significant variation (F (3, 20) = 36.046, p < 0.0001), and subsequent Dunnett's tests showed: p = 0.9939 for α-SI; **, p = 0.0014 for β-SI; ****, p = 0.0001 for γ-SI. All error bars represent SEM.

Statistical Analysis

Statistical tests were performed using Graphpad Prism 7.03. Each test is listed in the figure legends, but in general two-tailed *t*-tests were used to compare two conditions, one-way ANOVA and Dunnett's multiple comparisons test was used to compare the control condition to multiple other conditions, and two-way ANOVA and Sidak's multiple comparisons test was used to compare results within one variable in experiments with two variables.

Chapter III

APP TRAFFICKING AND LOCALIZATION IN PRIMARY NEURONS

Introduction

APP is well-known for its association with Alzheimer's disease, but in addition to its pathological connection, APP has been implicated in the development of neurons [216, 278], the maturation of synapses [218], the regulation of synaptic plasticity[5], and even the metabolism of cholesterol in the central nervous system (CNS) [252-255]. APP's various proteolytic pathways and different cleavage products underlie its diverse functions. One of the proteolysis pathways generates Aβ peptides, the major constituent of the amyloid plaques commonly found in AD patients' brains. Through decades of research, it is now clear that the different secretases and their proteolytic processing of APP are compartmentalized in different parts of cells, including the plasma membrane and the endosomal/lysosomal membrane. However, how newly synthesized APP arrives at those membrane compartments in synapses, neurites, and the soma of neurons remains understudied.

Early investigations using non-polarized cells and biochemistry methods reported that APP was first transported to the plasma membrane, where the majority was cleaved by α-secretase, and the remaining was internalized and cleaved by β-secretase [35, 45, 279]. However, this model of APP trafficking and cleavage has not been investigated

as thoroughly in the neurons of the CNS. Some reported that only a small fraction of neuronal APP reaches the plasma membrane [280]. Even if most APP is first transported to the plasma membrane before being cleaved, as shown in non-neuronal cells, there are still two different trafficking routes to follow: it can be sent to the somatodendritic plasma membrane right after synthesis and propagated along the neurite surface or it can be internalized and intracellularly transported to distal neurites before surface presentation. Evidence for both surface and intracellular transportation has been observed, but it remains unclear which is more prominent and more relevant to amyloidogenesis [281-283]. It is well demonstrated that a considerable amount of APP is cleaved by α-secretase, which is predominantly localized in the plasma membrane [45, 284]. Consequently, a shift of APP distribution from cell surface to intracellular membranes may result in an increase of amyloidogenic processing, a potential etiological factor in AD [285]. Accordingly, it has been shown that irregular APP trafficking, specifically an increase in intracellular retention [280] and a decrease in exportation to the plasma membrane [96, 266], cause increased Aβ production and therefore could contribute to more amyloidogenesis. Therefore, it is crucial to know if and how nascent APP is transported between surface and intracellular membranes and where it is processed by α-secretase.

Recently, Das et al. utilized fluorescent APP fusion proteins to illustrate the intracellular trafficking of nascent APP [286], which, along with a few other recent reports [243], has demonstrated the power of fluorescence live-cell imaging for studying APP in CNS neurons. Interestingly, they have shown that while a considerable

amount of newly synthesized APP co-localizes with BACE1 in the endoplasmic reticulum and Golgi at somatodendritic areas, they are then sorted into separate compartments before transport [286]. However, it has also been reported that APP can be co-transported with BACE1 without being cleaved [287], which illustrates the complexity of APP trafficking and processing in CNS neurons. These seemingly conflicting results demonstrate the need for further investigation of the APP trafficking and processing between surface and intracellular membranes. Furthermore, compared to β-cleavage, the subcellular location of α-secretase cleavage is drastically understudied. While most reports agree that α-cleavage occurs at the plasma membrane[158, 288], most studies have been performed in cell lines so it is not clear whether this occurs at the soma, axons, and/or dendrites.

Furthermore, Das et al. showed that APP and BACE1 converge upon stimulation in what they term acidic microdomains in the dendrites[286]. However, using similar methodology, Groemer et al. also showed that APP is cleaved in response to stimulation and the products are released by synaptic vesicles in the axons, although it is not clear there being cleaved by BACE1 [243]. Finally, the nature of the relationship between synaptic activity and APP trafficking is unclear.

Live-cell fluorescence imaging is the most practical option to resolve these issues as it offers adequate spatiotemporal resolution to deal with morphologically complex neurons. We started with an APP fusion protein with a pH-sensitive fluorescent protein at its N-terminal. It can measure surface and intracellular APP because of the pH gradient between extracellular space and intracellular compartments like

endosomes, lysosomes, and synaptic vesicles. We added a pH-insensitive BFP2 at its C-terminal to obtain an independent measurement of APP and its CTFs. Using it, we discovered that a considerable amount of nascent APP is trafficked to the surface at the soma and propagates to distal neurites along the neuronal surface. The APP in the plasma membrane is subject to removal by α-secretase cleavage and dynamin-dependent endocytosis. Our findings demonstrate that surface presentation and cleavage are major routes for newly synthesized APP in neurons.

Some of this chapter is reprinted (adapted) with permission from (DelBove, C. E., Deng, X., and Zhang, Q. (2018). The fate of nascent APP in hippocampal neurons: a live cell imaging study, *ACS Chemical Neuroscience*) [299]. Copyright (2018) American Chemical Society.

Validation of constructs

Ratiometric quantification of APP

We started with Groemer's pH-APP (gifted by the J. Klingauf lab) for several reasons. First, it is based on ratAPP695, matching our rat postnatal hippocampal culture. Secondly, its expression is driven by a human Synapsin 1 promoter (hpSynI), ensuring neuron-specific and moderate expression [289]. Thirdly, pHluorin was inserted near APP's N-terminal, right behind APP's short signaling peptide (SP), ensuring the same subcellular distribution pattern as native APP695 [243, 288]. The pH-sensitive pHluorin located in APP's ectodomain exhibits an increase in fluorescence increase or a

decrease during APP externalization or internalization respectively [243] because intracellular membrane compartments like synaptic vesicles and lysosomes are often acidic (pH5.5~6.5), whereas extracellular pH is generally neutral (pH7.35). However, using pHluorin alone has some limitations. First, it does not allow us to track intracellular APP since pHluorin is quenched in the acidic lumen. Second, N-terminal cleavage by α-secretase or β-secretase detaches pHluorin, yielding non-fluorescent CTFs. Third, a high concentration (e.g. 50 mM) of NH_4Cl is needed to unquench all intracellular APP for quantification [243, 290]. However, high concentration NH_4Cl significantly alters neuronal membrane properties and synaptic activity [291], such that total APP and CTFs cannot be continuously monitored while keeping neurons physiologically normal. We reasoned that adding a pH-insensitive fluorescent protein like BFP2 to APP's cytosolic domain (i.e. C-terminal) should address those issues because it provides an independent and persistent fluorescent signal for APP and CTFs. Previous studies have shown that an APP fusion protein with fluorescent proteins at both terminals behaves the same as endogenous APP. For example, Villegas et al. showed that dual-tagged APPs (i.e. CFP-APP-YFP and FLAG-APP-Myc) were the same as endogenous APP in terms of intracellular distribution and transportation [292]. Hence, we attached BFP2 (gifted by Yulong Li) to pH-APP's C-terminal to generate pH-APP-BFP2.

To independently visualize synapses and synaptic activity in the same neurons, we inserted Synaptophysin-pHTomato (SypHTm, also gifted by Yulong Li) [267] and a "self-cleavage" oligopeptide (T2A) [293] in front of the pH-APP-BFP2 (**Figure 4A**). By so

doing, the SypHTm is co-expressed with pH-APP-BFP2 and post-translationally separated.

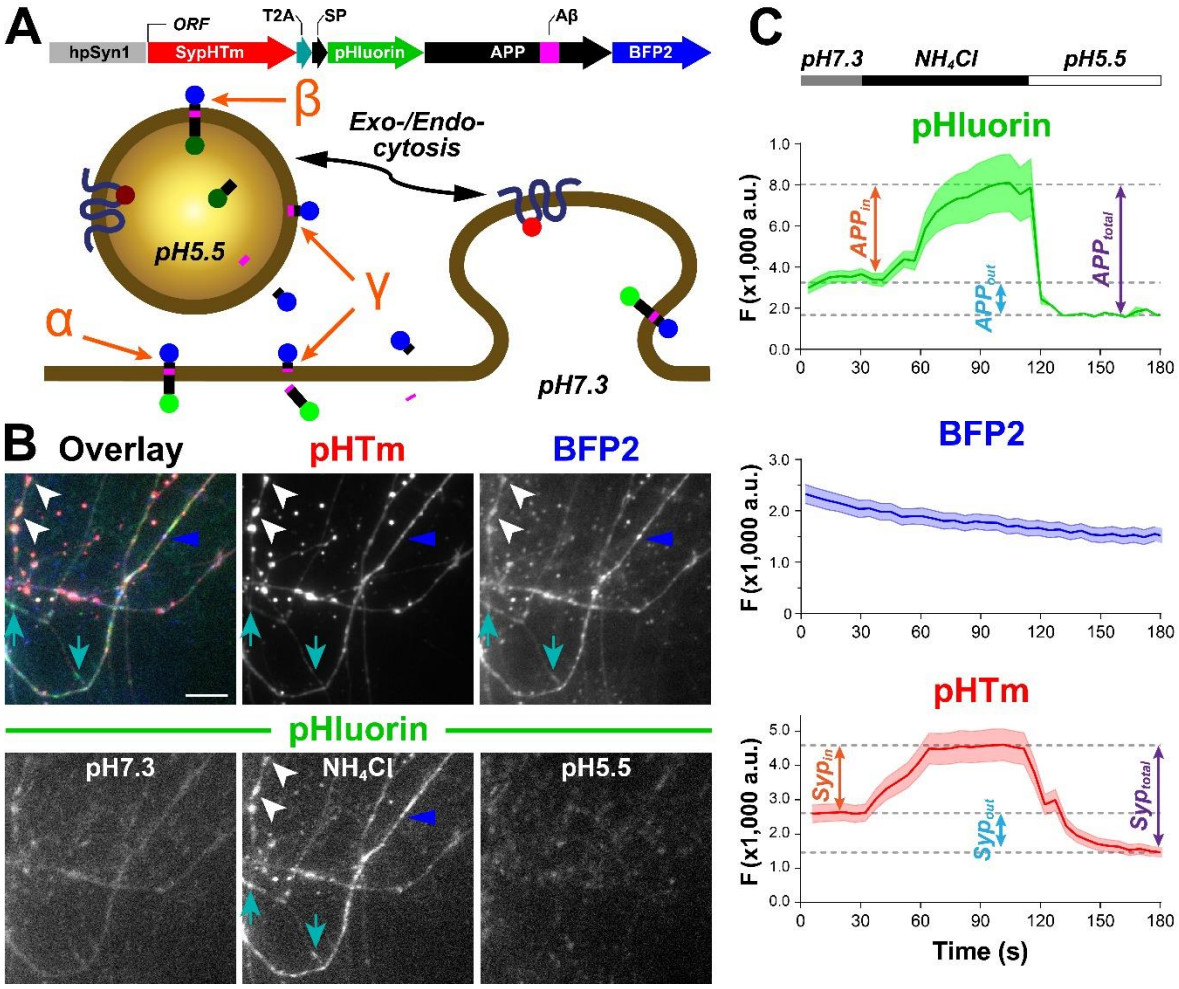

Figure 4. SypHTm:T2A:pH-APP-BFP2 reports APP distribution and marks synaptic vesicles. A, top diagram illustrates the components of SypHTm:T2A:pH-APP-BFP2 including the human Synapsin I promoter (hpSyn1) and an open reading frame (ORF) comprised of Synaptophysin-pHTomato (SypHTm), *thosea asigna* virus 2A peptide (T2A), APP signal peptide (SP), pH-sensitive green fluorescent protein (pHluorin), APP containing Aβ, and blue fluorescence protein 2 (BFP2). The lower cartoon demonstrates how extracellular pH and exo-/endocytosis affect pHluorin and pHTm fluorescence and how α-, β-, and γ-secretases cleave pH-APP-BFP2. **B,** top left, overlay of SypHTm (red), pHluorin (green) in 50 mM NH4Cl, and BFP2 (blue); top middle, SypHTm in 50 mM NH4Cl; top right, averaged BFP2 throughout the course of the experiment; bottom: pHluorin in normal Tyrode's solution (pH7.3), in 50 mM NH4Cl, and in pH5.5 Tyrode's solution. White arrowheads indicate synaptically co-localized SypHTm and pH-APP-BFP2, cyan arrows indicate non-synaptic pH-APP-BFP2, and the blue arrowheads indicate nonsynaptic CTF because of strong BFP2 and weak pHluorin signals. Scale bar, 10 µm. **C,** example of intensity

changes of pHluorin, BFP2 and pHTm fluorescence in one FOV (field of view) containing 39 ROIs (regions of interest) during sequential applications of pH7.3 Tyrode's solution, 50 mM NH4Cl and pH5.5 Tyrode's solution. Double-ended arrows indicate the calculations of surface, intracellular and total APP and Syp based on fluorescence intensity differences. Shadows show the SEM.

To visualize neurites and synapses with fluorescence microscopy, we used a modified transfection protocol [294] to achieve 10-30% expression in synaptically mature hippocampal cultures (i.e. DIV12-18), yielding sparsely labeled neurons, neurites and synapses. Fluorescence images showed that pHTm was more punctated whereas BFP2 and pHluorin were more diffused in the neurites (**Figure 4B, Figure 5**), consistent with the notion that Syp is a synaptic vesicle-specific protein whereas APP is not. We also observed that most pHTm puncta were overlapped with BFP2 and pHluorin (white arrowheads in **Figure 4B**) but not the other way around (cyan arrows in **Figure 4B**), suggesting APP and CTFs are more ubiquitously distributed across neurites than vesicular proteins. There were puncta with strong BFP2 and weak pHluorin fluorescence (blue arrowhead in **Figure 4B**), reflecting membrane compartments enriched with CTFs but not APP.

Next, we asked if the membrane orientation of SypHTm and pH-APP-BFP2 was correct (i.e. pHTm and pHluorin should be located extracellularly and/or luminally). To do so, we applied 50mM NH_4Cl to deacidify all intracellular membrane compartments, followed by pH5.5 buffer to quench all pHTm or pHluorin [291]. We observed significant pHTm and pHluorin fluorescence increase and decrease during 50mM NH_4Cl and pH5.5 treatments respectively (**Figure 4B&C**), which demonstrates the luminal localization of pHTm and pHluorin and thus the correct

transmembrane conformations of both fusion proteins. Expectedly, BFP2 fluorescence was very stable except for gradual decay as a result of photobleaching (**Figure 4C**). Hence, we can calculate the total pHluorin or pHTm fluorescence by subtracting the baseline fluorescence (at pH5.5) from the maximum fluorescence (at 50mM NH_4Cl), the surface/out pHluorin or pHTm fluorescence by subtracting the baseline fluorescence (at pH5.5) from the pretreatment fluorescence (at pH7.3), and the intracellular/in pHluorin or pHTm fluorescence by subtracting the pretreatment fluorescence (at pH7.3) from maximum fluorescence (at 50mM NH_4Cl) (**Figure 4C**). Unlike pHluorin, pHTm is only partially quenched at pH5.5, allowing us to identify expressing neurons, neurites and individual synapses without the use of NH_4Cl [267].

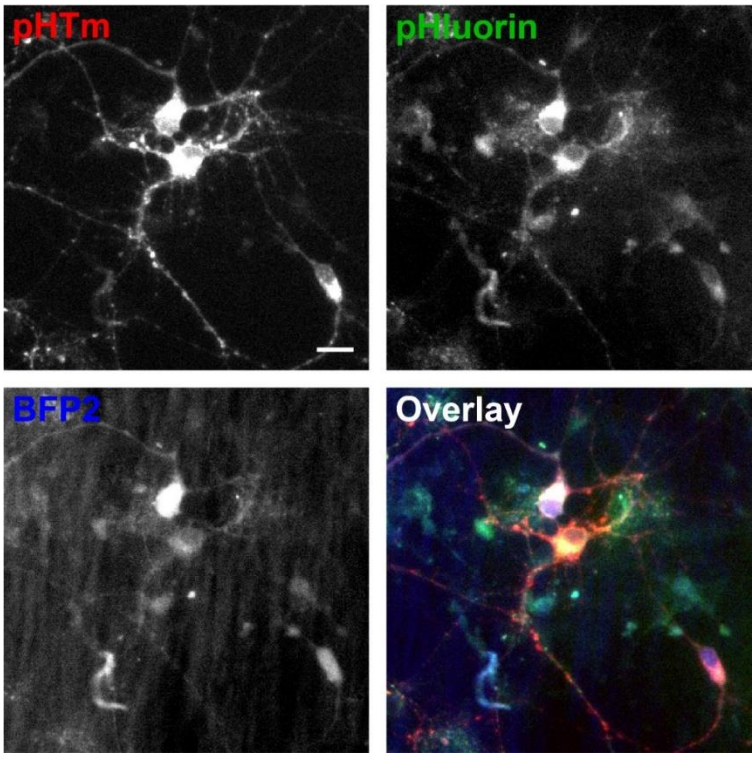

Figure 5: Example images showcasing the expression of SypHTm and pH-APP-BFP2 at multiple processes. These images show a single field of view containing multiple

transfected neurons in all 3 channels in NH4Cl, demonstrating the variety in expression in the somas. Scale bar, 50 μm.

Localization

We used object-based colocalization to determine if APP is preferentially located in the synapses. Object-based colocalization greatly reduces the false positive rate typically seen in correlation analysis methods based on intensity values. We performed an immunocytochemistry experiment using Synaptotagmin I (SytI), a synaptic vesicle specific protein, and paired GFP and mCherry antibodies with green and red fluorophore-tagged secondary antibodies, respectively, so that any residual fluorescence from the protein tags would only show up in an appropriate channel. We confirmed that SypHTm was mostly synaptic, whereas pH-APP-BFP2 was more diffused across the neurons (**Figure 6**). **Figure 6A** shows clearly that pH-APP-BFP2 puncta overlap much less with Syt1 puncta. Although there are a similar number of pH-APP-BFP2 and SypHTm puncta (**Figure 6B**), we determined that nearly twice as many SypHTm puncta were positive for SytI (**Figure 6C**). The localization of pH-APP-BFP2 is clearly not typical of a synaptic vesicle-specific protein.

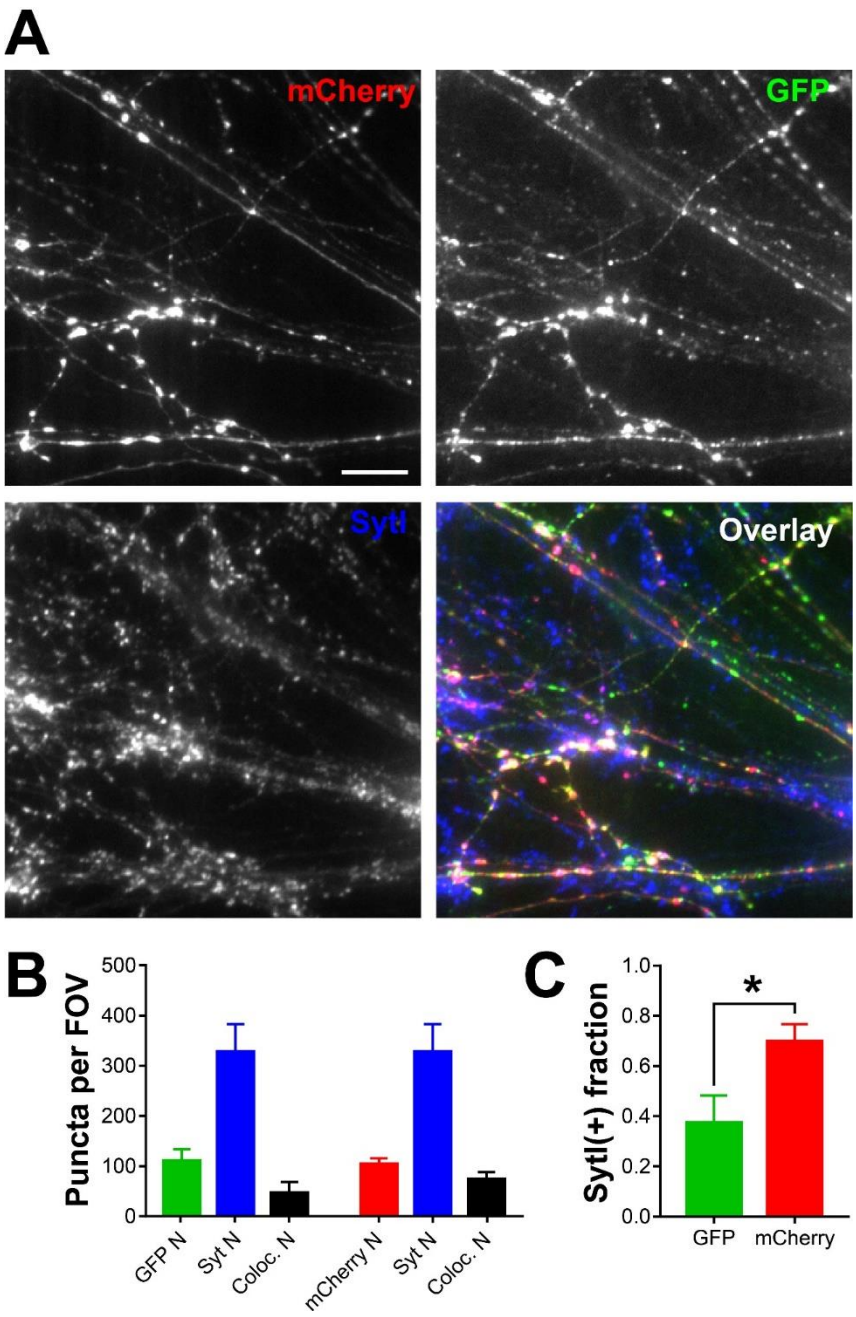

Figure 6. SypHTm is more colocalized with Synaptotagmin I than pH-APP-BFP2. A, sample images of immunocytochemistry performed on transfected cells using anti-mCherry (against pHTm, an mCherry derivative), anti-GFP (against both pHluorin and BFP2) and anti-Synaptotagmin I (Syt). Scale bar, 10 µm. **B,** object-based colocalization was performed using the *Synapse Counter* plug-in for ImageJ [295]. The graph shows the average numbers of puncta per field of view (FOV). The number of Synaptotagmin I-positive puncta is much greater than the number of mCherry and GFP-positive puncta because the majority of neurons, and therefore synapses, are untransfected. Error bars are SEM. and N = 3 FOVs. This colocalization analysis is likely an overestimate for synaptic pH-APP-BFP2 because membrane permeabilization during immunostaining caused loss of the plasma membrane

proteins like pH-APP-BFP2. **C,** the fraction of SytI-positive mCherry puncta is significantly higher than the fraction of SytI-positive GFP puncta (two-tailed paired *t*-test; *, $p = 0.0160$), although SypHTm and pH-APP-BFP2 are cotranslated from the same open reading frame. Error bars are SEM.

However, the surface fraction of SypHTm should therefore be lower than the surface fraction of pH-APP-BFP2. A combination of different but known factors resulted in a higher pHTm surface fraction in our high magnification data sets only that were not corrected for because of the risk of introducing additional error. Due to the incomplete quenching of pHTm, SypHTm experienced more photobleaching at high magnification (e.g. 100x), causing an overestimate of the surface fraction of SypHTm (the pretreatment fluorescence was always imaged first by definition and NH_4Cl application for total fluorescence was always the last [291]). Notably, this phenomenon was less severe at low magnification (e.g. 20x) due to significantly less illumination (**Figure 7A**). We therefore used low magnification images and found that surface pHluorin fraction was significantly more than surface pHTm fraction, while the intracellular pHluorin fraction was significantly less at the synapses (**Figure 7B**). At non-synaptic regions of the neurites, the trend remained but the difference was no longer statistically significant likely due to the lack of synaptic vesicles in neurite shafts (**Figure 7B**). Hence, we conclude that SypHTm and pH-APP-BFP2 distributed independently, matching their endogenous counterparts.

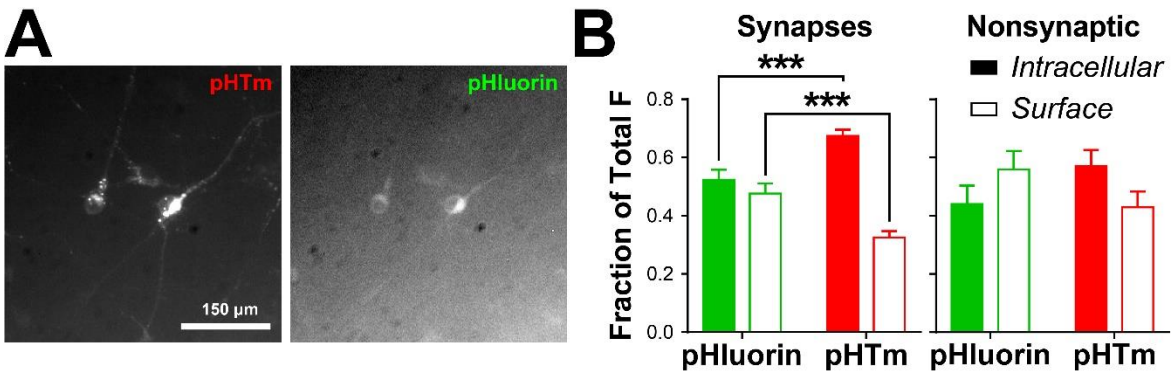

Figure 7: Surface fraction of pHluorin is higher than pHTm. A, Sample images of pHTm and pHluorin at 20x in 4K. Scale bar, 150 µm. **B,** quantification of intracellular (solid bars) and surface (open bars) pHluorin (green) and pHTm (red) fluorescence at synapses (left) and nonsynaptic areas (right). There was a significant difference between pHTm and pHluorin regarding surface or intracellular fractions according to a two-tailed paired *t* test (***, $p = 0.001$). No significant difference was found for the nonsynaptic ROIs (two-tailed paired t-test, ns, $p = 0.0543$). Synaptic ROIs, n = 47; nonsynaptic ROIs, n = 23. All error bars represent SEM.

Next, we asked if the dual-tagged pH-APP-BFP2 has the same distribution pattern in neuronal processes as endogenous APP. For reliable comparison, we performed fluorescent immunostaining for both endogenous APP and exogenously expressed pH-APP-BFP2 using an anti-APP antibody (recognizing APP's N-terminus) and an anti-GFP antibody (recognizing pHluorin) respectively. In addition, MAP2 immunostaining was used to identify dendrites, and Synapsin I immunostaining was used to identify synaptic boutons and axons bearing those boutons (**Figure 8A**). The amount of endogenous or exogenous APP in the synapses, axonal shafts, and dendritic shafts was normalized to total APP in the corresponding neurites. We found that endogenous APP and pH-APP-BFP2 were very similar in terms of their distributions in axon, dendrite and synaptic boutons — more in synaptic boutons, less in dendritic

shafts and the least in axon shafts (**Figure 8B**), clearly correlated to the total amount of surface and intracellular membranes in those subcellular structures.

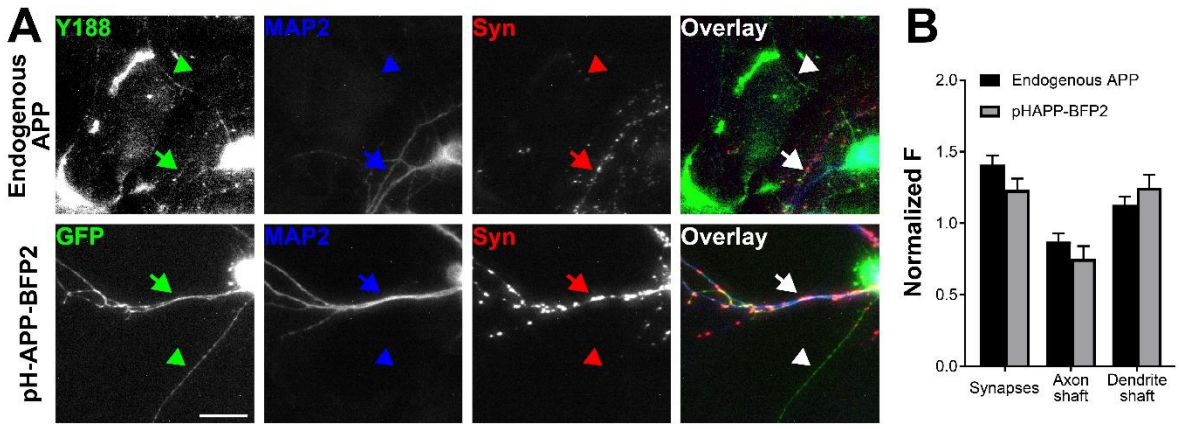

Figure 8. pH-APP-BFP2 is distributed in the same way as endogenous APP is. A, sample images of immunofluorescence labeling of untransfected (top) and transfected cells (bottom). The Y188 antibody was used to detect endogenous APP (green), and anti-GFP antibody was used to detect transgenically expressed pH-APP-BFP2 (green). Anti-MAP2 antibody was used to identify dendrites (arrows) and thin neurites with low expression of MAP2 (arrowheads). Anti-Syn was used to identify synaptic boutons. Scale bar, 100 μm. **B,** normalized average APP fluorescence in synaptic boutons, axon shafts and dendritic shafts, normalized to the average fluorescence of the whole processes. Two-way ANOVA detected a significant effect of localization at synapses, axonal shafts and dendritic shafts ($F(2, 30) = 25.29$, $p < 0.0001$). There was no significant difference between pH-APP-BFP2 and endogenous APP ($F(1, 30) = 0.9346$, $p = 0.3414$) and no interaction between the two factors ($F(2, 30) = 2.256$, $p = 0.1223$).

Next, we tested if pH-APP-BFP2 recapitulates endogenous APP in terms of its surface and intracellular distribution and cleavage in the soma specifically. To do so, we conducted live-cell imaging of pHluorin, BFP2, and pHTm and immunostaining of endogenous APP in parallel. To study nascent APP, we focused on the soma where APP is synthesized. The total APP (i.e. $pHluorin_{total}$) is calculated by the difference in pHluorin fluorescence between NH_4Cl-containing and pH5.5 Tyrode's solutions, the surface APP (i.e. $pHluorin_{out}$) by the difference between normal and pH5.5 Tyrode's solutions, and the intracellular APP ($pHluorin_{in}$) by the difference between NH_4Cl-

containing and normal Tyrode's solutions. To mitigate the variation of protein expression among different cells, we calculated the surface and intracellular APP as fractions of the total APP (i.e. pHluorin out/total and pHluorin in/total respectively). Furthermore, we estimated the ratio of holo-APP (uncleaved full length APP) vs. both APP and its CTFs by $pHluorin_{total}$/BFP2, which is influenced by the secretase-mediated cleavage of pH-APP-BFP2. Our data showed that a considerable amount of pH-APP-BFP2 resides on the surface membrane at the soma, as shown by sample images in **Figure 9A** and plots in **Figure 9B**. Next, we used three separate anti-APP primary antibodies to detect endogenous APP. We labeled surface APP with one antibody selectively recognizing APP's N-terminal epitope before cell membrane permeabilization, detected total APP with a second antibody specifically against APP's ectodomain different from the previous one, and measured total APP as well as any CTFs with a third antibody highly selective to a C-terminal epitope. All antibody information can be found in **Table 1**, and the latter two antibodies were applied after cell membrane permeabilization in order to label intracellular APP. Consistently, our triple immunostaining and quantitative fluorescence imaging of endogenous APP supported our live-cell imaging results (**Figure 9C&D**). Notably, the difference between $pHluorin_{total}$/BFP2 (via live cell imaging) and APP N/C (via immunostaining) was most likely caused by technological differences like BFP2 fluorescence and immunolabeling efficacy, which makes it inappropriate to directly compare to the fraction of pHluorin out/total. Nevertheless, together these two sets of results suggest that at least one third of APP is directly transported to the plasma membrane after

synthesis. To confirm if the pH-APP-BFP2 faithfully represents the trafficking and processing of endogenous APP, we blocked α-secretase using a selective inhibitor (GI 254023X) [276, 296]. As expected, this manipulation significantly increased holo-APP measured by both live-cell and immunofluorescence imaging (i.e. augments in $pHluorin_{total}$/BFP2 and APP-N_{total}/APP-C) (**Figure 9**), confirming that pH-APP-BFP2 is cleaved like endogenous APP. Although we predicted that blocking α-secretase would increase surface APP, we observed decreases in both the surface fractions of pH-APP-BFP2 and the ratio of out vs total endogenous holo-APP (**Figure 9**), although the result was not significant in the former (likely due to the large variance of autofluorescence as well as expression from neuronal somas, as seen in **Figure 5**). Nevertheless, the similarity in the direction and the degree of change (28% vs. 46% decrease via live cell imaging and immunostaining, respectively) vindicated our conclusion. In fact, previous studies about APP trafficking in non-neuronal cells have suggested that the amount of cell surface APP is strictly regulated to prevent aberrant increase[199, 262, 297, 298]. Our results from the two different methods suggest that surface APP spared by α-SI was mostly internalized, which is in good agreement with the idea that cell surface APP is homeostatically regulated. Furthermore, the consistency between the two different sets of results validated that pH-APP-BFP2 offers a reliable representation of endogenous APP.

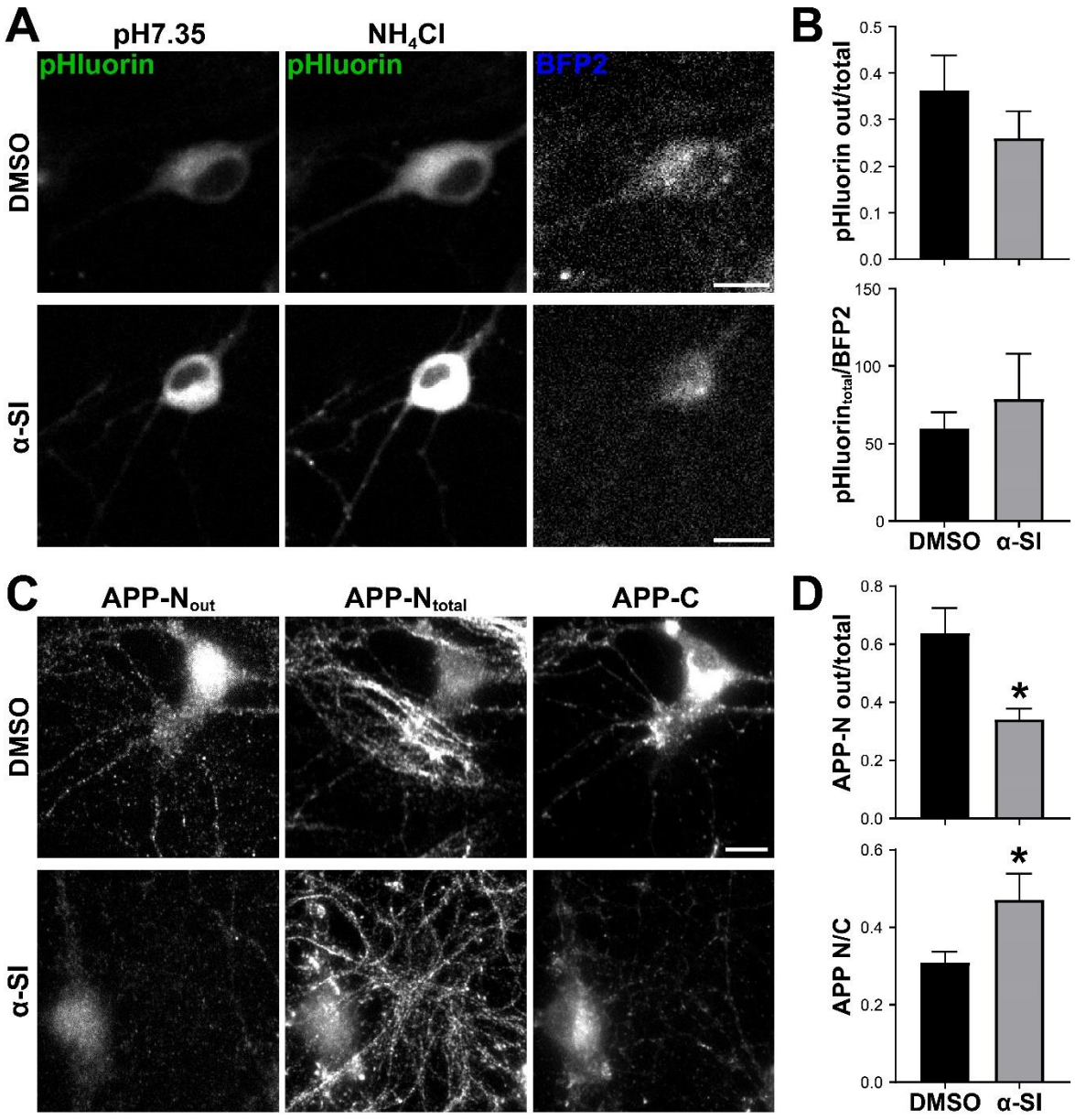

Figure 9. Fluorescence analysis of surface and intracellular membrane APPs. A, Sample pHluorin images for two pH conditions, and BFP2 images. Cultures were treated by DMSO control or α-secretase inhibitor (α-SI). Images depicted are background-subtracted. Scale bars, 50 µm. **B,** The average soma surface fraction of pHluorin (pHluorin out/total), and total pHluorin vs. BFP2 ($pHluorin_{total}$/BFP2) after DMSO and α-SI treatments. Surface vs total pHluorin was decreased by 28.1% in the α-SI group. However, an unpaired, two-tailed *t*-test failed to detect significance ($p = 0.2966$). Total pHluorin vs. BFP2 was increased by 32.0% in α-SI group, which also fails to reach significance (unpaired, two-tailed *t*-test, $p = 0.6137$). For DMSO, n = 6 and for α-SI, n = 9, where n is the number of somas. **C,** Sample images of triple immunofluorescence labeling for surface APP ($APP\text{-}N_{out}$), total APP ($APP\text{-}N_{total}$) and APP C-terminal (APP-C) after DMSO and α-SI treatments. Images depicted are background-subtracted. Scale bars, 50 µm. **D,** The average soma immunofluorescence ratios

of surface vs. total APP (APP-N out/total), and total APP N vs. C-terminals (APP N/C) after DMSO and α-SI treatments. Surface vs total APP was significantly decreased by application of α-SI according to an unpaired, two-tailed *t*-test (*, $p = 0.0152$). Total APP-N vs. APP-C was significantly increased by application of α-SI (unpaired, two-tailed *t*-test, *, $p = 0.0397$). For DMSO, n = 6 and for α-SI, n = 5, where n is the number of somas. Reprinted (adapted) with permission from (DelBove, C. E., Deng, X., and Zhang, Q. (2018) The fate of nascent APP in hippocampal neurons: a live cell imaging study, *ACS Chemical Neuroscience*)[299]. Copyright (2018) American Chemical Society.

Cleavage

We also asked if pH-APP-BFP2 was proteolytically processed like endogenous APP to ensure that it is a fair reporter of both localization and cleavage. Based on the inhibitors' selectivity, potency and usage reported in the literature, we selected GI 254023X, β-secretase inhibitor II (i.e. CAS 263563-09-3) and Compound E (i.e. CAS 209986-17-4) to block α-secretase, β-secretase and γ-secretase respectively. Since α-secretase and β-secretase release APP's N-terminal ectodomain including pHluorin whereas γ-secretase releases the cytosolic C-terminal domain including BFP2, these secretase inhibitors should alter N *vs.* C terminal ratio or total pHluorin *vs.* BFP2 ratio. For endogenous APP, we performed fluorescence immunostaining using antibodies selective for APP's N- and C-terminals (22C11 and Y188 respectively) (**Figure 10A**). As expected, immunofluorescence analyses showed that both α-secretase and β-secretase inhibition increased the N/C ratio for endogenous APP at synaptic boutons marked by Syp whereas γ-secretase inhibition decreased the ratio (**Figure 10B**). For pH-APP-BFP2, we conducted live cell imaging to measure total pHluorin *vs.* BFP2 ratio while using the SypHTm signal to identify synaptic boutons (**Figure 10C**). Again, live cell imaging showed that the changes of this ratio was very similar to the changes

of N/C ratio from the immunostaining of endogenous APP (**Figure 10D**). Notably, the fluorescent signals from the live cell imaging are more discrete than those from immunostaining, mostly owning to the neuron-specific gene expression, which makes the difference among the four groups more significant. This is further supported by the results from non-synaptic regions, in which the total pHluorin vs. BFP2 ratios are very similar to those of synaptic regions (**Figure 11**). Therefore, all of our comparisons between endogenous APP and exogenous pH-APP-BFP2 demonstrate that despite the extra fluorescent proteins at both ends, pH-APP-BFP2 exhibits the same membrane orientation, subcellular distribution, and proteolytic processing as those of endogenous APP.

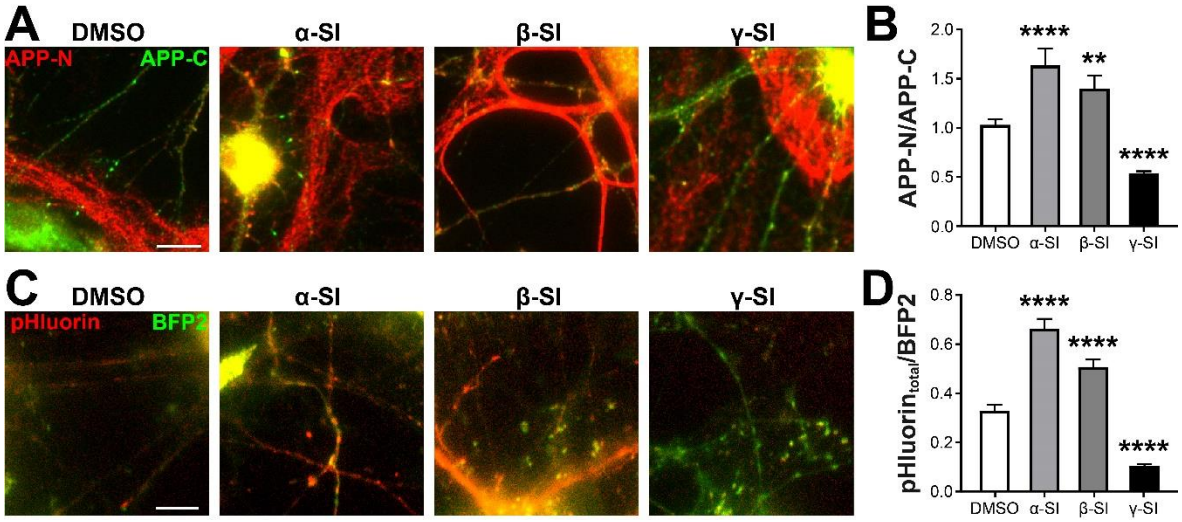

Figure 10. pH-APP-BFP2 is cleaved in the same way as endogenous APP is. A, sample images of immunofluorescence labeling for APP N- and C-terminals with and without secretase inhibitors (α/β/γ-SI). Scale bar, 50 μm. **B,** one-way ANOVA detected significant differences in the endogenous APP N/C ratio after α/β/γ-SI treatments ($F(3, 380) = 44.153$, $p < 0.0001$). Dunnett's multiple comparisons test showed that α/β-SI increased the ratio compared to DMSO (****, $p = 0.0001$; and **, $p = 0.0014$, respectively). γ-SI significantly decreased the ratio (****, $p = 0.0001$). DMSO, n = 160; α-SI, n = 21; β-SI, n = 38; γ-SI, n = 165, where n is the number of Syp-positive puncta (i.e. synaptic boutons). **C,** sample images of live cell imaging for total pHluorin (for APP's N-terminal, red color) and total BFP2 (for APP's C-terminal, green color) after α/β/γ-SI treatments. Scale bar, 10 μm. **D,**

pHluorin/BFP2 ratio after SI treatments. One-way ANOVA detected a significant effect ($F(3, 499) = 98.199$, $p < 0.0001$) and Dunnett's multiple comparisons test showed that α-SI and β-SI both increased the ratio compared to DMSO (****, $p = 0.0001$; ****, $p = 0.0001$) while γ-SI decreased it (****, $p = 0.0001$). DMSO, n = 132; α-SI, n = 126; β-SI, n = 80; γ-SI, n = 165, where n is the number of ROIs corresponding to Syp-marked synaptic boutons. All error bars represent SEM.

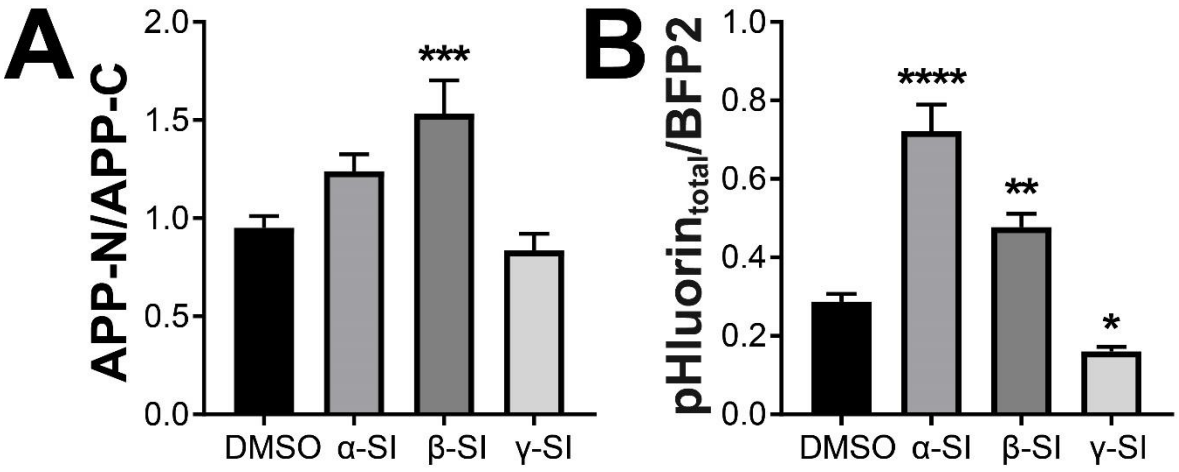

Figure 11. Effect of secretase inhibitors on nonsynaptic N/C-APP ratio. A, one-way ANOVA detected significant differences in the N/C ratio of endogenous APP after inhibitor treatments: $F(3, 533) = 7.64831$, $p = 0.000052$. Dunnett's multiple comparisons test showed that β-SI increased this ratio in comparison to DMSO control (***, $p = 0.000558$) in the nonsynaptic regions, while α-SI and γ-SI failed to cause a significant change ($p = 0.111772$ and 0.507811, respectively). n = 254 for DMSO, 62 for α-SI, 51 for β-SI, 170 for γ-SI, where n is the number of nonsynaptic regions taken from multiple fields of view from a single biological replicate (except DMSO – two slides were imaged). **B,** average total pHluorin *vs.* BFP2 ratio after four different treatments. One-way ANOVA detected a significant effect ($F(3, 743) = 50.2176$, $p < 0.0001$) and Dunnett's test showed that α-SI or β-SI treatment significantly increased the ratio compared to DMSO (****, $p = 0.0001$, **, $p = 0.0031$ respectively) while γ-SI significantly decreased it (*, $p = 0.0148$). DMSO, n = 209; α-SI, n = 175; β-SI, n = 107; γ-SI, n = 256, where n is the number of nonsynaptic ROIs. All error bars represent SEM.

Results

Nascent APP in live neurons

Dual-fluorescence tagging of APP combined with long-term live-cell imaging provides us a unique opportunity to investigate the fate of nascent APP. This is an

important research topic because APP has been widely implicated in neuronal survival[216], axon growth and pruning[214], and synaptogenesis[218], and because the disruption of these functions is linked to AD[27]. Here, we mounted hippocampal cultures in a weather-controlled station immediately after transfection, and continuously monitored the fate of newly expressed pH-APP-BFP2 as well as SypHTm by time-lapse imaging of pHluorin, BFP2, and pHTm for up to 24 hours (**Figure 12A&B**). Notably, pHluorin signal largely represented pH-APP-BFP2 residing in the plasma membrane because pHluorin is nearly completely quenched in acidic intracellular membrane compartments[300]. We observed that: (1) pHluorin and BFP2 signals appeared nearly simultaneously at 5 hours after transfection, whereas pHTm signal came up a couple of hours later likely due to the longer maturation time for pHTm[267, 301, 302] (**Figure 12C-E**); (2) while neuronal nuclei remained relatively pHluorin- and pHTm-free during imaging, BFP2 showed up in nuclei a few hours after its cytosolic appearance, which likely represents the nuclear entrance of the AICD [224]; (3) only the pHluorin signal exhibited a transient increase followed by a partial decrease at the soma (**Figure 12C-E**); (4) BFP2 fluorescence began to level off after 10 hours whereas pHTm fluorescence continued to rise for at least 20 hours (**Figure 12D&E**); (5) the ratio of pHluorin to BFP2 peaked, then declined, first in the soma, then in the immediately proximal stretch of neurites, and then further down to distal neurites (**Figure 12F**); (6) in a larger, separate data set (DMSO controls in **Figure 13B**), at the soma, pHluorin/BFP2 was 1.662 ± 0.284 (n = 7) during the 8-10th hour period, significantly higher than that of 4-6th hour period (0.967 ± 0.071, n = 7;

Tukey's multiple comparisons test, $p = 0.0205$) and that of 16-18th hour period (0.853 ± 0.134, n = 4; Tukey's multiple comparisons test, $p = 0.0214$). These observations indicate that, unlike synaptic vesicle proteins such as Synaptophysin (i.e. SypHTm), (a) a substantial amount of nascent APP is first transported to the surface of the soma; (b) APP transportation to the plasma membrane eventually reaches an equilibrium; (c) APP in the plasma membrane propagates to distal neurites via lateral diffusion, although the possibility of additional transportation via intracellular cargo vesicles cannot be excluded; and (d) APP in the plasma membrane is continuously removed while moving along the plasma membrane. Given pHluorin's N-terminal position and pH-sensitivity, two mechanisms can be in play for such removal: endocytosis-mediated APP internalization, N-terminal cleavage by α-secretase, or both.

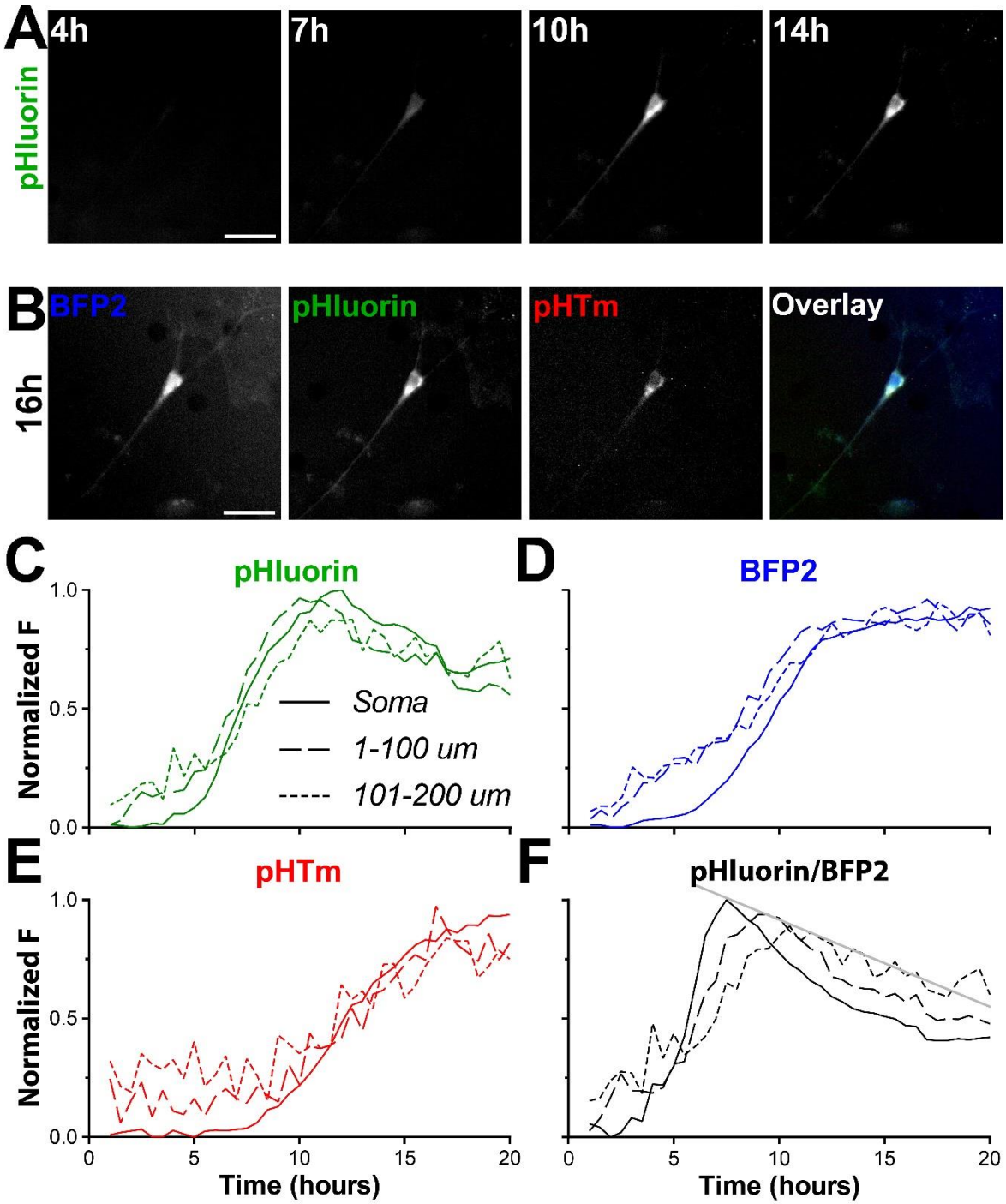

Figure 12. Surfacing and propagation of nascent APP at the soma. A, Snapshots of pHluorin fluorescence from a time-lapse video started after transfection. Scale bar, 100 µm. **B,** Sample images of pHluorin, BFP2, pHTm and overlay at 16 hours after transfection. Scale bar, 100 µm. **C-E**, Normalized fluorescence changes of pHluorin, BFP2, and pHTm at the soma and at 1-100 and 101-200 µm from the neuronal soma over time. **F,** Normalized ratio of pHluorin vs. BFP2 fluorescence at the soma and at 1-100 and 101-200 µm from the soma over time. The gray solid line illustrates that the peak is earlier in ROIs closer to the soma.

For **C-F**, 3 processes divided into two segments, which are 1-100 and 101-200 μm away from the soma, are averaged). Reprinted (adapted) with permission from (DelBove, C. E., Deng, X., and Zhang, Q. (2018) The fate of nascent APP in hippocampal neurons: a live cell imaging study, *ACS Chemical Neuroscience*)[299]. Copyright (2018) American Chemical Society.

To evaluate the contribution of those two mechanisms, we pharmacologically inhibited endocytosis or α-secretase activity. For the former, we inhibited dynamin because almost all endocytosis is dynamin-dependent. We chose Dyngo-4a, which is six times more potent than the popular Dynasore and does not interfere with dynamin-independent membrane trafficking [303]. Using long-term time-lapse imaging, we found that Dyngo-4a eliminated the decrease of pHluorin/BFP2 ratio with little effect on the transient increase and that the ratio reached a steady state at around 12 hours after transfection (**Figure 13A**). Notably, this ratio during the steady state was significantly higher than that of DMSO control (**Figure 13B**). This result suggested that endocytosis-mediated APP internalization contributes to the homeostatic regulation of APP in the plasma membrane. To study the contribution of α-secretase, we applied the previously tested α-SI. In contrast to Dyngo-4a, the inhibitor reduced the transient increase of pHluorin/BFP2 ratio, and it reached equilibrium earlier than the other two conditions (**Figure 13A**). Notably, the ratio at the steady state was similar to that of the DMSO control (**Figure 13B**). To test if either of the two mechanism(s) is generic to any neuronal membrane proteins, we analyzed the change of SypHTm. Unlike pH-APP-BFP2, SypHTm signal exhibited continuous increase up to the end of the long-term imaging, and this increase was not affected by either drug (**Figure 13C**). Based on the outcomes of the two pharmacological

interventions, we conclude that both dynamin-dependent endocytosis and α-secretase cleavage contribute to the homeostatic control of surface APP. Between the two mechanisms, the former is responsible for the internalization of excessive APP, whereas α-secretase has little effect in determining the amount of plasma membrane APP at steady state.

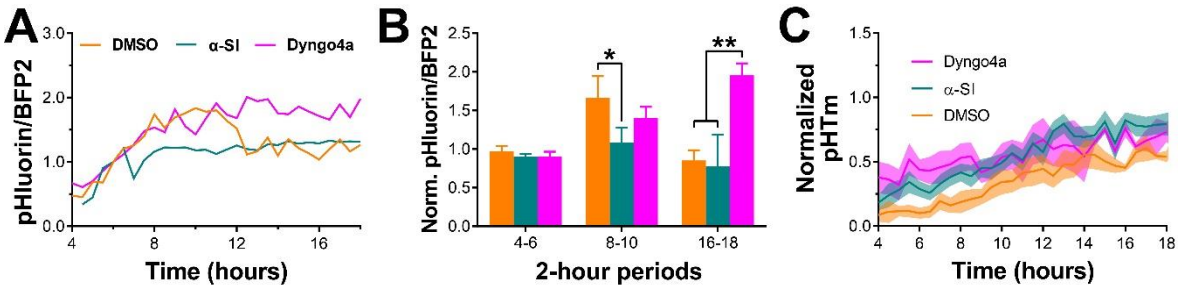

Figure 13. The effects of α-SI and Dyngo4a on nascent APP trafficking. A, Changes in pHluorin vs. BFP2 ratio at representative somas over time after treatments of DMSO, α-secretase inhibitor (α-SI) and Dyngo4a (a dynamin inhibitor). Each cell is normalized to the 6th hour, when all fluorescent signals are significantly and reliably above cell autofluorescence and background. **B,** Average pHluorin vs. BFP2 ratios at 4-6, 8-10 and 16-18 hour time periods after treatments of DMSO, α-SI and Dyngo4a. Ordinary two-way ANOVA detected effects based on time ($F(2, 46) = 4.932$, $p = 0.0115$), treatment ($F(2, 46) = 4.412$, $p = 0.0177$) and an interaction ($F(4, 46) = 3.316$, $p = 0.0181$). At time 4-6 hours, when all fluorescent reporters are reliably identifiable, Tukey's multiple comparisons test detected no significant differences between treatments (Dyngo4a vs. α-SI, ns, $p > 0.9999$; Dyngo4a vs. DMSO, ns, $p = 0.9687$; α-SI vs. DMSO, ns, $p = 0.959$). By 8-10 hours, there is a significant difference between DMSO and the α-SI (*, $p = 0.0401$) only (Dyngo4a vs. α-SI, ns, $p = 0.439$; Dyngo4a vs. DMSO, ns, $p = 0.6036$). At 16-18 hours, there is a significant difference between the Dyngo4a-treated cells and the other cells (Dyngo4a vs. DMSO, **, $p = 0.009$, Dyngo4a vs. α-SI, **, $p = 0.0049$) but there is no longer any difference between DMSO and α-SI (ns, $p = 0.9698$). **C,** Changes of normalized pHTm over time after treatments of DMSO, α-SI and Dyngo4a. The fluorescence of every cell is normalized to the minimum and maximum signal. Shadows represent SEM. At 4-6 and 8-10 hours: for DMSO, n = 7, for α-SI, n = 10, and for Dyngo4a, n = 5, where n is the number of somas. By 16-18 hours, for DMSO, n = 4, for α-SI, n = 4, and for Dyngo4a, n = 3. Reprinted (adapted) with permission from (DelBove, C. E., Deng, X., and Zhang, Q. (2018) The fate of nascent APP in hippocampal neurons: a live cell imaging study, *ACS Chemical Neuroscience*)[299]. Copyright (2018) American Chemical Society.

APP trafficking along processes does not respond to acute stimulation

A large body of evidence suggests that APP subcellular trafficking and surface turnover are influenced by neuronal activity, linking APP abnormalities to synaptic dysfunction commonly found in animal models and preclinical AD patients [27, 304]. Much of this work focuses on Aβ production [135, 249, 305], so we asked if APP trafficking between synapses or between surface and intracellular membranes was associated with acute neuronal activity changes. This question cannot be readily addressed using conventional biochemical approaches, so we took advantage of the fast response of pHluorin fluorescence and the high temporal resolution of optical imaging.

First, we examined if the mobility of APP and/or CTFs was affected by synaptic activity. We applied two different stimuli (a 1-minute 10-Hz electric field stimulation and a 1-minute 90-mM K^+ perfusion) each separated by a 1-minute resting period long enough for the synapses to recover. Since pHluorin fluorescence only represented surface APP at pH7.35 bath solution and could be altered by stimulation-induced exo-/endocytosis, we imaged BFP2 to track the movement of all APP and its C-terminal fragments (**Figure 14A**). Again, SypHTm was used to mark the positions of synaptic boutons in transfected neurons. The comparison between the sample kymographs of pHTm and BFP2 illustrates the random behaviors of BFP2 puncta, i.e. stationary or mobile, anterograde or retrograde, and toward or away from nearby synaptic boutons (**Figure 14B**). When plotted against time, neither the velocity (**Figure 14C**) nor the distance from the nearest synapse (**Figure 14D**) of the moving BFP2 puncta exhibited any significant difference between stimulation or resting periods, suggesting that APP

and/or CTFs move rather randomly instead of directionally (with respect to the synapses) and are not affected by acute activity change.

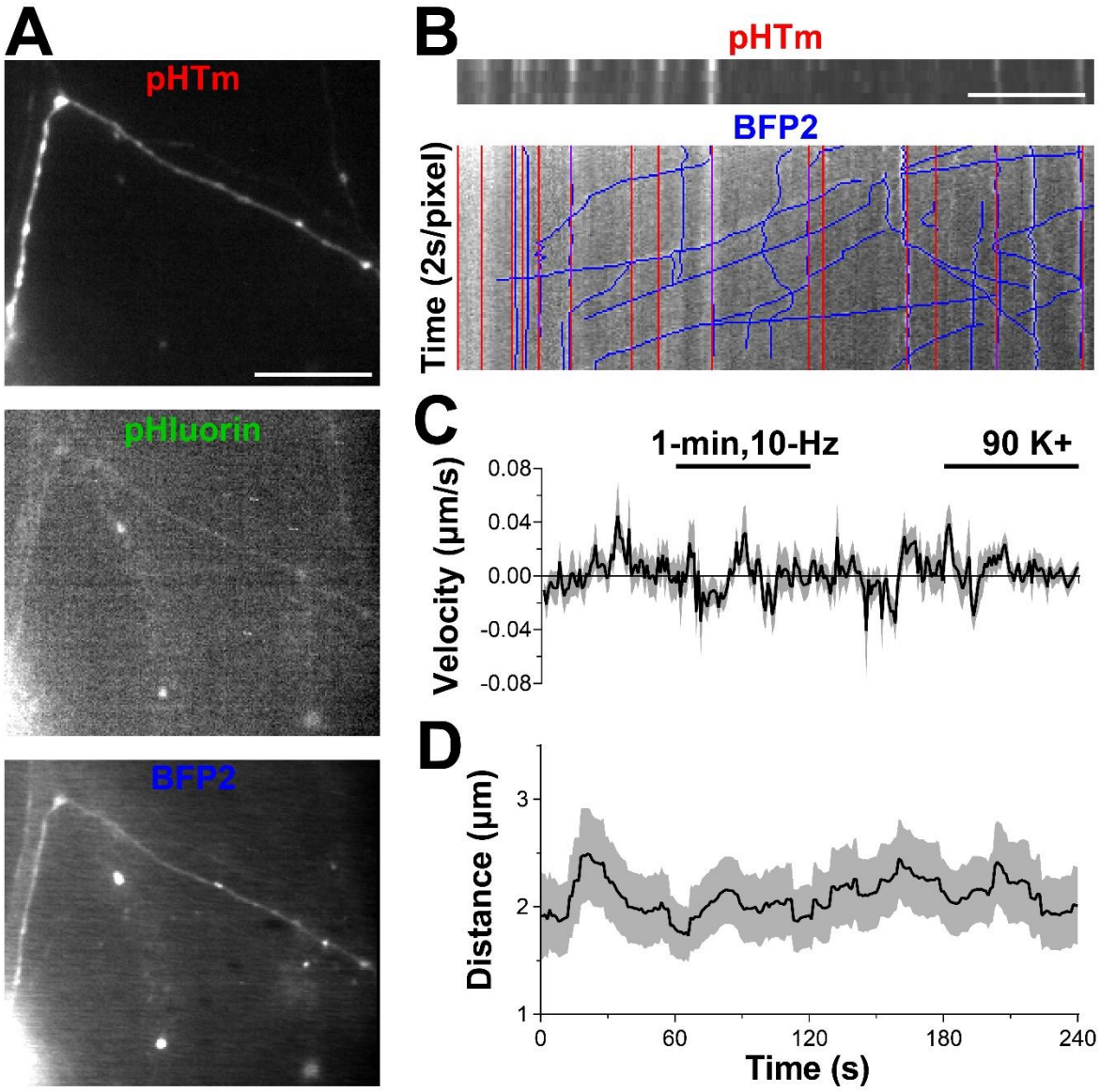

Figure 14. APP trafficking is not activity-associated. A, sample images of a process in 3 fluorescence channels. Scale bar, 10 μm. **B,** sample kymographs that show the changes in value over time during 10 Hz field stimulation and 90K stimulation along the process shown in **A**. BFP2 was imaged every two seconds, while pHTm was imaged every minute for relatively immobile synaptic boutons. Hand drawn BFP2 tracks are shown in blue, immobile synaptic boutons are in red, and purple is overlap. **C,** mean velocity of the moving BFP2 puncta. Movement towards the nearest synapse was defined as positive. **D,** mean distance from the moving BFP2 puncta to the nearest synapse. For **C**-**D**, only visible puncta contribute to the mean and s.e.m, with at most 81 puncta and at least 50 puncta at any

given time. There was a total of 241 tracks taken from 13 kymographs from 4 experiments. All shadows (**C**, **D**) represent SEM.

Response of APP at the synapses to acute activity

We next asked if APP's turnover between surface and intracellular membranes is correlated to activity-associated synaptic vesicle exo-/endocytosis. To do so, we utilized SypHTm fluorescence change as a measure for synaptic vesicle turnover [267]. If APP, like Syp, is selectively associated with synaptic vesicles, SypHTm and pHluorin fluorescence should exhibit correlated changes during stimulation. Again, we applied an intense stimulation, 90 mM K^+, and simultaneously measured the pHTm and pHluorin fluorescence changes at the same synapses. While we observed an increase of pHluorin fluorescence at synaptic boutons, neither the amount nor the rate of change was correlated to those of the pHTm fluorescence (**Figure 15A&B**). Furthermore, we did not observe consistent correlations for the total, surface, or intracellular pHluorin and pHTm fluorescence intensities at synaptic boutons (**Figure 15D-F**). These data suggest that, unlike Syp, synaptic APP is not proportional to synaptic bouton size or synaptic vesicle population, and its surface-intracellular turnover is affected but not directly mediated by synaptic vesicle turnover.

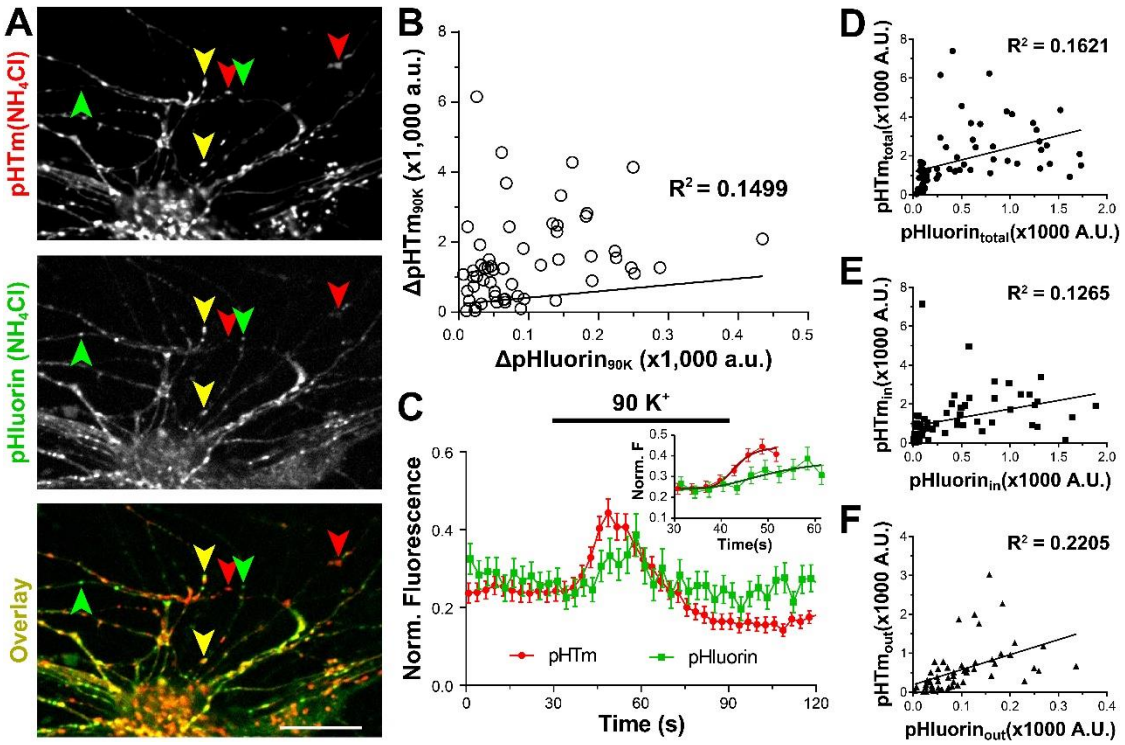

Figure 15. Subcellular distribution of APP at synaptic boutons exhibits limited correlation to synaptic vesicles and APP surfacing is delayed in comparison to SypHTomato after stimulation. A, sample images of pHTm and pHluorin in NH_4Cl and the overlay. Green arrowheads indicate puncta with high pHluorin and low pHTm fluorescence, red arrowheads indicate the opposite, and yellow arrowheads indicate puncta with similar brightness (i.e. overlapping). Scale bar, 20 µm. **B,** $pHTm_{90K}$ and $pHluorin_{90K}$ represent the maximal increase of fluorescence during 90 mM K^+ perfusion. n = 56 ROIs from 3 experiments. The line shows a linear regression of slope 1.25 ± 0.36. There is a small but significant correlation: Pearson's $R^2 = 0.1499$, $p = 0.0032$. One negative value was excluded. **C,** synaptic pHluorin and pHTm fluorescence normalized to the maximal values set by 50 mM NH_4Cl. The pHluorin increase during stimulation with 90 mM K^+ is significantly smaller than that of pHTm according to an unpaired two-tailed *t*-test ($p = 0.0224$). n = 56 ROIs from 3 FOV. The inset shows variable slope (4 parameters) curves fits to the rising phases of pHTm and pHluorin (30 - 60s) with the constraints Top = 0.4437 or Top = 0.3864, which are the maximums of pHTm and pHluorin, respectively. Based on the fittings, for pHTm, $t_{1/2}$ = 12.98 s; for pHluorin, $t_{1/2}$ = 20.15 s. Error bars represent SEM. **D,** total fluorescence ($F_{NH4Cl} - F_{pH5.5}$) of pHTm vs pHluorin. The line shows a linear regression of slope 1.252 ± 0.3585. Pearson's $R^2 = 0.1621$, $p = 0.0009$, n = 65 ROIs from 3 FOVs (excluding negative values). **E,** internal fluorescence ($F_{NH4Cl} - F_{4K}$) of pHTm vs pHluorin. The line shows a linear regression of slope 0.8808 ± 0.2939. Pearson's $R^2 = 0.1265$, $p = 0.0039$, n = 64 ROIs from 3 FOVs (excluding negative values). **F,** surface fluorescence ($F_{4K} - F_{pH5.5}$) of pHTm vs pHluorin. The line shows a linear regression of slope 3.86 ± 1.006. Pearson's $R^2 = 0.2205$, $p = 0.0003$, n = 54 ROIs from 3 FOVs (excluding negative values).

Discussion

In this chapter, we generated a dual-fluorescence APP fusion protein and utilized long-term time-lapse imaging to study the fate of nascent APP in live neurons. Our results illustrate that a substantial amount of newly synthesized APP is directly transported to the plasma membrane at the soma and propagates towards the distal direction in the plasma membrane. Moreover, neuronal surface APP is regulated by α-secretase cleavage and endocytosis together. Methodologically, we demonstrate that our dual-fluorescence APP fusion protein is a useful tool for studying APP trafficking and processing. Its combination with long-term time-lapse imaging is a powerful tool to investigate the fate of APP in polarized and morphologically complicated neurons, which are the most relevant cell type for AD research. Furthermore, the dual-tagged pH-APP-BFP2 can be a useful probe for other assays like fluorescence recovery after photobleaching (FRAP) because only unquenched (in the plasma membrane) pHluorin will be bleached.

Combined with reporters for synaptic activity (i.e. SypHTm), it is also possible to evaluate if and how APP trafficking and processing are associated with neuronal firing at synaptic and non-synaptic regions. Due to its abundance at presynaptic terminals [306], APP is believed to be functionally involved in synaptic vesicles exo-/endocytosis and thus neurotransmission [307]. However, Groemer et al. demonstrated that only about 10% of APP was recycled with synaptic vesicles [243]. A more recent study showed that APP is enriched in the presynaptic active zone but not free synaptic vesicles [308].

While our data showed that APP did surface during stimulation, the rate was much slower than that of Syp, a synaptic vesicle protein. Additionally, the surface fraction of APP at synaptic boutons was significantly more than that of Syp. One possibility is that APP is localized to the presynaptic active zone and endosome/lysosome membranes, but not to synaptic vesicles. Hence, only prolonged stimulation that forced vesicle regeneration from endosomes was able to move a limited fraction of intracellular APP to the presynaptic surface. Alternatively, it could reflect a tightly coupled vesicle retrieval mode [309] in which the surfacing and internalization of vesicular APP were balanced at the beginning of stimulation, but that was eventually unbalanced by extensive vesicle release. In addition, a continuous decay of pHluorin fluorescence after stimulation stopped suggests that the externalized APP has to be removed to keep the surface APP level steady.

Furthermore, we examined the lateral movement of BFP2 puncta, likely cargo vesicles carrying APP or CTF, as they were not confined to synaptic boutons and showed no pHluorin intensity changes during stimulation. We could not distinguish between APP and CTF because the pHluorin fluorescence of the former was quenched by the acidic luminal pH. Nevertheless, the lack of correlation between BFP2 mobility and neuronal activity or between its position and synaptic boutons suggests that the trafficking of APP and/or CTF in neurites is unlikely to be regulated by neuronal activity.

Based on our observations and its global expression, we speculate that APP is a housekeeping protein important for the maintenance of cell membranes. Given that

APP has a cholesterol-binding motif partially overlapping with its transmembrane domain [90], given that neurons have plasma membranes with the highest cholesterol level of any cells in the body, and given that cholesterol has been implicated in AD through genetic risk factors like ApoE4, there is an intriguing possibility that APP is part of the regulatory mechanism for neuronal membrane cholesterol which will be explored in Chapter V. While our study mostly used young neurons, major routes of APP trafficking and processing likely remain the same in aging neurons [310].

Chapter IV

THE COUPLING OF APP TRAFFICKING AND CLEAVAGE

Introduction

Accumulated evidence suggests that APP's surface and intracellular distributions are tightly regulated, which greatly influences APP's proteolytic products because of differentially compartmentalized secretases[45, 156]. Furthermore, APP localization is also essential for its stipulated functions; for example, being a receptor ligand requires its surface presentation. Therefore, when and how APP is transported to different membrane compartments are both physiologically and pathologically crucial. Long-term time-lapse imaging enabled us to track pH-APP-BFP2 immediately after its synthesis, which is a less studied aspect of APP. Available reports offered opposite theories: APP is either cleaved right after synthesis or is transported to distal neurites before cleavage[281]. While it is possible that nascent APP directly encounters β-secretase in intracellular compartments [280, 287], our data have shown that a large amount of APP clearly follows the regular route of plasma membrane proteins — first being transported to the plasma membrane at the soma. In addition to the well-studied anterograde transportation via cargo vesicles [311] (e.g. polarized axonal transport along microtubules [312]), we have found that it also laterally diffuses along the neuronal surface to the processes. Furthermore, APP in

the plasma membrane is also partially consumed by α-secretase and/or internalized through endocytosis, which are likely two of the constitutive mechanisms regulating the amount of APP in the plasma membrane.

The abilities to distinguish surface and intracellular APP by relative pHluorin signals and to estimate its cleavage by pHluorin/BFP2 ratio make pH-APP-BFP2 a versatile reporter for multiple aspects of APP behavior such as trafficking and processing. The best example in our results in the previous chapter is the finding that α-secretase cleavage, commonly occurring at the neuronal surface, caused a decrease instead of an increase in surface APP fraction, implying that the control of surface APP concentration is more strict than that of intracellular APP. Using this probe, it is now possible to study how changes in the activities of other secretases such as β- and γ-secretases affect APP distribution in different membrane compartments. We decided to focus on the processes and synapses in this chapter after we confirmed that full length APP is trafficked to the neuronal processes.

Results

Different secretases localize with and cleave APP in different membrane compartments [27, 313]. Moreover, inhibition of different secretases can affect APP distribution as well [196, 198]. Additionally, uncleaved APP or CTFs may relocate to other membranes, causing functional changes. Since the pHluorin and BFP2 signals allow us to estimate N- and C-terminal cleavage respectively, we investigated whether and

how inhibition of α-secretase, β-secretase and γ-secretase alter APP distribution. We applied the three ELISA-validated inhibitors (**Figure 3**) separately or in combination, and quantified surface, intracellular and total pHluorin as well as BFP2. For comparison, we calculated the ratios such as that for intracellular *vs.* total pHluorin in both synaptic and non-synaptic regions. For easy visualization, we converted those ratiometric values to color-coded charts (**Figure 16**) supplied with corresponding bar graphs (**Figure 17**) and scatter plots of the background subtracted fluorescence values (**Figure 18** and **19**).

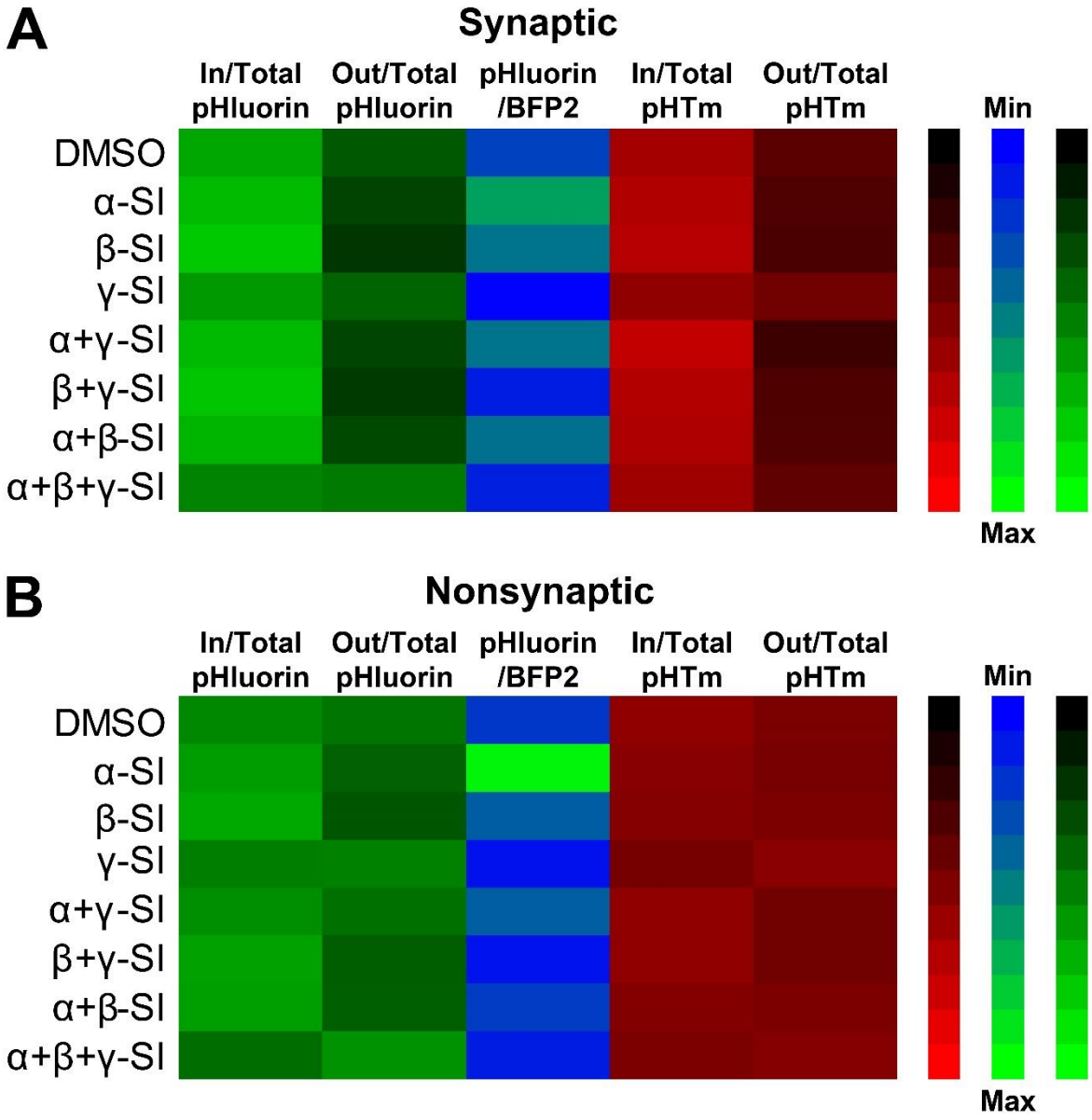

Figure 16. Changes of pHluorin and pHTm ratios after secretase inhibition. A, color-coded representation of the fluorescence ratios at synaptic boutons marked by SypHTm. Color coding and scale are shown in the right. **B,** color-coded representation of the fluorescence ratios at non-synaptic part of the neurites. Color coding and scale are shown in the right. Some bar graphs are shown in **Figure 17**. Statistics are shown in **Table 2** and **Table 3**. Raw data is shown in **Figure 18** and **Figure 19**.

α- and β-secretase inhibition

As expected, α-secretase inhibition doubled the total pHluorin *vs.* BFP2 ratio (from 0.33 ± 0.02 to 0.66 ± 0.04) at synaptic boutons (**Figure 16A, Figure 17B,** and **Figure 18D&E**), consistent with the notion that α-secretase cleavage is the major APP N-terminal cleavage and β-secretase alone is not sufficient to process the excessive APP. Instead of remaining in the plasma membrane, the uncleaved APP was accumulated intracellularly, as shown by a decrease of surface APP fraction and an increase of intracellular fraction. This holds true in non-synaptic regions as well (**Figure 16B** and **Figure 19D&E**), indicating that the surface APP level is more strictly controlled than the intracellular level. Notably, there were similar changes in surface and intracellular pHTm distributions although much smaller (**Figure 17C, Figure 18F**). As expected, β-secretase inhibition caused less of an increase in the total pHluorin *vs.* BFP2 ratio (~55%, from 0.33 ± 0.02 to 0.51 ± 0.03) than α-secretase inhibition did, and uncleaved APP again accumulated intracellularly at synaptic boutons (**Figure 16, Figure 18G&H** and **19G&H**). Changes in surface and intracellular pHTm (**Figure 18I** and **19I**) were similar to those of α-secretase inhibition and in the same direction as those of pHluorin.

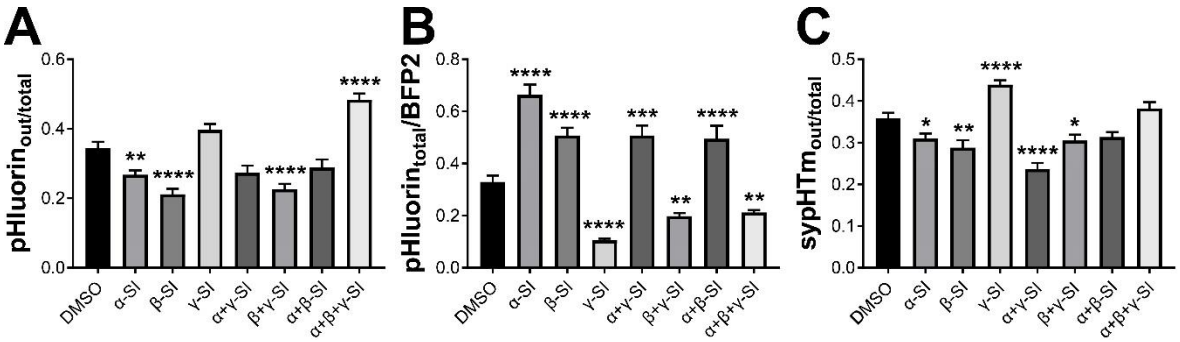

Figure 17: The effects of secretase inhibitors on APP and SypHTm at the synapses. A, Comparison of the mean surface fraction of pHluorin. **B,** Comparison of the mean surface fraction of pHluorin/BFP2. **C,** Comparison of the mean surface fraction of pHTm. The asterisks show the results of Dunnett's post comparisons test comparing all conditions to DMSO control after ordinary 1-way ANOVA. For full statistics, see **Table 2**.

γ-secretase inhibition

As we expected, γ-secretase inhibition reduced the total pHluorin *vs.* BFP2 ratio to 33% (from 0.33 ± 0.02 to 0.11 ± 0.01) due to a significant increase of uncleaved CTFs (**Figure 16, Figure 18J&K** and **19J&K**). Intriguingly, there was a significant increase of surface APP fraction (i.e. increase of surface vs total pHluorin ratio). Even more interesting is a greater increase of surface pHTm fraction (**Figure 18L** and **19L**), suggesting an imbalance of synaptic vesicle release and retrieval when γ-secretase was inhibited. While such an imbalance may be accountable for increased surface APP at synaptic boutons, it cannot explain the same increase at non-synaptic regions lacking synaptic vesicles. An alternative explanation is that other γ-secretase substrates, CTFs, or even membrane lipids are affected by γ-secretase inhibition, resulting in direct and consequently alter membrane APP trafficking.

Combination effects

Next, we applied different combinations of secretase inhibitors and tested their effects on APP trafficking and synaptic vesicle turnover (**Figure 16** and **Figure 18&19**). The inhibition of both α-secretase and γ-secretase caused a greater increase in APP than in CTF (i.e. ~55% increase of total pHluorin *vs.* BFP2 ratio), and, consistently, most uncleaved APP remained intracellular (**Figure 16**, **Figure 18M&N** and **19M&N**).

Additionally, the pHTm distribution changed in a manner similar to that of APP (**Figure 18O** and **19O**), i.e. there was more intracellular SypHTm. The inhibition of both β-secretase and γ-secretase caused a greater increase in CTF than APP (i.e. ~39% decrease in total pHluorin *vs.* BFP2 ratio), and most uncleaved APP again remained intracellular (**Figure 16**, **Figure 18P&Q** and **19P&Q**). Again, there was a small change in pHTm distribution, in the same direction as that of APP (**Figure 18R** and **19R**), i.e. there was more intracellular localization of SypHTm. Inhibition of both α-secretase and β-secretase also caused more increase in APP than CTF, (i.e. ~52% increase in total pHluorin *vs.* BFP2 ratio) (**Figure 18T** and **19T**), and uncleaved APP again accumulated in the intracellular compartments (**Figure 16**, **Figures 18S** and **19S**). The inhibition of three major secretases caused a greater CTF increase than APP increase, (i.e. ~36% decrease in total pHluorin *vs.* BFP2 ratio) (**Figure 18W** and **19W**). More interestingly, there was much greater increase of surface APP than that of intracellular APP (**Figure 16, Table 2**), accompanied by a similar change in SypHTm distribution (**Figure 18X** and **19X**). Collectively, these results implicate alternative N-terminal cleavage mechanism(s), a close association between APP processing and surface trafficking, strict control of surface APP level, and a loose association between APP surface turnover and synaptic vesicle recycling.

Synapses	n	out/total pHluorin	pHluorin/ BFP2	out/total pHTm
DMSO	132			
α-SI	126	$p = 0.0090$	$p = 0.0001$	$p = 0.0446$
β-SI	80	$p = 0.0001$	$p = 0.0001$	$p = 0.0044$
γ-SI	165	$p = 0.1003$	$p = 0.0001$	$p = 0.0001$
α+γ-SI	60	$p = 0.0986$	$p = 0.0004$	$p = 0.0001$
β+γ-SI	132	$p = 0.0001$	$p = 0.0011$	$p = 0.0172$
α+β-SI	96	$p = 0.1524$	$p = 0.0001$	$p = 0.1114$
α+β+γ-SI	128	$p = 0.0001$	$p = 0.0052$	$p = 0.6594$
ANOVA		F (7, 911) = 27.5087	F (7, 911) = 60.1197	F (7, 911) = 20.6126
		$p < 0.0001$	$p < 0.0001$	$p < 0.0001$

Table 2: Comparisons between conditions at the synapses for Figure 16 and 17. Dunnett's multiple comparisons test after ordinary one-way ANOVA was used to compare all conditions to DMSO, the control, and *p* values are listed. ANOVA **F,** degrees of freedom, and *p* values are listed below the multiple comparisons reults. The *p* values for in/total are identical to those of out/total.

Nonsynaptic	n	out/total pHluorin	pHluorin/ BFP2	out/total pHTm
DMSO	143			
α-SI	144	$p = 0.0187$	$p = 0.0001$	$p = 0.9966$
β-SI	111	$p = 0.0001$	$p = 0.9204$	$p = 0.9997$
γ-SI	322	$p = 0.2632$	$p = 0.7503$	$p = 0.0074$
α+γ-SI	99	$p = 0.9623$	$p = 0.9026$	$p = 0.5337$
β+γ-SI	88	$p = 0.0108$	$p = 0.9428$	$p = 0.5491$
α+β-SI	100	$p = 0.0241$	$p = 0.9999$	$p = 0.9996$
α+β+γ-SI	160	$p = 0.0002$	$p = 0.9714$	$p = 0.2901$
	ANOVA	F (7, 1159) = 18.2103	F (7, 1159) = 7.99344	F (7, 1159) = 5.76781
		$p < 0.0001$	$p < 0.0001$	$p < 0.0001$

Table 3: Comparisons between conditions at the nonsynaptic areas for Figure 16. Dunnett's multiple comparisons test after ordinary one-way ANOVA was used to compare all conditions to DMSO, the control, and *p* values are listed. ANOVA **F,** degrees of freedom, and *p* values are listed below the multiple comparisons reults. The *p* values for in/total are identical to those of out/total.

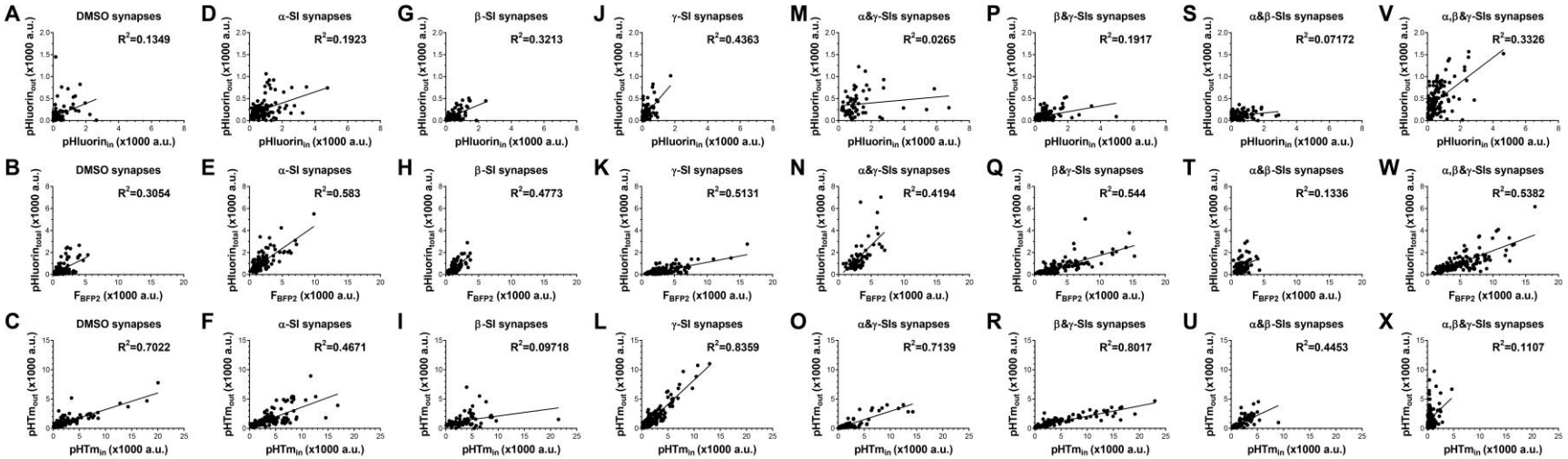

Figure 18. Secretase inhibition affects pHluorin and pHTm distribution at synaptic boutons. A-H, surface pHluorin vs internal pHluorin fluorescence. **I-P**, total pHluorin vs BFP2 fluorescence, which corresponds to APP N vs APP C. **Q-X**, surface pHTm vs internal pHTm. DMSO, n = 132; α-SI, n = 126; β-SI, n = 80; γ-SI, n = 165; α&γ-SIs, n = 60; β&γ-SIs, n = 132; α&β-SIs, n = 96; α&β&γ-SIs, n = 128, where n is equal to the number of synapses from at least three FOVs. Correlation statistics are listed in **Table 4**.

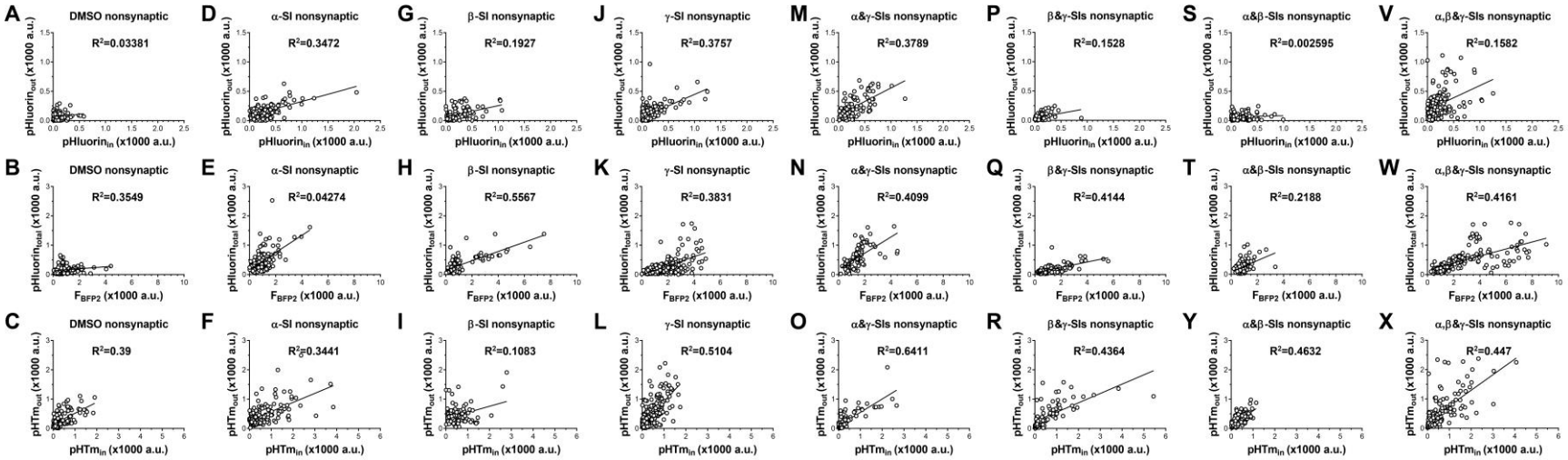

Figure 19. Secretase inhibition affects pHluorin and pHTm distribution at neurite shafts. A-H, surface pHluorin vs internal pHluorin fluorescence. **I-P**, total pHluorin vs BFP2 fluorescence, which corresponds to APP N vs APP C. **Q-X**, surface pHTm vs internal pHTm. DMSO, n = 145; α-SI, n = 144; β-SI, n = 111; γ-SI, n = 326; α&γ-SIs, n = 99; β&γ-SIs, n = 88; α&β-SIs, n = 101; α&β&γ-SIs, n = 160, where n is equal to the number of synapses from at least three FOVs. Correlation statistics are listed in **Table 5**.

pHluorin (in) vs. pHluorin (out)				
	N	Slope	R^2	p (2-tailed)
DMSO	132	0.1532 ± 0.03404	0.3054	<0.0001
α-SI	126	0.1257 ± 0.02314	0.583	<0.0001
β-SI	80	0.1549 ± 0.02548	0.4773	<0.0001
γ-SI	165	0.4345 ± 0.03869	0.5131	<0.0001
α+γ-SIs	60	0.03347 ± 0.02663	0.4194	<0.0001
β+γ-SIs	132	0.0658 ± 0.01185	0.544	<0.0001
α+β-SIs	96	0.03643 ± 0.01352	0.1336	0.0003
α+β+γ-SIs	128	0.2832 ± 0.03573	0.5382	<0.0001
BFP2 vs. pHluorin (total)				
	N	Slope	R^2	p (2-tailed)
DMSO	132	0.299 ± 0.03955	0.3054	<0.0001
α-SI	126	0.4138 ± 0.03143	0.583	<0.0001
β-SI	80	0.4388 ± 0.05199	0.4773	<0.0001
γ-SI	165	0.1146 ± 0.008744	0.5131	<0.0001
α+γ-SIs	60	0.5821 ± 0.08993	0.4194	<0.0001
β+γ-SIs	132	0.169 ± 0.01357	0.544	<0.0001
α+β-SIs	96	0.2881 ± 0.07569	0.1336	0.0003
α+β+γ-SIs	128	0.2242 ± 0.0185	0.5382	<0.0001
pHTm(in) vs. pHTm(out)				
	N	Slope	R^2	p (2-tailed)
DMSO	132	0.2832 ± 0.01618	0.7022	<0.0001
α-SI	126	0.3274 ± 0.0314	0.4671	<0.0001
β-SI	80	0.1203 ± 0.0415	0.09718	0.0049
γ-SI	165	0.8337 ± 0.02894	0.8359	<0.0001
α+γ-SIs	60	0.2865 ± 0.02382	0.7139	<0.0001
β+γ-SIs	132	0.1757 ± 0.007662	0.8017	<0.0001
α+β-SIs	96	0.4119 ± 0.04741	0.4453	<0.0001
α+β+γ-SIs	128	0.863 ± 0.2179	0.1107	0.0001

Table 4: Correlation statistics for synaptic data in Figure 18. Correlations between surface and internal pHluorin, pHluorin and BFP2, and surface and internal pHTm. The raw data is presented in scatterplots in **Figure 18**.

pHluorin (in) vs. pHluorin (out)				
	N	Slope	R^2	p (2-tailed)
DMSO	145	0.1043 ± 0.04664	0.03381	0.0268
α-SI	144	0.246 ± 0.02831	0.3472	<0.0001
β-SI	111	0.1926 ± 0.03775	0.1927	<0.0001
γ-SI	326	0.3881 ± 0.02797	0.3757	<0.0001
α+γ-SIs	99	0.4611 ± 0.05994	0.3789	<0.0001
β+γ-SIs	88	0.1611 ± 0.0409	0.1528	0.0002
α+β-SIs	101	0.01464 ± 0.029	0.002595	0.6147
α+β+γ-SIs	160	0.4167 ± 0.07646	0.1582	<0.0001
BFP2 vs. pHluorin (total)				
	N	Slope	R^2	p (2-tailed)
DMSO	145	0.03428 ± 0.01366	0.04274	0.0132
α-SI	144	0.292 ± 0.03304	0.3549	<0.0001
β-SI	111	0.1582 ± 0.01352	0.5567	<0.0001
γ-SI	326	0.1562 ± 0.01108	0.3831	<0.0001
α+γ-SIs	99	0.2751 ± 0.03352	0.4099	<0.0001
β+γ-SIs	88	0.09153 ± 0.01173	0.4144	<0.0001
α+β-SIs	101	0.1916 ± 0.03656	0.2188	<0.0001
α+β+γ-SIs	160	0.1195 ± 0.01126	0.4161	<0.0001
pHTm(in) vs. pHTm(out)				
	N	Slope	R^2	p (2-tailed)
DMSO	145	0.3758 ± 0.0393	0.39	<0.0001
α-SI	144	0.3106 ± 0.03599	0.3441	<0.0001
β-SI	111	0.2101 ± 0.05774	0.1083	0.0004
γ-SI	326	0.7949 ± 0.04326	0.5104	<0.0001
α+γ-SIs	99	0.4551 ± 0.03457	0.6411	<0.0001
β+γ-SIs	88	0.3185 ± 0.03903	0.4364	<0.0001
α+β-SIs	101	0.488 ± 0.05279	0.4632	<0.0001
α+β+γ-SIs	160	0.5308 ± 0.04697	0.447	<0.0001

Table 5: Correlation statistics for nonsynaptic data in Figure 19. Correlations between surface and internal pHluorin, pHluorin and BFP2 presented as raw data in scatterplots in **Figure 18**.

Discussion

Reducing Aβ production has been one of the major therapeutic strategies tested clinically. However, little is known about how secretase inhibition will impact APP's surface and intracellular distribution in neurites and synapses. It is well documented that different secretases cleave APP/CTF in different membrane compartments and that their activities are greatly affected by the environment such as membrane cholesterol concentration and pH [35]. However, the localization of APP or CTF is essential for specific functions they reportedly execute [314]. Therefore, secretase inhibition can change both APP distribution and function. Our findings not only support this notion but also suggest that neuronal surface membrane APP is tightly controlled except after γ-secretase inhibition. Notably, application of γ-secretase inhibitor alone or in combination with other inhibitors also significantly increased surface SypHTm, suggesting a side effect on synaptic vesicle turnover and likely synaptic transmission. However, it is unlikely that the surfacing of vesicular membrane components was the major cause of surface APP increase because (1) the later also occurred at neurite shafts, (2) its increase was much more than that of surface SypHTm in subsequent experiments, and (3) APP might be less abundant in synaptic vesicles than previously thought [243, 308]. We speculate that the excessive CTFs after γ-secretase inhibition might contribute to the unexpected increase in surface APP via heterodimerization with APP (discussed in detail later).

Chapter V

RELATIONSHIP BETWEEN APP LOCALIZATION AND CHOLESTEROL

Introduction

The strict control of surface membrane APP and its disruption by γ-secretase inhibition prompted us to identify a membrane factor that can link the two together. It is well known that all three secretases are sensitive to cholesterol in cell membranes, although this is thought to be due to likelihood of colocalization [100, 101, 105, 110, 260, 261]. Furthermore, recent structural studies using nuclear magnetic resonance spectroscopy (NMR) revealed a cholesterol-binding motif, implicating a specific interaction between cholesterol and APP in neuronal membrane [88-90]. This is interesting not only because neuronal membranes have much higher cholesterol content than most other types of cells in the human body [315], but also because cholesterol seems to be closely linked to AD. First, ApoE4, the highest genetic risk factor for sporadic AD, leads to a reduced cholesterol supply to neurons compared to the AD-protective or benign ApoE2&3 variants [316]. Second, when cholesterol transportation to the plasma membrane is disrupted by mutations like NPC1 (found in Niemann-Pick Type C1 disease) [317], AD-like histopathology, including abnormal Aβ metabolism, NFTs, and neurodegeneration, appear. Third, increasing membrane cholesterol shifts APP processing from the non-amyloidogenic mode to

amyloidogenic by suppressing α-secretase cleavage [101, 102, 318] and promoting β-secretase and γ-secretase cleavage [107, 109]. Fourth, APP and ApoE reciprocally modulate each other's expression [253, 319, 320]. Fifth, cholesterol and ApoE4 reportedly affects the clearance of Aβ aggregates. Sixth, cholesterol is essential for exo-/endocytosis of synaptic vesicles [321]. Seventh, age-related loss of membrane cholesterol is often accompanied by synaptic dysfunction during the preclinical stage of AD [322]. We manipulated both cholesterol concentration and APP's direct cholesterol binding to investigate the relationship between APP and cholesterol trafficking.

Results

Cholesterol depletion increases the surface fraction of APP

Hence, we examined how synaptic APP processing and trafficking change upon membrane cholesterol reduction. We incubated hippocampal cultures with 1 mM MβCD (methyl-β-cyclodextrin) for 90 minutes before proceeding with live cell imaging, which we confirmed caused a moderate (~10%) reduction of neuronal membrane cholesterol without detectable membrane damage or morphological change (**Figure 20**). The raw filipin signal was significantly decreased (**Figure 20A**). We decided to use AM1-43 to normalize the data to the total membrane in order to specifically narrow the changes to cholesterol concentration, and still found a significant difference (**Figure 20B**).

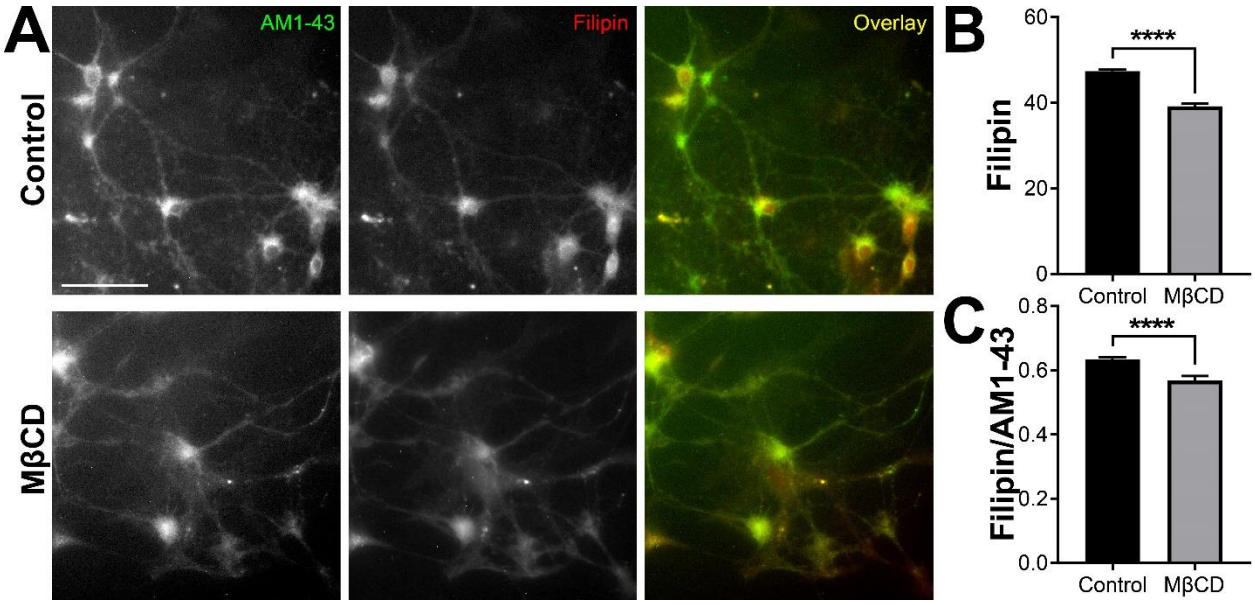

Figure 20. 90 minute 1 mM MβCD treatment moderately but significantly decreases neuronal membrane cholesterol. A, sample images of AM1-43 and filipin staining performed with and without the MβCD treatment. Scale bar, 150 µm. **B,** MβCD application decreases the background subtracted filipin fluorescence (unpaired two-tailed *t*-test: t = 12.47, df=2145, ****, $p < 0.0001$. Control, n = 1520; MβCD, n = 627 ROIs. Error bars represent SEM. **C,** MβCD decreases the filipin/AM1-43 ratio (unpaired two-tailed *t*-test: t = 4.99, df = 2145, ****, $p < 0.0001$). Control, n = 1520; MβCD, n = 627, where n is segmented ROIs from neuronal processes. Error bars represent SEM.

Immediately before live cell imaging, the coverslips were transferred to the microscope in pre-warmed 4K Tyrode with MBCD, but MBCD was not present during imaging. The appearance of the processes is visibly less punctated in the pH-APP channel after treatment, even after NH4Cl application (**Figure 21A**). The surface fraction of pH-APP is increased by MBCD in both synaptic and nonsynaptic regions (**Figure 21B**). However, we chose to focus on the synapses because the increase in pH-APP surface fraction after cholesterol depletion was larger, likely because synapses are highly enriched in both cholesterol and internal lipid compartments. We compared SypHTm to pH-APP to determine if changes in synaptic vesicles, such as

the size of the vesicle pool, could explain the results (**Figure 21C**). MβCD caused a 57.84% increase in pHluorin surface fraction but only a 20.71% increase in pHTm. The increases in pHluorin surface fraction ($p < 0.0001$) and SypHTm surface fraction ($p = 0.0004$) are both significant, however the effect size (η2) is much higher for pHluorin (0.1582) than pHTm (0.07463). We concluded that the effect on SypHTm, and thus the synaptic vesicles, is too small to explain the greatly increased surface fraction of pH-APP.

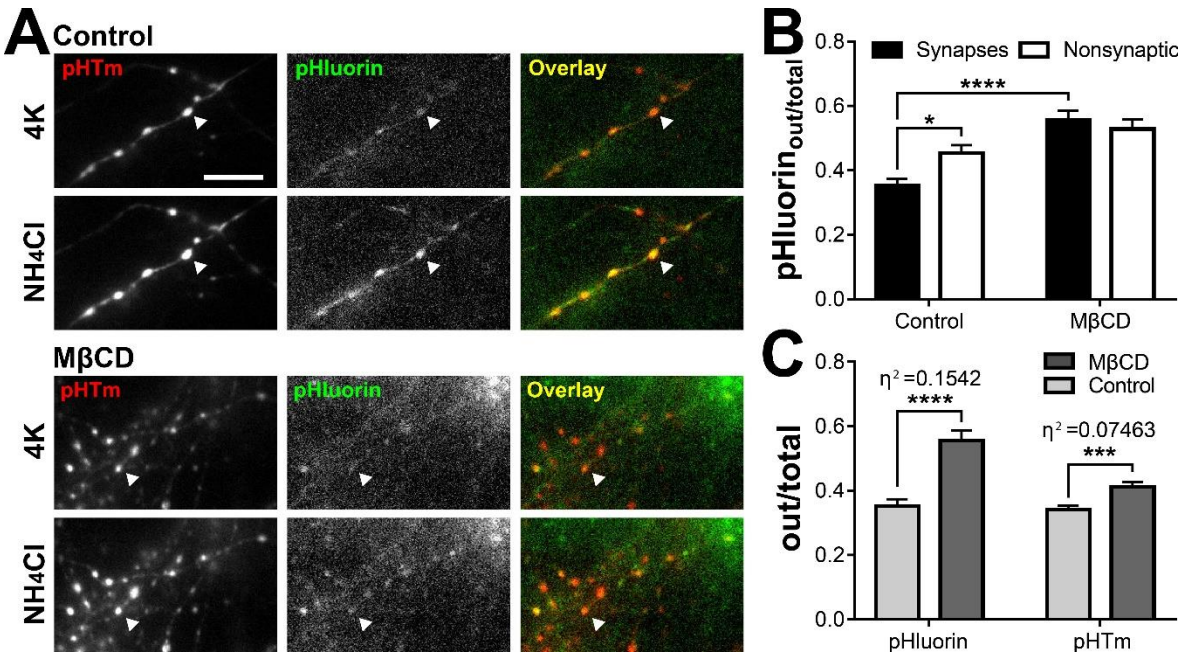

Figure 21: Cholesterol depletion by MβCD significantly increases APP surfacing at synaptic boutons. A, Representative images of processes with and without MβCD. The same processes are shown during application of 4K and NH_4Cl in two channels, pHTm and pHluorin. The overlay shows colocalization in yellow. Images shown are an average of 3 frames. Markers show examples of synapses. Scale bar is 10 µm. **B,** Two-way ANOVA was used to analyze the effects of treatment on pHluorin surface fraction in synaptic and nonsynaptic regions of the processes. The treatment causes a statistically significant difference ($F(1, 346) = 26.71$, $p < 0.0001$) although localization does not ($F(1, 346) = 1.898$, $p = 0.1692$), there is a significant interaction ($F(1, 346) = 5.673$, $p = 0.0178$). Sidak's multiple comparisons test clarifies that the difference between synaptic and nonsynaptic surface fraction is only significant for the control ($p = 0.0114$, MβCD $p = 0.7461$), and likewise a significant difference between treatments was only observed at the synapses ($p < 0.0001$, nonsynaptic $p = 0.0844$). **C,** A comparison of the surface fraction increases of pHTm and

pHluorin caused by MβCD, mean ± SEM. MβCD caused a 57.84% increase in pHluorin surface fraction but only a 20.71% increase in pHTm. The increases in pHluorin surface fraction (unpaired t-test p = <0.0001, t = 5.534, df = 163) and SypHTm surface fraction (p = 0.0004, t = 3.626, df = 163) are both significant, however the effect size (η^2) is much higher for pHluorin (0.1582) than pHTm (0.07463). N is the number of synaptic or nonsynaptic regions of interest, control synapses n = 90, control nonsynaptic n = 100, MβCD synapses n = 75, MβCD nonsynaptic n = 85. The experiment was repeated 5 times per condition and an equal number of ROIs was chosen from each FOV.

After making these two important observations, we decided to focus on synapses going forward due to the weakness of the nonsynaptic effect. **Figures 22 & 23** show the complete data set with all conditions for synapses only.

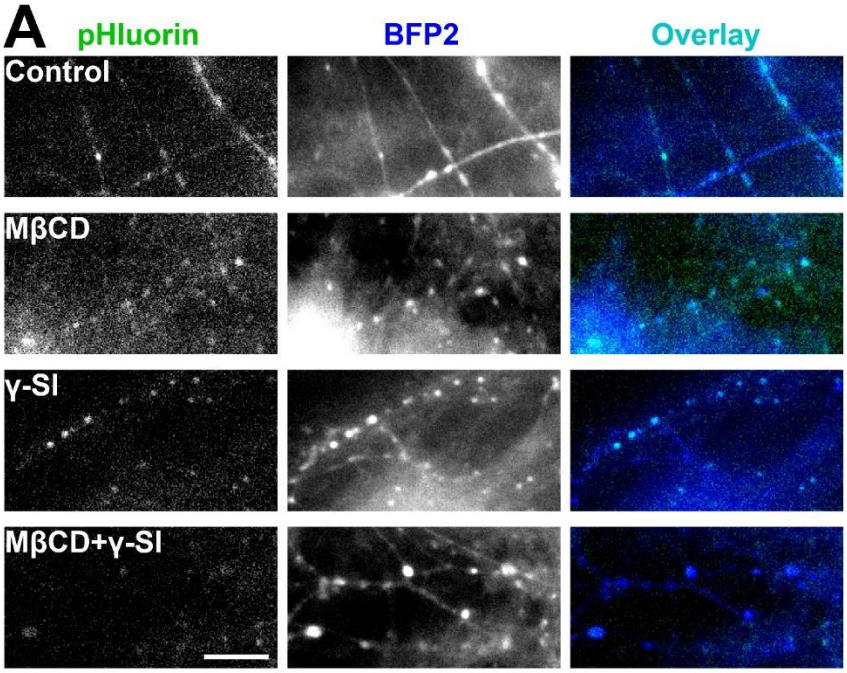

Figure 22: Images of membrane cholesterol affecting the distribution and cleavage of APP. A, sample images of pHluorin, BFP2 and their overlays with four different treatments. Scale bar, 10 μm.

By far the most visible change we observed was a significant reduction of total pHluorin fluorescence (**Figure 22A** and **Figure 23A**), consistent with an increase in α-secretase cleavage caused by lower membrane cholesterol [102, 323]. Looking at the raw

data (not shown) reveals that the reduction of surface pHluorin was less than that of intracellular pHluorin, which is what lead to the relative increase in the surface APP fraction (**Figure 23D**).

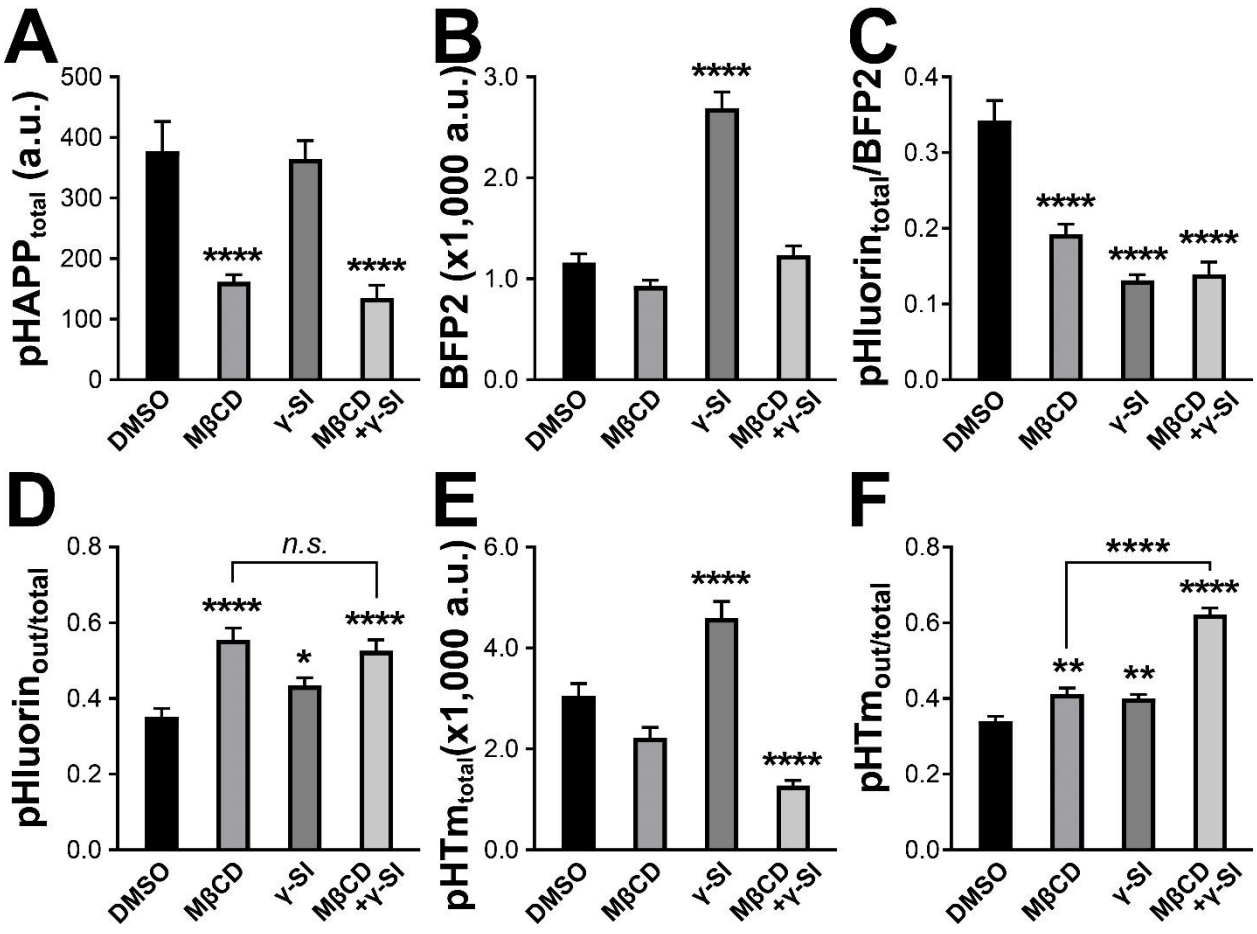

Figure 23. **Membrane cholesterol affects the distribution and cleavage of APP. A,** average total pHluorin fluorescence intensities in synaptic boutons marked by SypHTm. One-way ANOVA detected significant differences among treatments ($F(3, 360) = 14.93$, $p < 0.0001$). Dunnett's multiple comparisons test showed that MβCD significantly decreased total pHluorin fluorescence without or with γ-SI (****, $p = 0.0001$ for both). However, γ-SI alone made no difference ($p = 0.9834$). **B,** average BFP2 fluorescence intensities in synaptic boutons marked by SypHTm. One-way ANOVA detected significant differences among treatments ($F(3, 360) = 48.65$, $p < 0.0001$). Dunnett's multiple comparisons test showed that only γ-SI significantly increased BFP2 fluorescence compared to WT (****, $p = 0.0001$). **C,** average total pHluorin vs. BFP2 ratio in synaptic boutons marked by SypHTm. One-way ANOVA detected significant differences among treatments ($F(3, 360) = 35.04$, $p < 0.0001$). Dunnett's multiple comparisons test showed that MβCD, γ-SI and MβCD+γ-SI significantly decreased the ratio (****, $p = 0.0001$). **D,** average surface vs. total pHluorin ratio in synaptic boutons marked by SypHTm. One-way ANOVA detected significant differences among

treatments (F (3, 360) = 12.9832, $p < 0.0001$). Dunnett's multiple comparisons test showed that both MβCD and γ-SI significantly increased the ratio (****, $p = 0.0001$; *, $p = 0.0343$, respectively), as did the combination (****, $p = 0.0001$), but there is no additive effect for MβCD and γ-SI combined compared to MβCD alone (two-tailed unpaired t test, $p = 0.4855$). **E,** average total pHTm in synaptic boutons marked by SypHTm. One-way ANOVA detected significant differences among treatments (F (3, 360) = 30.86, $p < 0.0001$). Dunnett's multiple comparisons test showed that γ-SI significantly increased total pHTm (****, $p = 0.0001$), whereas MβCD and MβCD+γ-SI decreased it (ns, $p = 0.0888$; ****, $p = 0.0001$, respectively). **F,** average surface vs. total pHTm in synaptic boutons marked by SypHTm. One-way ANOVA detected significant differences among treatments (F (3, 360) = 76.19, $p < 0.0001$). Dunnett's multiple comparisons test showed that MβCD, γ-SI and MβCD+γ-SI significantly increased the ratio (**, $p = 0.0014$; **, $p = 0.003$; ****, $p = 0.0001$, respectively). Additionally, a two-tailed t-test showed a very significant difference between MβCD+γ-SI and MβCD (****, $p < 0.0001$). For all, DMSO, n = 90 (FOV = 5); MβCD, n = 75 (FOV = 5); γ-SI, n = 119 (FOV = 7); MβCD+γ-SI, n = 80 ROIs (FOV = 4), where n is the number of ROIs corresponding to SypHTm-marked synaptic boutons. This data set includes data from **Figure 21**.

We next investigated whether a cholesterol-related change in secretase activity increased the surface APP fraction indirectly. Because α-secretase mostly cleaves cell surface APP (**Figure 13**), MβCD-induced potentiation of α-secretase – which we are observing here - is unlikely to be directly responsible for the increase of surface APP fraction. In fact, this demonstrates that the mechanism driving APP to the surface after cholesterol depletion outpaces α-cleavage. Furthermore, β-secretase suppression caused by MβCD[324, 325] also cannot explain the increase because our previous results showed that direct β-secretase inhibition resulted in a reduction, not an increase, in surface APP fraction (see **Figure 24** for some example images and **Figure 17A** and **Table 2** for the data). Although γ-secretase activity is expected to be reduced by membrane cholesterol loss [105, 111], and we do indeed observe and increase in surface fraction after direct γ-inhibition, MβCD treatment does not increase BFP2 fluorescence (**Figure 23B**). This suggests that our mild MβCD treatment was

insufficient to suppress γ-secretase. Therefore, it is likely that MβCD-induced surface APP fraction increase was completely separate from that mediated by γ-secretase inhibition. Taken together, altered secretase activity after MβCD treatment does not appear to be account for the increased surface fraction of APP.

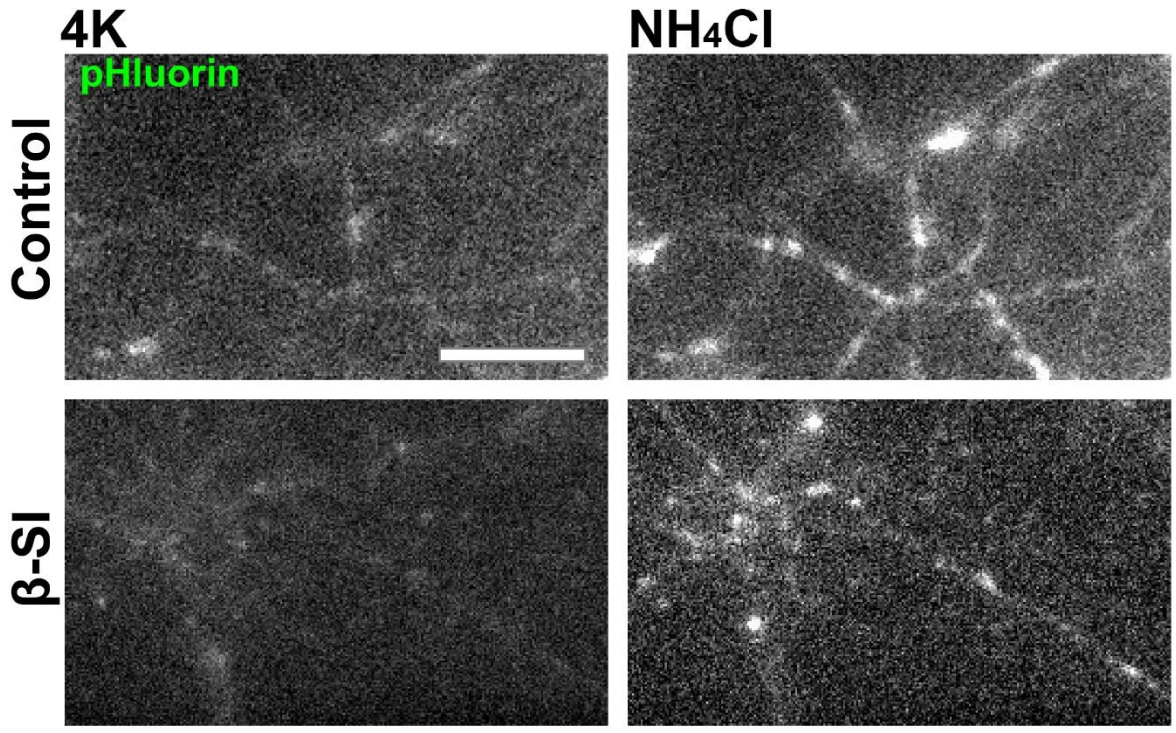

Figure 24: β-secretase inhibitors visibly decrease surface expression of pHluorinAPP-BFP2. Representative images of β-SI-treated and control processes in normal Tyrode and 50 mM NH4Cl. These images are among those quantified in Chapter IV. Scale bar is 10 μm.

Interaction between γ-secretase and cholesterol

By combining MβCD and γ-secretase inhibitor treatments, we further tested if their effects on surface APP was additive. The total pHluorin signal was reduced to the same degree as MβCD alone (**Figure 23A**), and the BFP2 signal was increased by the addition of the γ-secretase inhibitor (**Figure 23B**). As such, the total pHluorin *vs.*

BFP2 ratio was reduced to a similar degree as that of γ-secretase inhibitor (unpaired two-tailed *t*-test, $p = 0.6324$) and more than that of MβCD alone (unpaired two-tailed *t*-test, $p = 0.0140$) (**Figure 23C**), suggesting MβCD alone does not completely block γ-secretase activity. Analysis of the surface pHluorin fraction showed that the increase in surface APP was more than that of γ-secretase inhibition alone, but no more than that by MβCD alone (**Figure 23D**). Moreover, the combined treatment caused a greater decrease of total SypHTm (**Figure 23E**) and a higher surface SypHTm fraction than MβCD or γ-secretase inhibitor alone (**Figure 23F**), which was similar to what we previously observed (**Figure 18L&19L**). These data further suggest that the MβCD treatment had limited impact on γ-secretase activity, and thus acted on surface APP distribution through mechanism(s) different from γ-secretase inhibition.

Cholesterol-binding deficient APP mutants have an increased surface fraction

If membrane cholesterol modulates APP surface distribution independent of the three major secretases, does that involve a direct interaction between APP and cholesterol? In fact, a cholesterol-binding motif in APP has been identified recently based on NMR studies [88-91], which has yet to be physiologically validated. To test the importance of direct cholesterol binding to surface fraction, we introduced two point mutations (G700A and I703A) into SypHTm:T2A:pH-APP-BFP2. These amino acid residues were essential for cholesterol-binding [90] and distant enough from the cleavage sites for the three major secretases. We expressed this mutant as well as the wild type control in cultured neurons (**Figure 25A**). Again, we focused on SypHTm-

marked synaptic boutons where APP changes occurred the most. Both mutants caused a significant increase of surface APP fraction (**Figure 25B**) with little change in surface SypHTm fraction (**Figure 25C**). This suggests that APP-cholesterol binding either prevents APP surface-localization or promotes its internalization, and it is independent of synaptic vesicle turnover, which is again different from that of γ-secretase inhibition.

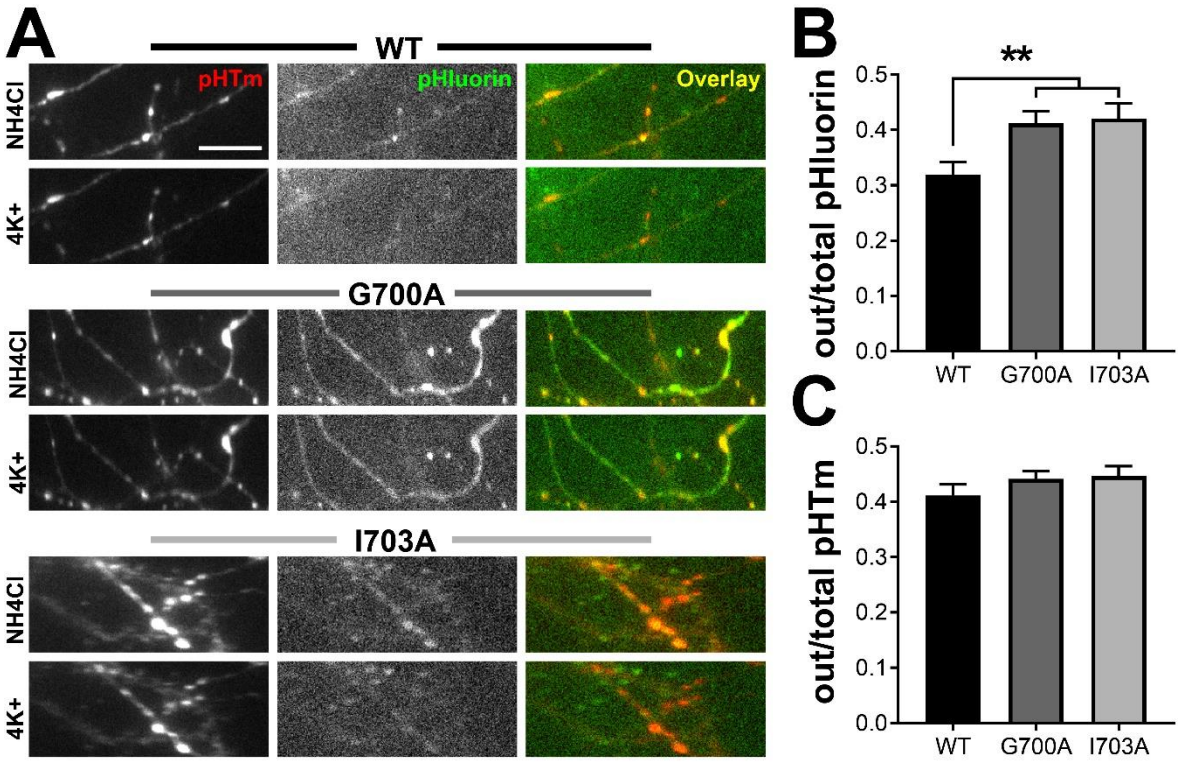

Figure 25: Cholesterol binding-deficient mutant APP accumulates on the cell surface. A, Representative images of WT (top) and the mutants G700A and I703A. The images of pHluorin and pHTm in NH_4Cl and 4K show the total and surface pHluorin (scale bar is 10 μm). **B,** G700A and I703A mutations cause an increase in the surface fraction of pHluorin at the synapses (one-way ANOVA, F (2, 245) = 5.652, p = 0.0040, Dunnett's: WT vs G700A p = 0.008, WT vs I703A p = 0.0077). **C,** The pHTm surface fraction is unchanged by the introduction of mutations to pH-APP-BFP2 (one-way ANOVA, F (2, 245) = 1.267, p = 0.2835). For **B** and **C,** WT n = 84, G700A n = 96, and I703A n = 68, where n is the number of synapses from multiple fields of view.

We determined that the γ-secretase cleavage was not affected by the mutation: the

mean value of BFP2 fluorescence was not significantly altered compared to the wild type (not shown), and both mutants responded as expected to the γ-secretase inhibitor. The overall ratio of N/C APP was not changed by the mutations (**Figure 26A**). However, because G700A has an increased total pHluorin signal (see **Figure 32** in the **Appendix** for details), we determined it is likely somewhat resistant to α- or β-cleavage. In some experiments, we chose I703A to focus on because we wanted to separate cleavage from cholesterol binding.

γ-secretase and APP mutations

Next, we asked if these increases can be augmented by inhibiting γ-secretase. All three genotypes were equally cleavable by γ-secretase and thus susceptible to γ-secretase inhibition, because their total pHluorin vs. BFP2 ratio were all significantly decreased (**Figure 26A**). When measuring surface APP fraction, γ-secretase inhibitor did not increase it any further in the two mutants (**Figure 26B**), which was the same as the result of MβCD plus γ-secretase inhibitor treatment. Also, we do not think this was due to a ceiling effect because the increase of surface APP fraction in both mutants was still far less than MβCD-caused increase (**Figure 23**). Again, this outcome suggests APP's binding to cholesterol involves in controlling APP distribution in the plasma membrane and acts independently from γ-secretase. Taken together, all our data have demonstrated that APP's neuronal surface distribution is closely regulated, inversely related to γ-secretase activity as well as the plasma membrane cholesterol, and both γ-secretase and cholesterol-binding to APP acts independently.

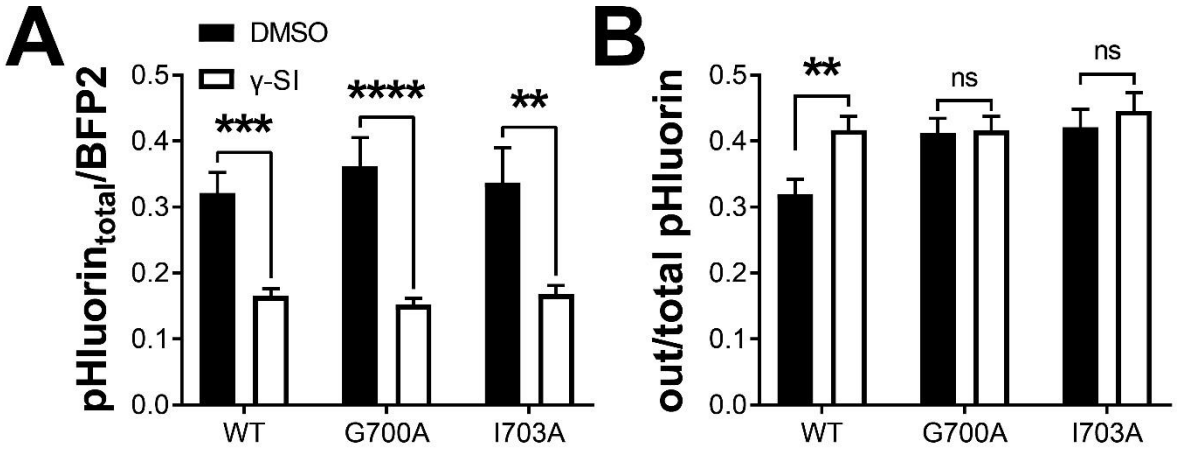

Figure 26: The effect of γ-inhibition on the APP mutants. A, All mutants are affected by the γ-SI, demonstrating that γ-secretase is able to cleave them. Two-way ANOVA indicated that only application of the secretase inhibitor affected the pHluorin total to BFP2 ratio. In summary, there was no effect due to mutation ($F(2, 531) = 0.1346$, $p = 0.8741$), significant variance from γ-SI treatment ($F(1, 531) = 54.6$, $p < 0.0001$), and no interaction ($F(2, 531) = 0.5277$, $p = 0.5903$). The results of Sidak's multiple comparisons test comparing only the untreated and the γ-SI treated samples within each APP variant are shown on the plot (WT, ***, $p = 0.0002$; G700A, ****, $p < 0.0001$; I703A, **, $p = 0.0013$). **B,** Two-way ANOVA was used to investigate the effects of γ-inhibition on the mutants. Although the interaction between APP sequence and γ-SI treatment did not quite reach significance with $\alpha = 0.05$ (interaction $F(2, 531) = 2.421$, $p = 0.0898$), when Sidak's multiple comparisons test was used only to compare vehicle control to γ-SI, γ-SI significantly increased the surface fraction of the wild-type ($p = 0.0062$) but not the mutants (G700A, $p = 0.9984$ and I703A, $p = 0.8847$). ANOVA confirmed that γ-SI treatment ($F(1, 531) = 4.791$, $p = 0.0290$) and cholesterol-binding deficiency ($F(2, 531) = 4.022$, $p = 0.0185$) cause significant alterations in pHluorin surface fraction unlikely to occur by chance when the entire data set is considered. N is the total number of synapse ROIs from at least 3 experiments for every condition: WT n = 84, G700A n = 96, I703A n = 68, WT+γ-SI n = 112, G700A+γ-SI n = 114 and I703A+γ-SI n = 63. All error bars represent SEM.

Effects of APP mutations on cholesterol level

To determine whether the mutation causes changes in cholesterol trafficking, we transfected cells with SypHTm-pH-APP and performed AM1-43 and filipin staining. AM1-43 was used to define the processes and pHTm was used to manually identify transfected cells (**Figure 27A**). We found that cells transfected with I703A have a significantly lower raw filipin signal than cells transfected with the wild type (**Figure**

27B), however we did not see any change in G700A. We applied the filipin at 4°C to decrease permeabilization of the cells as much as possible, so the filipin decrease suggests a decrease in surface cholesterol level specifically. Next, we used AM1-43 to normalize the filipin signal to the total membrane signal to ensure that the effect was cholesterol-specific and to determine if G700A affects cholesterol concentration in the membrane rather than the actual amount measured with raw filipin. We found that the decrease in filipin/AM1-43 in I703A-expressing cells compared to WT is even more pronounced than the decrease in raw filipin (**Figure 27C**), and that G700A does decrease the cholesterol concentration to a lesser extent. This indicates that it is specifically the plasma membrane cholesterol concentration that is decreased in mutant-expressing cells. I703A APP has a stronger effect on cholesterol than G700A APP. Perhaps G700A's cleavage resistance is responsible for its diminished effects on cholesterol.

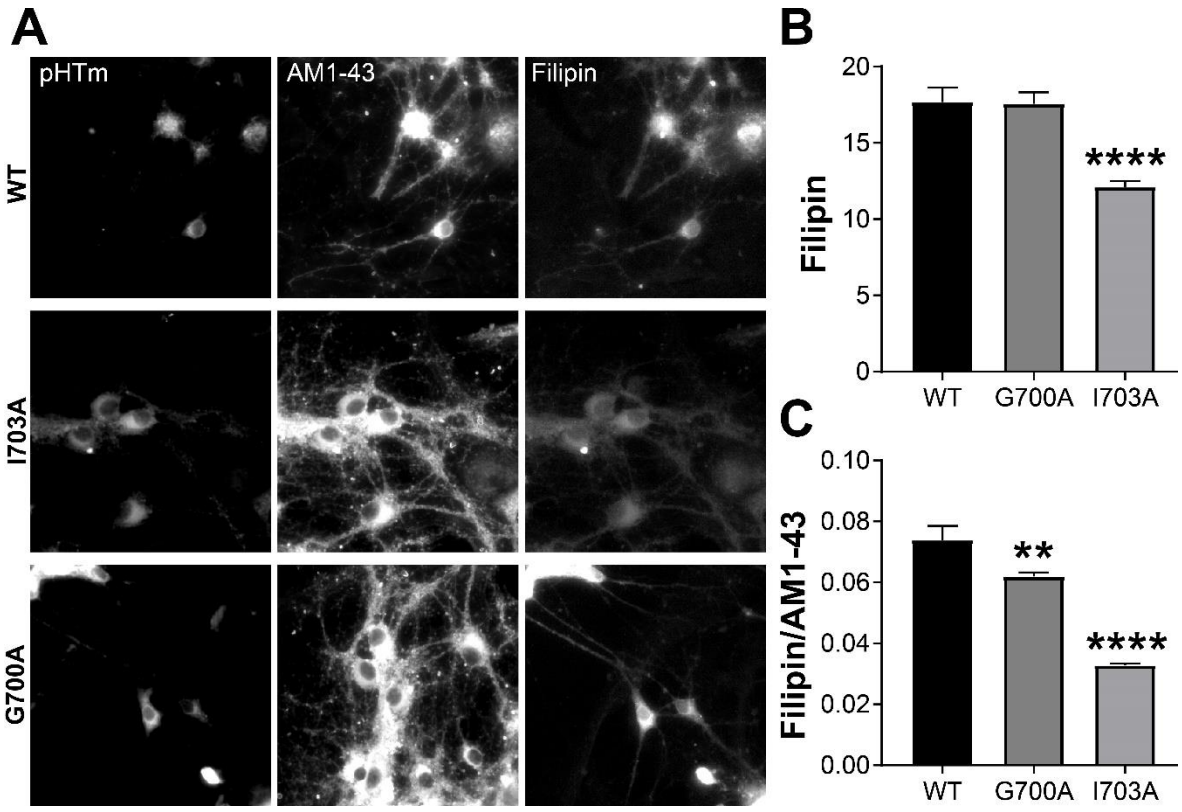

Figure 27: Cholesterol-binding deficient mutant APP decreases cholesterol in neuronal processes. A, Background-subtracted sample images of filipin staining experiments. Cells were transfected with SypHTm-pH-APP, either WT APP, G700A or I703A. After fixation, pHTm is visible and was used to differentiate transfected cells from untransfected neighbors. AM1-43 was used to identify processes and for normalization (see **Figure 28**, which shows that pHluorin signal is negligible). **B,** Quantification of the raw filipin signal in arbitrary units. One-way ANOVA was used to compare the three conditions and significant variance was detected ($F(2, 911) = 28.349$, $p < 0.0001$). Cells transfected with I703A have a significantly lower raw filipin signal compared to WT according to Dunnett's multiple comparisons test (****, $p = 0.0001$), but no there was no difference between G700A and WT (ns, $p = 0.9908$). **C,** Mean filipin/AM1-43 in transfected process segments. When AM1-43 is used to normalize the filipin signal, Dunnett's multiple comparisons test, performed after one-way ANOVA ($F(2, 911) = 89.127$, $p < 0.0001$), demonstrates that both G700A (**, $p = 0.004$) and I703A (****, $p = 0.0001$) are different from WT. For **B** and **C,** the n for WT is 264, the n for G700A is 206, and n for I703A is 444, where n is the number of process segments from 3 fields of view each.

It should be noted that some pHluorin may still be visible in the green channel after fixation, although the pHluorin signal was too weak to differentiate transfected cells from non-transfected cells even at the soma by visual inspection. We tested to

determine whether pHluorin makes a difference in the apparent AM1-43 signal in the processes before normalization. By comparing transfected cells with neighboring untransfected cells, we found that pHluorin's impact on the apparent AM1-43 signal is negligible (**Figure 28A**). Since there is little difference in signal even between transfected and untransfected cells, we reasoned that AM1-43 signal can be used to accurately measure and compare the total membrane in SypHTm-pH-APP-expressing cells. Furthermore, there is bleed-through of AM1-43 in the red channel. Unlike pHluorin, we found that pHTm's apparent signal was still much higher in the processes of transfected cells than untransfected cells (**Figure 28B**). In the soma, this difference is detectable by eye – apparently transfected somas were chosen based on pHTm signal and the connected processes were quantified in **Figure 27** and **Figure 28**.

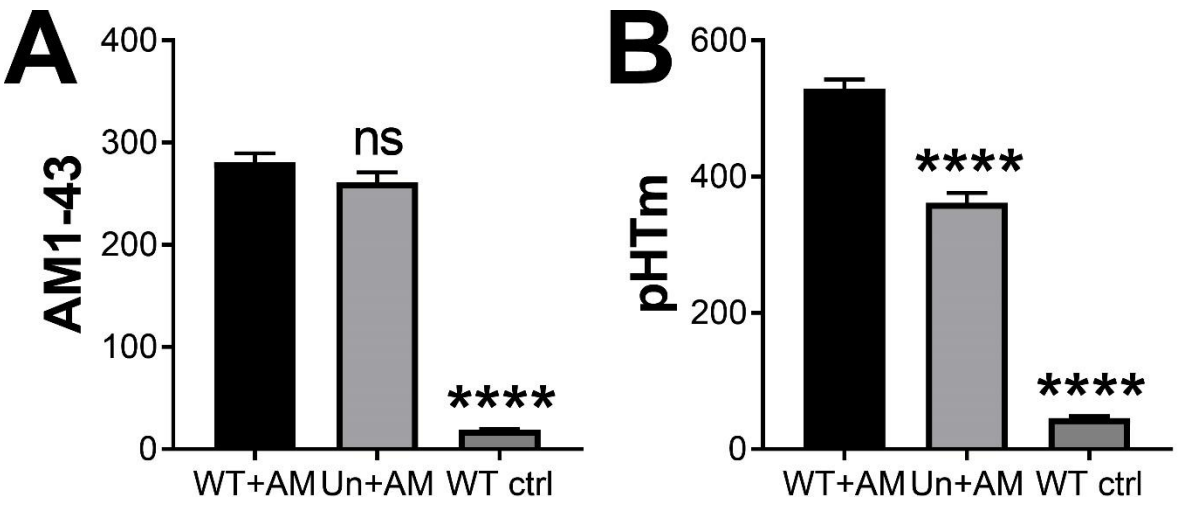

Figure 28: pHluorin is negligible in AM1-43 treated cells, but pHTomato is detectable. **A,** Apparent mean intensity of AM1-43 in transfected processes treated with AM1-43, neighboring untransfected cells treated with AM1-43, and transfected cells that were not treated with AM1-43. Although pHluorin, which spectrally overlaps with AM1-43, is present in transfected cells, it is not detectable at this magnification. One-way ANOVA was used to compare the three conditions and significant variance was detected (F (2, 826)

= 220.96, $p < 0.0001$). Dunnett's multiple comparisons test showed that there is a drastic difference in signal between transfected cells that have or have not been treated with AM1-43 (****, $p = 0.0001$), but no difference between transfected and untransfected AM1-43 treated-cells despite pHluorin (ns, $p = 0.1365$). **B,** Apparent mean intensity of pHTm in transfected processes treated with AM1-43, neighboring untransfected cells treated with AM1-43, and transfected cells that were not treated with AM1-43. One-way ANOVA was used to compare the three conditions and significant variance was detected ($F(2, 826) = 269.77$, $p < 0.0001$). Although AM1-43 bleed-through clearly affects the signal in treated vs untreated transfected cells (Dunnett's multiple comparisons test, ****, $p = 0.0001$), there is still a significant difference between transfected and untransfected cells after AM1-43 (Dunnett's multiple comparisons test, ****, $p = 0.0001$). For both **A** and **B,** n for WT+ AM1-43 is 400, n for neighboring untransfected cells + AM1-43 is 256, and n for WT transfected untreated is 173, where n is the number of process segments.

Cholesterol depletion compromises cells transfected with APP mutants

Since cholesterol is critical for neuronal membrane integrity [321, 322, 326] and functionally essential for the origination as well as the recycling of synaptic vesicles [327, 328], we set out to test the functional significance of APP's cholesterol-binding and surface distribution for presynaptic terminals. To simulate neuronal membrane cholesterol reduction during aging [329, 330], we again used the mild MβCD treatment (1 mM for 90 min) in cultures expressing wild type or I703A APP. We found that the MβCD treatment caused significant swelling of synaptic boutons (i.e. SypHTm puncta) in mutant but not wildtype-expressing neurons (**Figure 29A**), which was confirmed by a significant increase in the area of SypHTm puncta (**Figure 29B**). Intriguingly, MβCD significantly increased the surface APP fraction at synaptic boutons in both wildtype and I703A (**Figure 29C**), suggesting that membrane cholesterol reduction was still able to drive the surface APP increase regardless of the point mutation. Similarly, MβCD also increased surface SypHTm at synaptic boutons in both cases (**Figure 29D**).

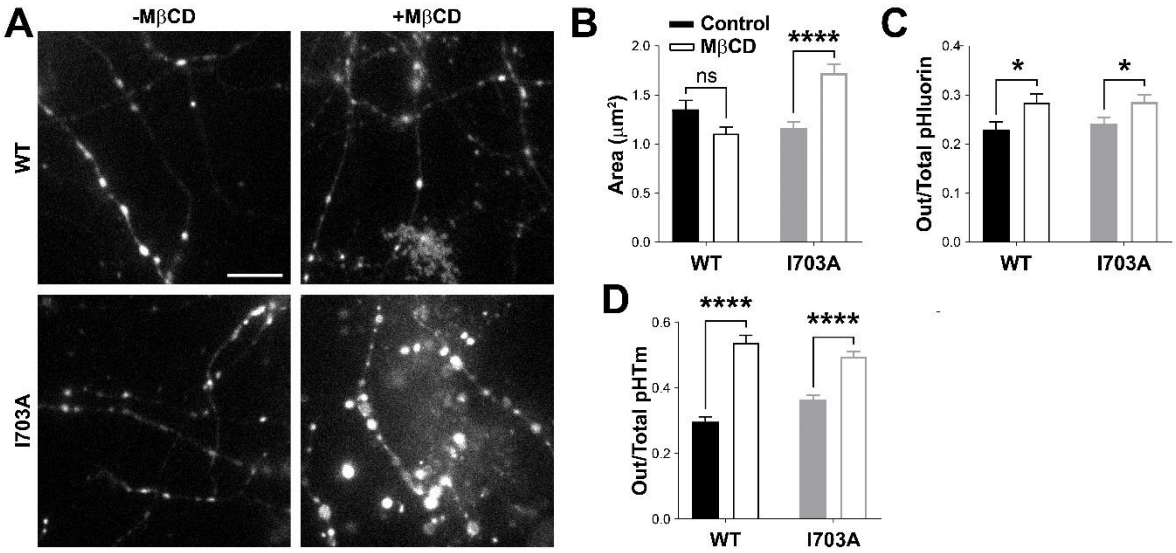

Figure 29: Point mutation in the cholesterol-binding motif renders presynaptic terminals vulnerable to membrane cholesterol reduction. A, sample pHTm images of cells expressing wild type (WT) and mutant (I703A) pH-APP-BFP2 with or without MβCD treatment. Fields of view were not excluded based on failure to respond to NH_4Cl (provided that they responded to pH 5.5), because dead or otherwise compromised cells and synapses are intended to be included in this analysis. The scale bar is 10 μm. **B,** mean area of synapses. Two-way ANOVA found a significant interaction between the mutation and treatment ($F(1, 746) = 21.34$, $p < 0.0001$), a singificant difference between the WT and I703A ($F(1, 746) = 6.341$, $p = 0.0120$), but treatment itself failed to reach significance ($F(1, 746) = 3.33$, $p = 0.0684$). Sidak's mutliple comparisons test showed, in fact, that the MβCD's effect on synapse size is specific to I703A ($p < 0.0001$) and does not occur in the WT ($p = 0.1589$). WT, n = 129 (FOV = 3); WT + MβCD, n = 135 (FOV = 4); I703A, n = 230 (FOV = 3); I703A + MβCD, n = 256 (FOV = 5), where n is the number of ROIs corresponding to SypHTm-marked synaptic boutons. **C,** average surface vs. total pHluorin ratios of two genotypes with or without MβCD treatment. Two-way ANOVA detected a significant difference after MβCD ($F(1, 746) = 11.16$, $p = 0.0009$). No interaction ($F(1, 746) = 0.1938$, $p = 0.7355$) and no effect due to the mutation ($F(1, 746) = 0.1938$, $p = 0.6599$) detected. Sidak's multiple comparisons test showed that MβCD significantly increased the ratio in WT and I703A (*, $p = 0.0446$; *, $p = 0.0232$, respectively. Same data set as B). **D,** average surface vs. total pHTm ratios of two genotypes with or without MβCD treatment. Two-way ANOVA detected significant differences between treatments ($F(1, 746) = 134.7$, $p < 0.0001$) but not genotype ($F(1, 746) = 0.5147$, $p = 0.4733$), however there was an interaction ($F(1, 746) = 11.81$, $p = 0.0006$). Sidak's multiple comparisons test showed that MβCD had a significant effect on the ratio for WT and I703A (****, $p < 0.0001$ and ****, $p < 0.0001$.

To understand how the synaptic swelling occurred and how the mutated APP was involved, we set up time-lapse imaging for pHluorin, BFP2 and pHTm during the

MβCD treatment (**Figure 30**). As described before, I703A had brighter pHluorin and pHTm fluorescence than the wild type to start with. During the course of the MβCD treatment, pHluorin fluorescence was significantly increased further at synaptic boutons expressing both wildtype and I703A (**Figure 31A**). However, the increase in wild type was relatively small and mostly occurred at the beginning of the MβCD treatment whereas the increase in I703A was significantly large and continued through the whole treatment, matching the abnormal swelling of synaptic boutons. In contrast, BFP2 fluorescence remained the same in both cases, indicating either unchanged γ-secretase activity or APP/CTF degradation by other means (**Figure 31B**).

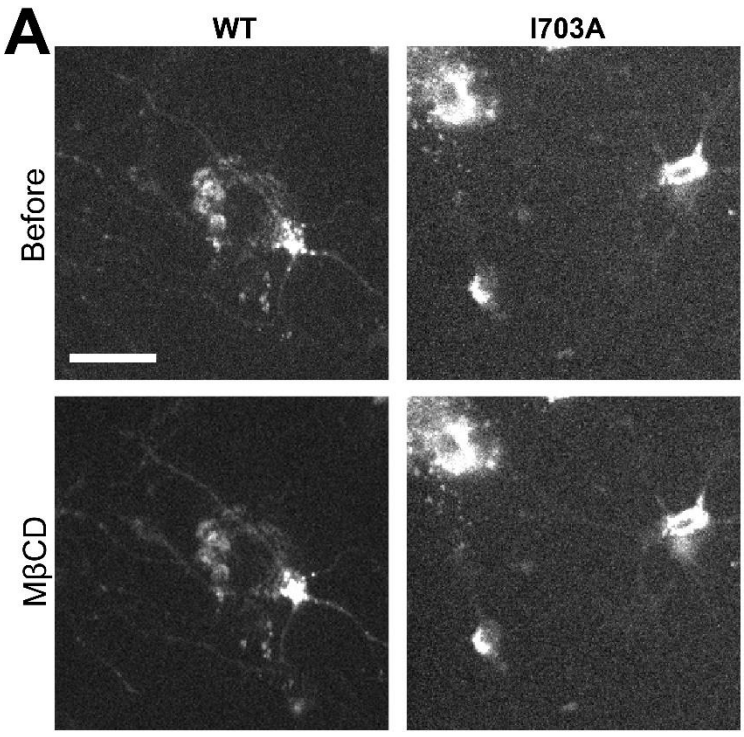

Figure 30: Example images of pHTm during the MβCD mutant time course. These images show the pHTm channel immediately before and immediately after 90 minutes of MβCD perfusion. The scale bar is 50 μm.

The increase of surface APP at synaptic boutons was unlikely caused by excessive exocytosis of synaptic vesicles as pHTm showed no further increase in both wildtype and I703A groups during MβCD treatment (**Figure 31C**). A more detailed look at this data set, including statistics and G700A pH-APP-BFP2, can be found in the Appendix in **Figures 33** and **34**. Together, this set of experiments suggests that, when membrane cholesterol was reduced, disruption of cholesterol-binding unleashed the restriction on APP surfacing, which was independent of synaptic vesicle turnover and was detrimental to synaptic boutons.

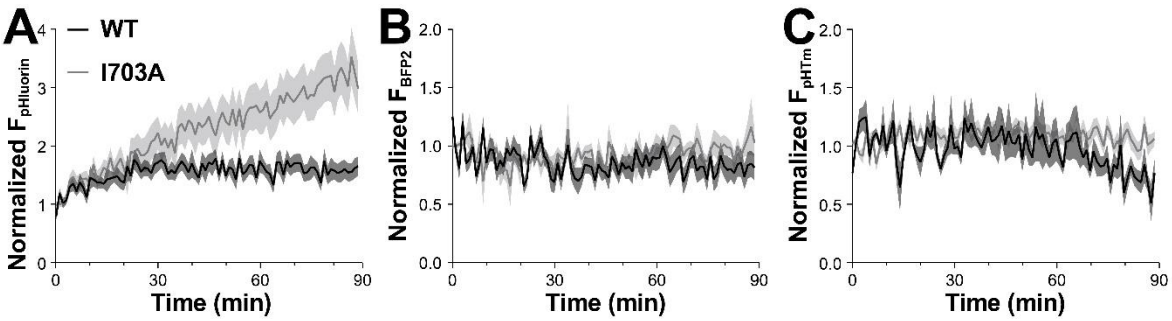

Figure 31: Point mutation in the cholesterol-binding motif causes unregulated pHluorin surface trafficking after MβCD. A-C, average fluorescence changes over time after application of MβCD. WT, n = 48 ROIs; I703A, n = 53 ROIs. (A), BFP2 (B) and pHTm (C) in WT (black) and I703A mutant (gray) during 90-min 1 mM MβCD treatment. Only pHluorin in the mutant group exhibited a consistent increase throughout the treatment. Fluorescence intensities were normalized to pretreatment baseline (set as 1). Shadows represent SEM.

Discussion

Cholesterol has been suspected as a pathological factor in AD, although it remains unclear whether it is the cholesterol in lipoproteins, in cell membranes, or in both that is responsible [297]. For example, cholesterol has been related to Aβ clearance via

low density lipoprotein receptor-related protein 1 (LRP1) [331] and to Aβ production via altering secretase activity [332]. The fact that our moderate MβCD treatment significantly reduced the total pHluorin fluorescence is in agreement with the latter idea, especially because α-secretase cleavage was greatly promoted by lowering the plasma membrane cholesterol. Despite the overall APP reduction, we discovered that the surface fraction of APP was relatively increased, likely due to reduced internalization. When we combined MβCD with the γ-secretase inhibitor, we found no further increase in surface APP fraction, pointing to a dominant role of membrane cholesterol in determining the surface APP concentration. Furthermore, the increase of surface APP is not directly caused by a change in γ-secretase activity because the I703A mutation increased surface APP without affecting γ-secretase cleavage. However, it is possible that γ-secretase, by regulating membrane cholesterol, indirectly contributes to the increase of surface APP [85], which is consistent with the dominance of MβCD and the I703A mutation over the γ-secretase inhibitor in increasing surface APP.

Another explanation for the MβCD-associated increase in the surface APP fraction is that reducing membrane cholesterol interrupts the retrieval of synaptic vesicles [327, 333], which is supported by the increase of surface SypHTm. In fact, a more recent study demonstrated concentration-dependent differences in the effects of MβCD on the synapse [334]. Mild cholesterol reduction impaired endocytosis whereas severe depletion impaired both endo- and exocytosis. However, in our tests, the increase of surface APP did not match that of surface SypHTm proportionally and it is

questionable whether synaptic vesicles had enough APP to be accountable for the increase. Cossec et al. also found that cholesterol depletion increased the level of surface APP, consistent with our results that increasing plasma membrane cholesterol decreases the surface fraction of APP via clathrin-mediated endocytosis (CME) [96]. If so, the explanation for our data can involve more than synaptic vesicle endocytosis as CME is essential for many other forms of surface membrane internalization. For example, the well-established LRP1-mediated endocytosis of APP is via CME as well [335]. Reduced clustering in lipid rafts is also a potential contributor to reduced endocytosis [336].

Recently, a structure-based study revealed a cholesterol-binding motif made of the C-terminal of APP's ectodomain and the N-terminal of its transmembrane domain [90], supporting the notion that APP directly and specifically interacts with cholesterol in cell membranes. Interestingly, overexpression of APP was recently found to decrease neuronal activity via reducing cholesterol turnover, and APP's transmembrane domain containing part of the cholesterol binding motif is required for this effect [254]. Our tests using the APP point mutation confirm that this cholesterol-binding capability is physiologically significant. The fact that the mutation increased surface distribution without changing SypHTm distribution or secretase cleavage suggests that cholesterol-binding either facilitates APP internalization or prevents its surfacing independent of synaptic vesicle turnover. Adding a γ-secretase inhibitor failed to increase its surface fraction, further confirming that cholesterol directly regulates APP surface distribution. More importantly, the overexpressed APP mutant rendered

the mild MβCD treatment destructive to neurons, i.e. causing severe swelling of synaptic boutons. The synaptic swelling was accompanied by massive surfacing of mutated APP, indicating dysregulation of APP and lipid membranes. The fact that mutant APP showed an increase in surface localization during MβCD treatment implies that APP surfacing is driven by membrane cholesterol but may not require direct binding between APP and cholesterol. Instead, it may be the APP internalization that requires direct cholesterol binding, which is consistent with the net increase of surface APP caused by the mutation without other treatments.

Our results with the mutants APP during cholesterol depletion support the notion that APP is essential for maintaining cholesterol homeostasis and for the integrity of presynaptic membranes, which points to a less appreciated link between APP and APOE [337]. Additionally, the decreased filipin staining demonstrated that cholesterol trafficking is indeed disrupted by expression of APP with the I703A mutation. Our results support the idea that APP facilitates trafficking of cholesterol to the cell surface via direct binding. The association between APP and membrane cholesterol may also help to reconcile various cellular functions proposed for APP, because membrane cholesterol, especially via membrane microdomains, has broad physiological impacts on various cellular processes like transmembrane signaling and membrane trafficking [329, 338]. We postulate that APP is a cholesterol sensor for cholesterol homeostasis between presynaptic surface and intracellular membranes. It is well documented that presynaptic terminals, especially the synaptic vesicles they contain, have a much higher concentration of cholesterol in comparison to that of the

plasma membrane [339], whereas other intracellular organelles like endosomes have far less membrane cholesterol than the plasma membrane. This means that activity-evoked vesicle release will lead to a substantial increase of cholesterol in the surface membrane and a correspondingly profound decrease in vesicular and other intracellular membrane at the presynaptic terminals. Intriguingly, APP resembles the well-studied sterol regulatory element binding protein (SREBP) [340] in several aspects including intracellular membrane localization, cholesterol-sensitivity, cleavage by regulated intramembrane proteolysis, and the function of their proteolytic products (i.e. transcription factor for cholesterol metabolism genes). It is very likely that disrupted cholesterol homeostasis and APP processing are intertwined during Alzheimer's disease pathogenesis, especially SAD.

Chapter VI

CONCLUSIONS AND FUTURE DIRECTIONS

Potential mechanisms directing APP localization

To best deal with technical challenges such as cell type heterogeneity and morphological complexity imposed by CNS neurons, we conducted live cell imaging. First, we generated pH-APP-BFP2 by adding pH-insensitive BFP2 to pH-APP's C-terminal. We also co-expressed a pH-sensitive red fluorescence reporter selective for synaptic vesicles, Synaptophysin-pHTomato (SypHTm) [267], which enables us to evaluate the spatiotemporal correlations between APP and synaptic vesicles. We performed multichannel live cell imaging to investigate APP's subcellular distribution, trafficking and association with synaptic transmission as well as the coupling between APP trafficking and cleavage, and its relationship to membrane cholesterol. Our results not only revealed an intricate coupling of APP's trafficking and processing, but also its involvement in membrane cholesterol homeostasis, especially at the plasma membrane at presynaptic terminals.

Our results showed that in primary neurons a substantial quantity of APP is transported to the cell surface immediately after it is produced before being cleaved by α-secretase or endocytosed. We speculated that α-secretase and dynamin-mediated endocytosis are part of a tightly regulated mechanism that controls the

surface concentration of APP. Next, we show that inhibition of alpha and beta secretases resulted in a decrease in surface APP. An examination of the background subtracted absolute values reveals that β-inhibition's effect is likely due to a buildup of APP internally, likely in the endosomes. However, treatment with the α-secretase inhibitor actually resulted in an overall increase in surface APP, at least according to the raw fluorescence values, although the increase was greater in the internal APP. This indicates that α-secretase cleavage is indeed likely to be part of the mechanism that controls the surface level of APP, while β-secretase cleavage is not. However, γ-inhibition caused an increase in APP surface fraction, although it cannot cleave full-length APP. A cleavage-independent role for γ-secretase in APP trafficking has been observed before[196, 198, 199]. It is most likely heavily involved in the regulation of both APP and cholesterol homeostasis [85].

We are not the first to perform live cell imaging experiments using APP, but our results are very useful for interpreting the current literature. By labeling APP and BACE1 with two different fluorescent proteins or two complementary parts of one fluorescent protein, Roy and his colleagues revealed activity-dependent and independent convergence of these two proteins in different intracellular compartments in hippocampal neurons [286, 287]. This convergence occurred in the dendrites, which suggests that the nearly 70% of secreted Aβ that can be attributed to synaptic activity [341] is produced at the dendrites. Interestingly, Groemer et al. tagged APP's N-terminal with a pH-sensitive green fluorescence protein (i.e. pHluorin) to evaluate the coupling between APP trafficking and synaptic vesicle

turnover [243]. By contrast, this paper demonstrated progressive fluorescence loss after rounds of stimulation at the synapse, which they attribute to cleavage (and speculate is β-cleavage). Groemer followed up on this paper by tagging BACE1 as Das et al. did [288]. In this paper, Bauereiss et al. use live cell imaging to demonstrate that APP and BACE1 are both trafficked to the cell surface separately [288]. They also reported (in agreement with the literature [45, 158]) that α-secretase cleavage does indeed predominate at the surface. This is consistent with our results, although these experiments were performed is a cell line and not neurons.

Taken together with our own results, we speculate that the activity-dependent proteolysis of APP/CTF by BACE1 mostly occurs at somatodendritic regions, whereas APP/CTF at the distal synaptic boutons behaves differently. While we did find that at some synapses there is an activity-dependent increase of APP on the cell surface, we speculate that this is due to its association with membrane cholesterol. In Groemer et al.'s paper, the experiments that showed cleavage in response to stimulation were performed in such a way as to minimize photobleaching. Between rounds, the cells were exposed to NH4Cl which is the only time images were taken. Therefore, it cannot be determined where the remaining APP is. It is possible, in light of our results that appear to show increased α-cleavage at the synapse in a short time in response to MβCD, that α-cleavage in response to the increased surfacing is decreasing the signal. Furthermore, Bauereiss et al. demonstrated that APP and BACE1 are also endocytosed separately [288]. This has been observed before and is likely controlled by ARF6[342]. This can be interpreted as supporting the idea that synaptic vesicle turnover is unlikely to

increase the convergence of APP and BACE1 at the synapses. Combining pH-APP-BFP2 with red fluorescent protein-tagged secretases like ADAM10 and BACE1 and applying acute stimulation could be used to address those questions in the future.

In Chapter IV, we focused heavily on the axons. Although we did find that the surface fraction of APP was changed by the BACE inhibitor at the synapses, this result does not confirm that β-cleavage occurs at the synapses because the proteins were given a minimum of 24 hours to redistribute. It is possible that the secretase inhibitors change the subcellular localization as well, not just the surface fraction at the processes. Follow-up experiments could examine the dendrites. A fuller picture focusing on the dendrites and the soma would add dimension to our results, especially in combination with tagged secretases. For example, if β-cleavage largely occurs in the somatodendritic region, will the change in surface fraction be even more profound there? Did β-inhibition cause a decrease in surface fraction to synaptic and nonsynaptic areas along axons (identified based on morphology) because some fraction of β-cleavage occurs there?

Finally, in Chapter V we demonstrated that cholesterol depletion and cholesterol binding-deficient mutations both caused increases in surface fraction. In spite of the fact that the overall APP level was decreased, and the surface concentration was also decreased, cholesterol depletion still caused an overall increase in surface fraction. This would suggest that α-secretase cleavage, most likely upregulated by the cholesterol depletion, is not the sole arbiter of APP surface fraction. Cholesterol concentration controls APP surface fraction as well via a mechanism that requires

direct APP binding. Future experiments may determine whether the cholesterol depletion increases exocytosis to the cell surface or decreases endocytosis.

A role for APP in cholesterol homeostasis

Acute regulation of cholesterol at the synapses

While our data showed that APP did surface during stimulation, the rate was much slower than that of Syp, a synaptic vesicle protein. Additionally, the surface fraction of APP at synaptic boutons was significantly more than that of Syp. One possibility is that APP is localized to the presynaptic active zone and endosome/lysosome membranes, but not to synaptic vesicles. Hence, only prolonged stimulation that forced vesicle regeneration from endosomes was able to move a limited fraction of intracellular APP to the presynaptic surface. Alternatively, it could reflect a tightly coupled vesicle retrieval mode [309] in which the surfacing and internalization of vesicular APP were balanced at the beginning of stimulation, but that was eventually unbalanced by extensive vesicle release. In addition, a continuous decay of pHluorin fluorescence after stimulation stopped suggests that the externalized APP has to be removed to keep the surface APP level steady.

However, in our tests, the increase of surface APP did not match that of surface SypHTm proportionally and it is questionable whether synaptic vesicles had enough APP to be accountable for the increase. Cossec et al. also found that cholesterol depletion increased the level of surface APP, consistent with our results that

increasing plasma membrane cholesterol decreases the surface fraction of APP via clathrin-mediated endocytosis (CME) [96]. If so, the explanation for our data can involve more than synaptic vesicle endocytosis as CME is essential for many other forms of surface membrane internalization. For example, the well-established LRP1-mediated endocytosis of APP is via CME as well [335]. Reduced clustering in lipid rafts is also a potential contributor to reduced endocytosis [336].

Based on our observation about its surfacing in relationship to activity, γ-secretase inhibition, MβCD and its own cholesterol-binding motif, we propose that APP can be a multifunctional player in retrieving surfaced membrane cholesterol, balancing intracellular membrane turnover and sensing endosomal cholesterol sensing, all of which agree well with APP's abundance in both surface and intracellular membrane sections and at presynaptic terminals. The mutual regulation between APP and LRP1 [343, 344] also supports this idea. In the future, we could determine if disabling LRP1 (e.g. knockdown) or the more ubiquitous dynamin (e.g. Dynasore, a membrane-permeable dynamin inhibitor) will affect this MβCD-associated surface APP fraction increase. While our study demonstrates the physiological relevance of APP-cholesterol binding and the functional significance of APP's cholesterol-binding motif, it also raises many interesting questions about the relationship between membrane cholesterol, APP and secretases. With the increasing capabilities of fluorescent microscopy, the time seems ripe to test these questions in CNS neurons in vitro or even in vivo. With the help of optogenetics, these questions can and should be put into the context of synaptic

activity and the neuronal network, which will not only reveal the intrinsic function of APP but also its pathological relevance to AD.

Mutual regulation of APP, secretases, and cholesterol concentration

Surprisingly, the effect of the APP mutant was seemingly dominant negative as endogenous wildtype APP was still being expressed. The explanation for that may reside in APP's homodimerization or heterodimerization with CTF. Intriguingly, the cholesterol-binding motif partially overlaps with the proposed dimerization motif [90, 345], and competition between cholesterol-binding and APP/CTF-dimerization has been observed in a biophysical study [91]. Hence, it is possible that the mutant dimerized with wildtype APP or CTF and rendered them insensitive to membrane cholesterol change. Furthermore, the dimerization may also be accountable for the increase of surface APP after γ-secretase inhibition. Interestingly, Eggert et al. demonstrated that APP homodimers are preferentially located in the endosomes in HeLa cells, and that induced homodimerization reduces surface APP fraction [346]. We postulate that the competition with intracellularly accumulated CTFs after γ-secretase inhibition reduced APP homodimers and allowed more APP to reach the plasma membrane. Eggert et al. also showed that APP homodimerization reduced co-transport with the sorting protein, SorLA. Notably, the SorLA binding sites are in the APP N-terminus/ectodomain [347], which has been cleaved off of the CTFs. Therefore, APP/CTF heterodimers are likely to bind SorLA and potentially other sorting and transport proteins, thus escaping from the endosomes and ultimately reaching the

plasma membrane in higher concentrations than are otherwise possible. An additional molecular explanation Eggert et al. proposed was that APP dimerization blocks LRP1 binding. Unlike SorLA, LRP1 binds to the YENPTY motif in the cytoplasmic domain of APP [348] via the adaptor protein FE65 [348, 349]. Because the cytoplasmic domain is intact in the CTFs, APP/CTF heterodimers can be as resistant to LRP1 binding as APP homodimers. Long term inhibition of LRP1 binding to APP in cell lines [350] and knocking out LRP1 in primary neurons [335] both resulted in drastic increases in APP surface fraction and production of sAPPα. If γ-secretase inhibition increases the surface fraction of APP through promotion of heterodimerization of APP and CTF, it logically follows that α-secretase or β-secretase inhibition would decrease the surface fraction by increasing full length APP and decreasing the production of CTFs, which is in fact what we observe (**Figure 16**). The further increase of surface APP by the combination of all three secretase inhibitors was seemingly contradictory since a higher total pHluorin *vs.* BFP2 ratio indicated more holo-APP than that of γ-secretase inhibitor alone (**Figure 18K&W**). However, a comparison to α&β-secretase inhibition (**Figure 18T&W**) suggests that there was also significantly more CTF after inhibiting all three secretases. It is possible that other N-terminal cleavage events such as η-secretase cleavage [48] took over and generated more alternative CTFs equally capable of forming heterodimers with extra APP. It would also be interesting to test the formation of APP-CTF heterodimer and the impact of CTF overexpression on APP surface distribution, especially with γ-secretase inhibition, membrane cholesterol reduction, and/or with an APP point mutation. As

fluorescent methods like FRET have been developed to study APP/CTF dimerization in cells [345], it is possible to incorporate such an assay using spectrally compatible fluorophores.

APP and cholesterol pathology in Alzheimer's disease

Disrupted cholesterol homeostasis

John Hardy, one of the originators of the amyloid cascade hypothesis, wrote in 2017 that disrupted phospholipid regulation is most likely the key event in Alzheimer's disease pathogenesis [351]. The data still support the idea that amyloid deposition is the starting point in familial Alzheimer's disease, as he wrote decades ago[24]. But, sporadic Alzheimer's disease accounts for the overwhelming majority of Alzheimer's patients, and it is now becoming clear that sporadic Alzheimer's disease starts in the membranes.

Based on our data, it is very likely that APP acts as a regulator of cholesterol. Disrupted cholesterol regulation can be linked to most of the difference pathogenic processes that occur during Alzheimer's disease[85, 352-354]. There is strong evidence in the literature for mutual regulation of γ-secretase, APP and its cleavage products, and cholesterol, and our work now demonstrates that APP regulates cholesterol through direct binding.

Disrupted cholesterol can lead to overproduction of amyloid beta, as cholesterol accumulation and swelling occurs in the endosomes in AD [355, 356]. However, cholesterol trafficking is also critical for the normal functioning of the synapses, and

therefore normal cognition [254]. APOE4 or APP-mediated cholesterol deficits, such as an accumulation in the endosomes that would eventually prevents the synaptic vesicle pool from fully replenishing itself, are an alternate explanation for the synaptic dysfunction that takes place early in sporadic Alzheimer's disease before amyloid plaque deposition.

Implications for anti-amyloid therapies

Perhaps APP itself, not just Aβ, could be targeted in the future. Our results suggest that blocking APP-cholesterol direct binding would result in an increase of APP trafficking to the cell surface, and a decrease in plasma membrane cholesterol. This would increase cleavage through the non-amyloidogenic pathway and decrease production of Aβ. However, our results also warned against the dangers of this approach. It seems, based on the plasma membrane swelling and apparent rupture that occurred in the cells expressing the cholesterol mutants when cholesterol is depleted, that APP cannot perform its important regulatory functions if it is trapped at the cell surface.

In cases of sporadic Alzheimer's disease, dysfunction in cholesterol homeostasis is likely to precede and is partially responsible for Aβ overproduction. It is difficult to target cholesterol trafficking in the brain; there is conflicting evidence about whether decreasing systemic cholesterol using statins has any effect on Alzheimer's disease [357]. This is likely because cholesterol typically does not cross the blood brain barrier [53]. Therefore, APOE itself remains an extremely promising drug target, as does LRP1,

clusterin, ABCA7, TREM2, PLCG2, and many other proteins involved in cholesterol homeostasis in the brain.

Some of this chapter is reprinted (adapted) with permission from (DelBove, C. E., Deng, X., and Zhang, Q. (2018). The fate of nascent APP in hippocampal neurons: a live cell imaging study, *ACS Chemical Neuroscience*) [299]. Copyright (2018) American Chemical Society.

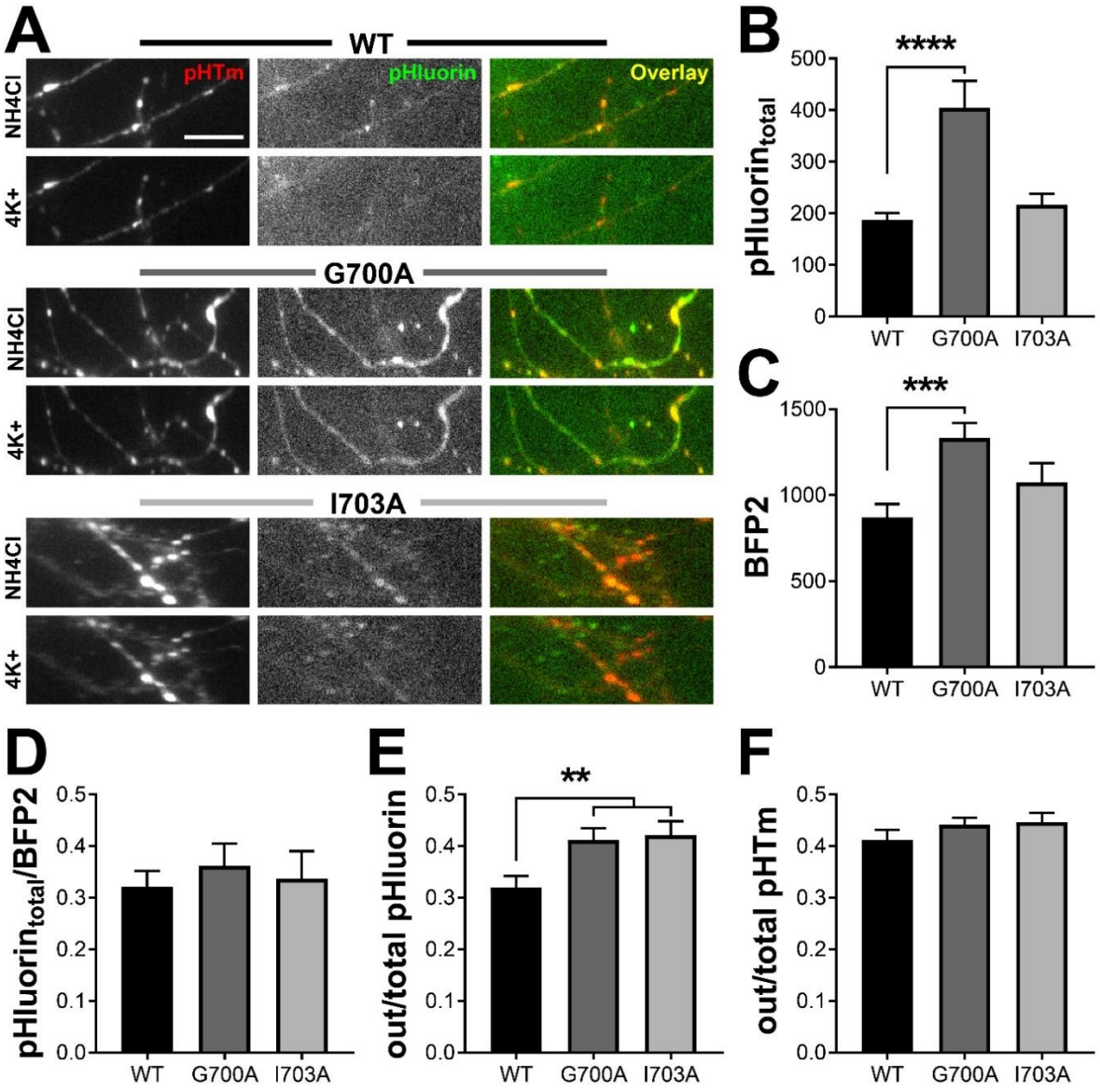

Figure 32: G700A but not I703A appears to affect cleavage of pH-APP-BFP2. A, Representative images of WT (top) and the mutants G700A and I703A are reproduced from **Figure 25** for reference. The scale bar is 10 μm. **B,** The G700A mutation, but not I703A, causes an increase in the total pHluorin at the synapses (one-way ANOVA, F (2, 245) = 11.16, $p < 0.0001$, Dunnett's multiples comparisons test: WT vs G700A, ****, $p = 0.0001$; WT vs I703A, ns, $p = 0.8177$). This suggests that cleavage is affected. **C,** G700A, but not I703A, causes an increase in BFP2 at the synapses (one-way ANOVA, F (2, 245) = 6.927, $p = 0.0012$, Dunnett's multiples comparisons test: WT vs G700A, ***, $p = 0.0005$; WT vs I703A, ns, $p = 0.2299$). **D,** Neither mutation affects the ratio of total pHluorin to BFP2 at the synapses (one-way ANOVA, F (2, 245) = 0.2601, $p = 0.7712$, Dunnett's multiples comparisons test: WT vs G700A, ns, $p = 0.6976$; WT vs I703A, ns, $p = 0.9539$). When taken together with **Figure 26A** which demonstrates that application of the γ-SI still affects the ratio, the data suggests that that the increase in both pHluorin and BFP2 is likely due to decreased α- or β-

cleavage. For context, **E** and **F** are reproduced from **Figure 25** for reference to assist in the interpretation of the major findings. **E,** G700A and I703A mutations cause an increase in the surface fraction of pHluorin at the synapses (one-way ANOVA, F (2, 245) = 5.652, p = 0.0040, Dunnett's: WT vs G700A, p = 0.008; WT vs I703A, p = 0.0077). **F,** The pHTm surface fraction is unchanged by the introduction of mutations to pH-APP-BFP2 (one-way ANOVA, F (2, 245) = 1.267, p = 0.2835). For **B** and **C,** WT n = 84, G700A n = 96, and I703A n = 68, where n is the number of synapses from multiple fields of view.

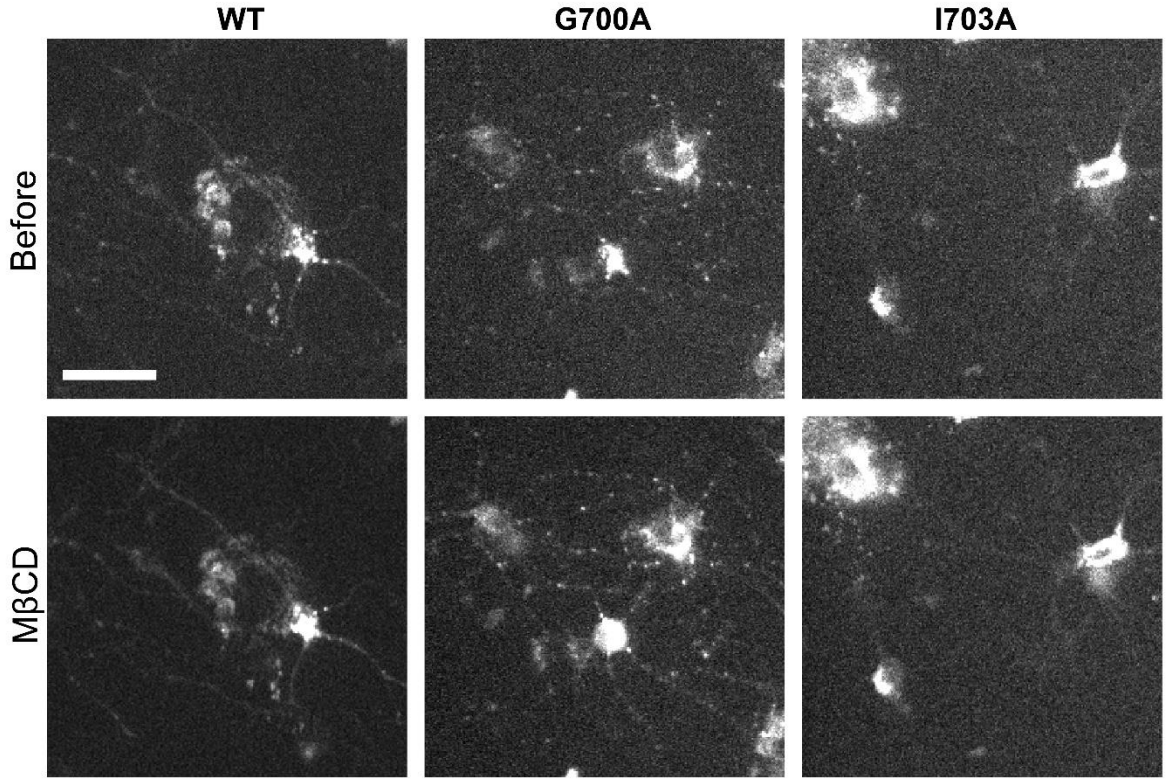

Figure 33: Images of pHTm during all 3 MβCD time course experiments. These images depict the first and last frame, and show the channel used to identify the synapses. The scale bar is 50 μm.

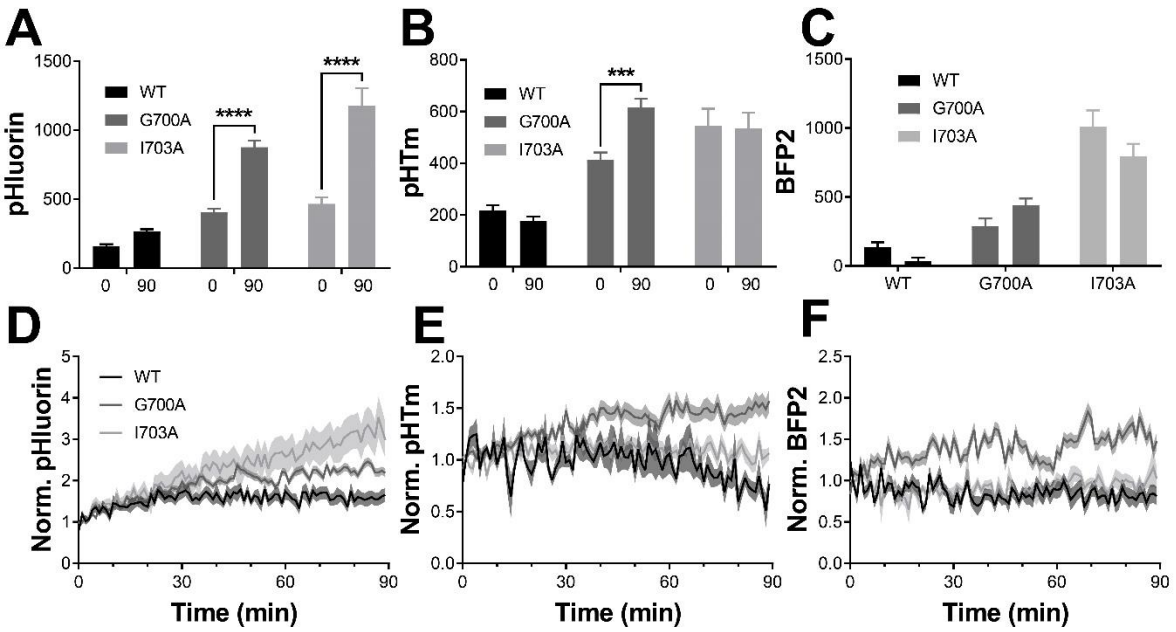

Figure 34: Detailed quantification of the effects of 90 minutes of MβCD on cells transfected with mutant pH-APP-BFP2. A, a direct comparison of the background subtracted value of pHluorin in the first and last frame of the time course experiment. After two-way ANOVA (Interaction, F (2, 352) = 11.86, $p < 0.0001$, Time, F (1, 352) = 79.37, $p < 0.0001$, Mutation, F (2, 352) = 50.05, $p < 0.0001$), Sidak's multiple comparisons test shows that only the mutants have a substantially increased pHluorin signal; (WT, ns, $p = 0.5751$; G700A, ****, $p < 0.0001$; I703A, ****, $p < 0.0001$). The p values are adjusted for multiple conditions and the surface fraction could not be directly measured, but the WT does show an increase as we would expect.
B, pHTm is only substantially increased by MβCD at the end of 90 minutes in the G700A transfected cell. Two-way ANOVA: (Interaction, F (2, 352) = 5.683, $p = 0.0037$; Time, F (1, 352) = 2.239, $p = 0.1355$; Mutation, F (2, 352) = 38.28, $p < 0.0001$). Sidak's was used to compare only the first and last frame within each APP variant: WT, ns, $p = 0.8995$; G700A, ***, $p = 0.0003$; I703A, ns, $p = 0.998$. **C,** No significant change in BFP2 after the time course**.** Two-way ANOVA: (Interaction, F (2, 352) = 4.109, $p = 0.0172$; Time, F (1, 352) = 0.9444, $p = 0.3318$; Mutation, F (2, 352) = 63.29, $p < 0.0001$). First and last frames compared with Sidak's: WT, ns, $p = 0.7113$; G700A, ns, $p = 0.2135$; I703A, ns, $p = 0.107$. **D-F**, average fluorescence changes over time after application of MβCD. WT, n = 48 ROIs; I703A, n = 53 ROIs. (**D**), BFP2 (**E**) and pHTm (**F**) in WT (black), G700A mutant (dark gray) and I703A mutant (light gray) during 90-min 1 mM MβCD treatment. The I703A mutant pHluorin exhibited a consistent increase throughout the treatment, while G700A appeared to level off at a higher level than the WT. Fluorescence intensities were normalized to pretreatment baseline (set as 1). Shadows represent SEM.

REFERENCES

[1] Alzheimer's Association. (2018) 2018 Alzheimer's disease facts and figures, *Alzheimer's & Dementia 14*, 367-429.

[2] Ziegler-Graham, K., Brookmeyer, R., Johnson, E., and Arrighi, H. M. (2008) Worldwide variation in the doubling time of Alzheimer's disease incidence rates, *Alzheimer's & Dementia 4*, 316-323.

[3] Montgomery, W., Ueda, K., Jorgensen, M., Stathis, S., Cheng, Y., and Nakamura, T. (2018) Epidemiology, associated burden, and current clinical practice for the diagnosis and management of Alzheimer's disease in Japan, *ClinicoEconomics and Outcomes Research: CEOR 10*, 13-28.

[4] Dodge, H. H., Buracchio, T. J., Fisher, G. G., Kiyohara, Y., Meguro, K., Tanizaki, Y., and Kaye, J. A. (2012) Trends in the Prevalence of Dementia in Japan, *Int. J. Alzheimers Dis. 2012*, 956354.

[5] Goren, A., Montgomery, W., Kahle-Wrobleski, K., Nakamura, T., and Ueda, K. (2016) Impact of caring for persons with Alzheimer's disease or dementia on caregivers' health outcomes: findings from a community based survey in Japan, *BMC Geriatr. 16*, 122.

[6] Sperling, R. A., Aisen, P. S., Beckett, L. A., Bennett, D. A., Craft, S., Fagan, A. M., Iwatsubo, T., Jack, C. R., Jr., Kaye, J., Montine, T. J., Park, D. C., Reiman, E. M., Rowe, C. C., Siemers, E., Stern, Y., Yaffe, K., Carrillo, M. C., Thies, B., Morrison-Bogorad, M., Wagster, M. V., and Phelps, C. H. (2011) Toward defining the preclinical stages of Alzheimer's disease: recommendations from the National Institute on Aging-Alzheimer's Association workgroups on diagnostic guidelines for Alzheimer's disease, *Alzheimer's & Dementia 7*, 280-292.

[7] Romanelli, M. F., Morris, J. C., Ashkin, K., and Coben, L. A. (1990) Advanced Alzheimer's Disease Is a Risk Factor for Late-Onset Seizures, *Arch. Neurol. 47*, 847-850.

[8] Palop, J. J., and Mucke, L. (2010) Synaptic depression and aberrant excitatory network activity in Alzheimer's disease: two faces of the same coin?, *Neuromolecular Med. 12*, 48-55.

[9] Rosen, J., and Zubenko, G. S. (1991) Emergence of psychosis and depression in the longitudinal evaluation of Alzheimer's disease, *Biol. Psychiatry 29*, 224-232.

[10] Lyketsos, C. G., Steele, C., Baker, L., Galik, E., Kopunek, S., Steinberg, M., and Warren, A. (1997) Major and minor depression in Alzheimer's disease: prevalence and impact, *J. Neuropsychiatry Clin. Neurosci. 9*, 556-561.

[11] Landes, A. M., Sperry, S. D., and Strauss, M. E. (2005) Prevalence of Apathy, Dysphoria, and Depression in Relation to Dementia Severity in Alzheimer's Disease, *J. Neuropsych. Clin. Neurosci. 17*, 342-349.

[12] Ropacki, S. A., and Jeste, D. V. (2005) Epidemiology of and Risk Factors for Psychosis of Alzheimer's Disease: A Review of 55 Studies Published From 1990 to 2003, *Am. J. Psychiatry 162*, 2022-2030.

[13] Tromp, D., Dufour, A., Lithfous, S., Pebayle, T., and Després, O. (2015) Episodic memory in normal aging and Alzheimer disease: Insights from imaging and behavioral studies, *Ageing Res. Rev. 24*, 232-262.

[14] Donaghy, P. C., and McKeith, I. G. (2014) The clinical characteristics of dementia with Lewy bodies and a consideration of prodromal diagnosis, *Alzheimers Res.*

Ther. 6, 46.
[15] Schneider, J. A., Arvanitakis, Z., Bang, W., and Bennett, D. A. (2007) Mixed brain pathologies account for most dementia cases in community-dwelling older persons, *Neurology 69*, 2197-2204.
[16] Viswanathan, A., Rocca, W. A., and Tzourio, C. (2009) Vascular risk factors and dementia: how to move forward?, *Neurology 72*, 368-374.
[17] Campion, D., Dumanchin, C., Hannequin, D., Dubois, B., Belliard, S., Puel, M., Thomas-Anterion, C., Michon, A., Martin, C., Charbonnier, F., Raux, G., Camuzat, A., Penet, C., Mesnage, V., Martinez, M., Clerget-Darpoux, F., Brice, A., and Frebourg, T. (1999) Early-Onset Autosomal Dominant Alzheimer Disease: Prevalence, Genetic Heterogeneity, and Mutation Spectrum, *Am. J. Hum. Genet. 65*, 664-670.
[18] Lista, S., O'Bryant, S. E., Blennow, K., Dubois, B., Hugon, J., Zetterberg, H., Hampel, H., and Shen, Y. (2015) Biomarkers in Sporadic and Familial Alzheimer's Disease, *J. Alzheimers Dis. 47*, 291-317.
[19] Bateman, R. J., Aisen, P. S., De Strooper, B., Fox, N. C., Lemere, C. A., Ringman, J. M., Salloway, S., Sperling, R. A., Windisch, M., and Xiong, C. (2010) Autosomal-dominant Alzheimer's disease: a review and proposal for the prevention of Alzheimer's disease, *Alzheimers Res. Ther. 3*, 1.
[20] Olsson, B., Lautner, R., Andreasson, U., Öhrfelt, A., Portelius, E., Bjerke, M., Hölttä, M., Rosén, C., Olsson, C., Strobel, G., Wu, E., Dakin, K., Petzold, M., Blennow, K., and Zetterberg, H. (2016) CSF and blood biomarkers for the diagnosis of Alzheimer's disease: a systematic review and meta-analysis, *Lancet N. 15*, 673-684.
[21] Reinhard, C., Hebert, S. S., and De Strooper, B. (2005) The amyloid-beta precursor protein: integrating structure with biological function, *EMBO J. 24*, 3996-4006.
[22] Kang, J., Lemaire, H. G., Unterbeck, A., Salbaum, J. M., Masters, C. L., Grzeschik, K. H., Multhaup, G., Beyreuther, K., and Muller-Hill, B. (1987) The precursor of Alzheimer's disease amyloid A4 protein resembles a cell-surface receptor, *Nature 325*, 733-736.
[23] Szaruga, M., Veugelen, S., Benurwar, M., Lismont, S., Sepulveda-Falla, D., Lleo, A., Ryan, N. S., Lashley, T., Fox, N. C., Murayama, S., Gijsen, H., De Strooper, B., and Chávez-Gutiérrez, L. (2015) Qualitative changes in human gamma-secretase underlie familial Alzheimer's disease, *J. Exp. Med. 212*, 2003-2013.
[24] Hardy, J., and Allsop, D. (1991) Amyloid deposition as the central event in the aetiology of Alzheimer's disease, *Trends Pharmacol. Sci. 12*, 383-388.
[25] Scheuner, D., Eckman, C., Jensen, M., Song, X., Citron, M., Suzuki, N., Bird, T. D., Hardy, J., Hutton, M., Kukull, W., Larson, E., Levy-Lahad, E., Viitanen, M., Peskind, E., Poorkaj, P., Schellenberg, G., Tanzi, R., Wasco, W., Lannfelt, L., Selkoe, D., and Younkin, S. (1996) Secreted amyloid beta-protein similar to that in the senile plaques of Alzheimer's disease is increased in vivo by the presenilin 1 and 2 and APP mutations linked to familial Alzheimer's disease, *Nat. Med. 2*, 864-870.
[26] De Felice, F. G., Wu, D., Lambert, M. P., Fernandez, S. J., Velasco, P. T., Lacor, P. N., Bigio, E. H., Jerecic, J., Acton, P. J., Shughrue, P. J., Chen-Dodson, E., Kinney, G. G., and Klein, W. L. (2008) Alzheimer's disease-type neuronal tau

hyperphosphorylation induced by A beta oligomers, *Neurobiol. Aging 29*, 1334-1347.
[27] Selkoe, D. J., and Hardy, J. (2016) The amyloid hypothesis of Alzheimer's disease at 25 years, *EMBO Mol. Med. 8*, 595-608.
[28] DaRocha-Souto, B., Scotton, T. C., Coma, M., Serrano-Pozo, A., Hashimoto, T., Sereno, L., Rodriguez, M., Sanchez, B., Hyman, B. T., and Gomez-Isla, T. (2011) Brain Oligomeric beta-Amyloid but Not Total Amyloid Plaque Burden Correlates With Neuronal Loss and Astrocyte Inflammatory Response in Amyloid Precursor Protein/Tau Transgenic Mice, *J. Neuropathol. Exp. Neurol. 70*, 360-376.
[29] Tang, Y., Scott, D. A., Das, U., Edland, S. D., Radomski, K., Koo, E. H., and Roy, S. (2012) Early and selective impairments in axonal transport kinetics of synaptic cargoes induced by soluble amyloid beta-protein oligomers, *Traffic 13*, 681-693.
[30] Wang, Z., Jackson, R. J., Hong, W., Taylor, W. M., Corbett, G. T., Moreno, A., Liu, W., Li, S., Frosch, M. P., Slutsky, I., Young-Pearse, T., Spires-Jones, T. L., and Walsh, D. M. (2017) Human brain-derived Abeta oligomers bind to synapses and disrupt synaptic activity in a manner that requires APP, *J. Neurosci.*
[31] Yang, T., Li, S. M., Xu, H. X., Walsh, D. M., and Selkoe, D. J. (2017) Large Soluble Oligomers of Amyloid beta-Protein from Alzheimer Brain Are Far Less Neuroactive Than the Smaller Oligomers to Which They Dissociate, *J. Neurosci. 37*, 152-163.
[32] Lee, H. G., Castellani, R. J., Zhu, X. W., Perry, G., and Smith, M. A. (2005) Amyloid-beta in Alzheimer's disease: the horse or the cart? Pathogenic or protective?, *Int. J. Exp. Pathol. 86*, 133-138.
[33] Selkoe, D. J. (1991) The molecular pathology of Alzheimer's disease, *Neuron 6*, 487-498.
[34] Hardy, J. A., and Higgins, G. A. (1992) Alzheimer's disease: the amyloid cascade hypothesis, *Science 256*, 184-185.
[35] Haass, C., Kaether, C., Thinakaran, G., and Sisodia, S. (2012) Trafficking and Proteolytic Processing of APP, *Cold Spring Harb. Perspect. Med. 2*, a006270.
[36] Haass, C., Koo, E. H., Mellon, A., Hung, A. Y., and Selkoe, D. J. (1992) Targeting of cell-surface beta-amyloid precursor protein to lysosomes: alternative processing into amyloid-bearing fragments, *Nature 357*, 500-503.
[37] Kuhn, P.-H., Wang, H., Dislich, B., Colombo, A., Zeitschel, U., Ellwart, J. W., Kremmer, E., Roßner, S., and Lichtenthaler, S. F. (2010) ADAM10 is the physiologically relevant, constitutive α-secretase of the amyloid precursor protein in primary neurons, *EMBO J. 29*, 3020-3032.
[38] Wang, Y. Q., Qu, D. H., and Wang, K. (2016) Therapeutic approaches to Alzheimer's disease through stimulating of non-amyloidogenic processing of amyloid precursor protein, *Eur. Rev. Med. Pharmacol. Sci. 20*, 2389-2403.
[39] Cai, H., Wang, Y., McCarthy, D., Wen, H., Borchelt, D. R., Price, D. L., and Wong, P. C. (2001) BACE1 is the major beta-secretase for generation of Abeta peptides by neurons, *Nat. Neurosci. 4*, 233-234.
[40] De Strooper, B. (2003) Aph-1, Pen-2, and Nicastrin with Presenilin Generate an Active gamma-Secretase Complex, *Neuron 38*, 9-12.
[41] De Strooper, B., Kopan, R., Annaert, W., Cupers, P., Saftig, P., Craessaerts, K.,

Mumm, J. S., Schroeter, E. H., Schrijvers, V., Wolfe, M. S., Ray, W. J., and Goate, A. (1999) A presenilin-1-dependent big gamma-secretase-like protease mediates release of Notch intracellular domain, *Nature 398*, 518-522.

[42] Steiner, H., Winkler, E., Edbauer, D., Prokop, S., Basset, G., Yamasaki, A., Kostka, M., and Haass, C. (2002) PEN-2 Is an Integral Component of the γ-Secretase Complex Required for Coordinated Expression of Presenilin and Nicastrin, *J. Biol. Chem. 277*, 39062-39065.

[43] Lee, S. F., Shah, S., Li, H., Yu, C., Han, W., and Yu, G. (2002) Mammalian APH-1 interacts with presenilin and nicastrin and is required for intramembrane proteolysis of amyloid-beta precursor protein and Notch, *J. Biol. Chem. 277*, 45013-45019.

[44] St George-Hyslop, P., Yu, G., Nishimura, M., Arawaka, S., Levitan, D., Zhang, L., Tandon, A., Song, Y.-Q., Rogaeva, E., Chen, F., Kawarai, T., Supala, A., Levesque, L., Yu, H., Yang, D.-S., Holmes, E., Milman, P., Liang, Y., Zhang, D. M., Xu, D. H., Sato, C., Rogaev, E., Smith, M., Janus, C., Zhang, Y., Aebersold, R., Farrer, L., Sorbi, S., Bruni, A., and Fraser, P. (2000) Nicastrin modulates presenilin-mediated notch/glp-1 signal transduction and betaAPP processing, *Nature 407*, 48-54.

[45] Andrew, R. J., Kellett, K. A., Thinakaran, G., and Hooper, N. M. (2016) A Greek Tragedy: the Growing Complexity of Alzheimer Amyloid Precursor Protein Proteolysis, *J. Biol. Chem.*

[46] Zhang, Z., Song, M., Liu, X., Su Kang, S., Duong, D. M., Seyfried, N. T., Cao, X., Cheng, L., Sun, Y. E., Ping Yu, S., Jia, J., Levey, A. I., and Ye, K. (2015) Delta-secretase cleaves amyloid precursor protein and regulates the pathogenesis in Alzheimer's disease, *Nat. Commun. 6*, 8762.

[47] Baranger, K., Marchalant, Y., Bonnet, A. E., Crouzin, N., Carrete, A., Paumier, J.-M., Py, N. A., Bernard, A., Bauer, C., Charrat, E., Moschke, K., Seiki, M., Vignes, M., Lichtenthaler, S. F., Checler, F., Khrestchatisky, M., and Rivera, S. (2015) MT5-MMP is a new pro-amyloidogenic proteinase that promotes amyloid pathology and cognitive decline in a transgenic mouse model of Alzheimer's disease, *Cell Mol Life Sci 73*, 217-236.

[48] Willem, M., Tahirovic, S., Busche, M. A., Ovsepian, S. V., Chafai, M., Kootar, S., Hornburg, D., Evans, L. D. B., Moore, S., Daria, A., Hampel, H., Müller, V., Giudici, C., Nuscher, B., Wenninger-Weinzierl, A., Kremmer, E., Heneka, M. T., Thal, D. R., Giedraitis, V., Lannfelt, L., Müller, U., Livesey, F. J., Meissner, F., Herms, J., Konnerth, A., Marie, H., and Haass, C. (2015) η-Secretase processing of APP inhibits neuronal activity in the hippocampus, *Nature 526*, 443-447.

[49] Baranger, K., Bonnet, A. E., Girard, S. D., Paumier, J.-M., García-González, L., Elmanaa, W., Bernard, A., Charrat, E., Stephan, D., Bauer, C., Moschke, K., Lichtenthaler, S. F., Roman, F. S., Checler, F., Khrestchatisky, M., and Rivera, S. (2017) MT5-MMP Promotes Alzheimer's Pathogenesis in the Frontal Cortex of 5xFAD Mice and APP Trafficking in vitro, *Front. Mol. Neurosci. 9*.

[50] Hook, G., Yu, J., Toneff, T., Kindy, M., and Hook, V. (2014) Brain Pyroglutamate Amyloid-β is Produced by Cathepsin B and is Reduced by the Cysteine Protease Inhibitor E64d, Representing a Potential Alzheimer's Disease Therapeutic, *J. Alzheimers Dis. 41*, 129-149.

[51] Bien, J., Jefferson, T., Causevic, M., Jumpertz, T., Munter, L., Multhaup, G., Weggen,

S., Becker-Pauly, C., and Pietrzik, C. U. (2012) The metalloprotease meprin beta generates amino terminal-truncated amyloid beta peptide species, *J. Biol. Chem. 287*, 33304-33313.
[52] Yu, J.-T., Tan, L., and Hardy, J. (2014) Apolipoprotein E in Alzheimer's Disease: An Update, *Annu. Rev. Neurosci. 37*, 79-100.
[53] Pfrieger, F. W., and Ungerer, N. (2011) Cholesterol metabolism in neurons and astrocytes, *Prog. Lipid Res. 50*, 357-371.
[54] Zhang, J., and Liu, Q. (2015) Cholesterol metabolism and homeostasis in the brain, *Protein & Cell 6*, 254-264.
[55] Mauch, D. H., Nägler, K., Schumacher, S., Göritz, C., Müller, E.-C., Otto, A., and Pfrieger, F. W. (2001) CNS Synaptogenesis Promoted by Glia-Derived Cholesterol, *Science 294*, 1354-1357.
[56] Makoto, M., Qi-Wen, F., Ichiro, I., and Katsuhiko, Y. (2000) Apolipoprotein E Exhibits Isoform-Specific Promotion of Lipid Efflux from Astrocytes and Neurons in Culture, *J. Neurochem. 74*, 1008-1016.
[57] Coon, K. D., Myers, A. J., Craig, D. W., Webster, J. A., Pearson, J. V., Lince, D. H., Zismann, V. L., Beach, T. G., Leung, D., Bryden, L., Halperin, R. F., Marlowe, L., Kaleem, M., Walker, D. G., Ravid, R., Heward, C. B., Rogers, J., Papassotiropoulos, A., Reiman, E. M., Hardy, J., and Stephan, D. A. (2007) A high-density whole-genome association study reveals that APOE is the major susceptibility gene for sporadic late-onset Alzheimer's disease, *J Clin Psychiatry 68*, 613-618.
[58] Grothe, M. J., Villeneuve, S., Dyrba, M., Bartrés-Faz, D., and Wirth, M. (2017) Multimodal characterization of older APOE2 carriers reveals selective reduction of amyloid load, *Neurology 88*, 569-576.
[59] Corder, E. H., Saunders, A. M., Strittmatter, W. J., Schmechel, D. E., Gaskell, P. C., Small, G. W., Roses, A. D., Haines, J. L., and Pericakvance, M. A. (1993) Gene Dose of Apolipoprotein-E Type-4 Allele and the Risk of Alzheimers-Disease in Late-Onset Families, *Science 261*, 921-923.
[60] Evans, R. M., Hui, S., Perkins, A., Lahiri, D. K., Poirier, J., and Farlow, M. R. (2004) Cholesterol and APOE genotype interact to influence Alzheimer disease progression, *Neurology 62*, 1869-1871.
[61] Namba, Y., Tomonaga, M., Kawasaki, H., Otomo, E., and Ikeda, K. (1991) Apolipoprotein E immunoreactivity in cerebral amyloid deposits and neurofibrillary tangles in Alzheimer's disease and kuru plaque amyloid in Creutzfeldt-Jakob disease, *Brain Res. 541*, 163-166.
[62] Schmechel, D. E., Saunders, A. M., Strittmatter, W. J., Crain, B. J., Hulette, C. M., Joo, S. H., Pericak-Vance, M. A., Goldgaber, D., and Roses, A. D. (1993) Increased amyloid beta-peptide deposition in cerebral cortex as a consequence of apolipoprotein E genotype in late-onset Alzheimer disease, *Proc. Natl. Acad. Sci. U.S.A. 90*, 9649-9653.
[63] Morris, J. C., Roe, C. M., Xiong, C., Fagan, A. M., Goate, A. M., Holtzman, D. M., and Mintun, M. A. (2010) APOE predicts amyloid-beta but not tau Alzheimer pathology in cognitively normal aging, *Ann. Neurol. 67*, 122-131.
[64] Huynh, T.-P. V., Davis, A. A., Ulrich, J. D., and Holtzman, D. M. (2017)

Apolipoprotein E and Alzheimer's disease: the influence of apolipoprotein E on amyloid-β and other amyloidogenic proteins, *J. Lipid Res. 58*, 824-836.
[65] Dong, H. K., Gim, J.-A., Yeo, S. H., and Kim, H.-S. (2017) Integrated late onset Alzheimer's disease (LOAD) susceptibility genes: Cholesterol metabolism and trafficking perspectives, *Gene 597*, 10-16.
[66] Bu, G. (2009) Apolipoprotein E and its receptors in Alzheimer's disease: pathways, pathogenesis and therapy, *Nat. Rev. Neurosci. 10*, 333-344.
[67] Shibata, M., Yamada, S., Kumar, S. R., Calero, M., Bading, J., Frangione, B., Holtzman, D. M., Miller, C. A., Strickland, D. K., Ghiso, J., and Zlokovic, B. V. (2000) Clearance of Alzheimer's amyloid-β1-40 peptide from brain by LDL receptor–related protein-1 at the blood-brain barrier, *J. Clin. Investig. 106*, 1489-1499.
[68] Fagan, A. M., Watson, M., Parsadanian, M., Bales, K. R., Paul, S. M., and Holtzman, D. M. (2002) Human and Murine ApoE Markedly Alters Aβ Metabolism before and after Plaque Formation in a Mouse Model of Alzheimer's Disease, *Neurobiol. Dis. 9*, 305-318.
[69] Holtzman, D. M., Bales, K. R., Tenkova, T., Fagan, A. M., Parsadanian, M., Sartorius, L. J., Mackey, B., Olney, J., McKeel, D., Wozniak, D., and Paul, S. M. (2000) Apolipoprotein E isoform-dependent amyloid deposition and neuritic degeneration in a mouse model of Alzheimer's disease, *Proc. Natl. Acad. Sci. U.S.A. 97*, 2892-2897.
[70] Eloise, K., Satu, H., Teemu, L., Heini, H., Sirkka, G., Hannu, H., and J., K. P. (2009) Apolipoprotein E–dependent accumulation of Alzheimer disease–related lesions begins in middle age, *Ann. Neurol. 65*, 650-657.
[71] Castellano, J. M., Kim, J., Stewart, F. R., Jiang, H., DeMattos, R. B., Patterson, B. W., Fagan, A. M., Morris, J. C., Mawuenyega, K. G., Cruchaga, C., Goate, A. M., Bales, K. R., Paul, S. M., Bateman, R. J., and Holtzman, D. M. (2011) Human apoE Isoforms Differentially Regulate Brain Amyloid-β Peptide Clearance, *Sci. Transl. Med. 3*, 89ra57-89ra57.
[72] Lee, C. Y. D., Tse, W., Smith, J. D., and Landreth, G. E. (2012) Apolipoprotein E Promotes β-Amyloid Trafficking and Degradation by Modulating Microglial Cholesterol Levels, *J. Biol. Chem. 287*, 2032-2044.
[73] Jiang, Q., Lee, C. Y. D., Mandrekar, S., Wilkinson, B., Cramer, P., Zelcer, N., Mann, K., Lamb, B., Willson, T. M., Collins, J. L., Richardson, J. C., Smith, J. D., Comery, T. A., Riddell, D., Holtzman, D. M., Tontonoz, P., and Landreth, G. E. (2008) ApoE promotes the proteolytic degradation of Abeta, *Neuron 58*, 681-693.
[74] Yeh, F. L., Wang, Y., Tom, I., Gonzalez, L. C., and Sheng, M. (2016) TREM2 Binds to Apolipoproteins, Including APOE and CLU/APOJ, and Thereby Facilitates Uptake of Amyloid-Beta by Microglia, *Neuron 91*, 328-340.
[75] Giri, M., Zhang, M., and Lü, Y. (2016) Genes associated with Alzheimer's disease: an overview and current status, *Clin. Interv. Aging 11*, 665-681.
[76] Guerreiro, R., Wojtas, A., Bras, J., Carrasquillo, M., Rogaeva, E., Majounie, E., Cruchaga, C., Sassi, C., Kauwe, J. S. K., Younkin, S., Hazrati, L., Collinge, J., Pocock, J., Lashley, T., Williams, J., Lambert, J.-C., Amouyel, P., Goate, A., Rademakers, R., Morgan, K., Powell, J., St. George-Hyslop, P., Singleton, A., and

Hardy, J. (2013) TREM2 Variants in Alzheimer's Disease, *N. Engl. J. Med. 368*, 117-127.
[77] Atagi, Y., Liu, C. C., Painter, M. M., Chen, X. F., Verbeeck, C., Zheng, H. H., Li, X., Rademakers, R., Kang, S. S., Xu, H. X., Younkin, S., Das, P., Fryer, J. D., and Bu, G. J. (2015) Apolipoprotein E Is a Ligand for Triggering Receptor Expressed on Myeloid Cells 2 (TREM2), *J. Biol. Chem. 290*, 26043-26050.
[78] Huynh, T.-P. V., Liao, F., Francis, C. M., Robinson, G. O., Serrano, J. R., Jiang, H., Roh, J., Finn, M. B., Sullivan, P. M., Esparza, T. J., Stewart, F. R., Mahan, T. E., Ulrich, J. D., Cole, T., and Holtzman, D. M. (2017) Age-Dependent Effects of apoE Reduction Using Antisense Oligonucleotides in a Model of β-amyloidosis, *Neuron 96*, 1013-1023.e1014.
[79] Liu, C.-C., Zhao, N., Fu, Y., Wang, N., Linares, C., Tsai, C.-W., and Bu, G. (2017) ApoE4 Accelerates Early Seeding of Amyloid Pathology, *Neuron 96*, 1024-1032.e1023.
[80] Vassar, R. (2017) Seeds of Destruction: New Mechanistic Insights into the Role of Apolipoprotein E4 in Alzheimer's Disease, *Neuron 96*, 953-955.
[81] M., T. L., Shivesh, G., P., K. K., Vaiva, L., Mark, M. C., Pinal, K., Nicole, C., Manel, B. A., Zhengdeng, L. A., Neil, B., J., G. S., Bill, H., J., V. E. L., and Jo, L. M. (2015) APOE-modulated Aβ-induced neuroinflammation in Alzheimer's disease: current landscape, novel data, and future perspective, *J. Neurochem. 133*, 465-488.
[82] Kim, J., Basak, J. M., and Holtzman, D. M. (2009) The role of apolipoprotein E in Alzheimer's disease, *Neuron 63*, 287-303.
[83] Heneka, M. T., Carson, M. J., Khoury, J. E., Landreth, G. E., Brosseron, F., Feinstein, D. L., Jacobs, A. H., Wyss-Coray, T., Vitorica, J., Ransohoff, R. M., Herrup, K., Frautschy, S. A., Finsen, B., Brown, G. C., Verkhratsky, A., Yamanaka, K., Koistinaho, J., Latz, E., Halle, A., Petzold, G. C., Town, T., Morgan, D., Shinohara, M. L., Perry, V. H., Holmes, C., Bazan, N. G., Brooks, D. J., Hunot, S., Joseph, B., Deigendesch, N., Garaschuk, O., Boddeke, E., Dinarello, C. A., Breitner, J. C., Cole, G. M., Golenbock, D. T., and Kummer, M. P. (2015) Neuroinflammation in Alzheimer's disease, *Lancet N. 14*, 388-405.
[84] Szekely, C. A., Breitner, J. C., Fitzpatrick, A. L., Rea, T. D., Psaty, B. M., Kuller, L. H., and Zandi, P. P. (2008) NSAID use and dementia risk in the Cardiovascular Health Study: role of APOE and NSAID type, *Neurology 70*, 17-24.
[85] Tamboli, I. Y., Prager, K., Thal, D. R., Thelen, K. M., Dewachter, I., Pietrzik, C. U., St. George-Hyslop, P., Sisodia, S. S., De Strooper, B., Heneka, M. T., Filippov, M. A., Muller, U., van Leuven, F., Lutjohann, D., and Walter, J. (2008) Loss of gamma-Secretase Function Impairs Endocytosis of Lipoprotein Particles and Membrane Cholesterol Homeostasis, *J. Neurosci. 28*, 12097-12106.
[86] Grimm, M. O., Grimm, H. S., Patzold, A. J., Zinser, E. G., Halonen, R., Duering, M., Tschape, J. A., De Strooper, B., Muller, U., Shen, J., and Hartmann, T. (2005) Regulation of cholesterol and sphingomyelin metabolism by amyloid-beta and presenilin, *Nat. Cell Biol. 7*, 1118-1123.
[87] Grimm, M. O. W., Tschape, J. A., Grimm, H. S., Zinser, E. G., and Hartmann, T. (2006) Altered membrane fluidity and lipid raft composition in presenilin-deficient cells, *Acta Neurol. Scand. 114*, 27-32.

[88] Beel, A. J., Sakakura, M., Barrett, P. J., and Sanders, C. R. (2010) Direct binding of cholesterol to the amyloid precursor protein: An important interaction in lipid–Alzheimer's disease relationships?, *Biochim. Biophys. Acta 1801*, 975-982.
[89] Beel, A. J., Mobley, C. K., Kim, H. J., Tian, F., Hadziselimovic, A., Jap, B., Prestegard, J. H., and Sanders, C. R. (2008) Structural Studies of the Transmembrane C-Terminal Domain of the Amyloid Precursor Protein (APP): Does APP Function as a Cholesterol Sensor?†‡, *Biochemistry 47*, 9428-9446.
[90] Barrett, P. J., Song, Y., Van Horn, W. D., Hustedt, E. J., Schafer, J. M., Hadziselimovic, A., Beel, A. J., and Sanders, C. R. (2012) The amyloid precursor protein has a flexible transmembrane domain and binds cholesterol, *Science 336*, 1168-1171.
[91] Song, Y., Hustedt, E. J., Brandon, S., and Sanders, C. R. (2013) Competition between homodimerization and cholesterol binding to the C99 domain of the amyloid precursor protein, *Biochemistry 52*, 5051-5064.
[92] Song, Y., Mittendorf, K. F., Lu, Z., and Sanders, C. R. (2014) Impact of Bilayer Lipid Composition on the Structure and Topology of the Transmembrane Amyloid Precursor C99 Protein, *J. Am. Chem. Soc. 136*, 4093-4096.
[93] Di Scala, C., Yahi, N., Lelievre, C., Garmy, N., Chahinian, H., and Fantini, J. (2013) Biochemical Identification of a Linear Cholesterol-Binding Domain within Alzheimer's beta Amyloid Peptide, *ACS Chem. Neurosci. 4*, 509-517.
[94] Di Scala, C., Chahinian, H., Yahi, N., Garmy, N., and Fantini, J. (2014) Interaction of Alzheimer's beta-Amyloid Peptides with Cholesterol: Mechanistic Insights into Amyloid Pore Formation, *Biochemistry 53*, 4489-4502.
[95] Ayciriex, S., Gerber, H., Osuna, G. M. G., Chami, M., Stahlberg, H., Shevchenko, A., and Fraering, P. C. (2016) The lipidome associated with the gamma-secretase complex is required for its integrity and activity, *Biochem. J 473*, 321-334.
[96] Cossec, J.-C., Simon, A., Marquer, C., Moldrich, R. X., Leterrier, C., Rossier, J., Duyckaerts, C., Lenkei, Z., and Potier, M.-C. (2010) Clathrin-dependent APP endocytosis and Aβ secretion are highly sensitive to the level of plasma membrane cholesterol, *Biochim. Biophys. Acta 1801*, 846-852.
[97] Guardia-Laguarta, C., Coma, M., Pera, M., Clarimon, J., Sereno, L., Agullo, J. M., Molina-Porcel, L., Gallardo, E., Deng, A., Berezovska, O., Hyman, B. T., Blesa, R., Gomez-Isla, T., and Lleo, A. (2009) Mild cholesterol depletion reduces amyloid-beta production by impairing APP trafficking to the cell surface, *J. Neurochem. 110*, 220-230.
[98] Cam, J. A., Zerbinatti, C. V., Knisely, J. M., Hecimovic, S., Li, Y., and Bu, G. (2004) The low density lipoprotein receptor-related protein 1B retains beta-amyloid precursor protein at the cell surface and reduces amyloid-beta peptide production, *J. Biol. Chem. 279*, 29639-29646.
[99] Cam, J. A., Zerbinatti, C. V., Li, Y., and Bu, G. (2005) Rapid endocytosis of the low density lipoprotein receptor-related protein modulates cell surface distribution and processing of the beta-amyloid precursor protein, *J. Biol. Chem. 280*, 15464-15470.
[100] von Arnim, C. A., von Einem, B., Weber, P., Wagner, M., Schwanzar, D., Spoelgen, R., Strauss, W. L., and Schneckenburger, H. (2008) Impact of cholesterol level upon APP and BACE proximity and APP cleavage, *Biochem. Biophys. Res.*

Commun. 370, 207-212.
[101] Kojro, E., Gimpl, G., Lammich, S., Marz, W., and Fahrenholz, F. (2001) Low cholesterol stimulates the nonamyloidogenic pathway by its effect on the alpha - secretase ADAM 10, *Proc. Natl. Acad. Sci. U. S. A. 98*, 5815-5820.
[102] Bodovitz, S., and Klein, W. L. (1996) Cholesterol modulates alpha-secretase cleavage of amyloid precursor protein, *J. Biol. Chem. 271*, 4436-4440.
[103] Galbete, J. L., Rodriguez-Martin, T., Peressini, E., Modena, P., Bianchi, R., and Forloni, G. (2000) Cholesterol decreases secretion of the secreted form of amyloid precursor protein by interfering with glycosylation in the protein secretory pathway, *Biochem. J 348*, 307-313.
[104] Wang, J., Wu, F., and Shi, C. (2013) Substitution of membrane cholesterol with beta-sitosterol promotes nonamyloidogenic cleavage of endogenous amyloid precursor protein, *Neuroscience 247*, 227-233.
[105] Xiong, H., Callaghan, D., Jones, A., Walker, D. G., Lue, L.-F., Beach, T. G., Sue, L. I., Woulfe, J., Xu, H., Stanimirovic, D. B., and Zhang, W. (2008) Cholesterol retention in Alzheimer's brain is responsible for high beta- and gamma-secretase activities and Aβ production, *Neurobiol. Dis. 29*, 422-437.
[106] Brambillaa, A., Lonati, E., Milani, C., Rizzo, A. M., Farina, F., Botto, L., Masserini, M., Palestini, P., and Bulbarelli, A. (2015) Ischemic conditions and beta-secretase activation: The impact of membrane cholesterol enrichment as triggering factor in rat brain endothelial cells, *Int. J. Biochem. Cell Biol. 69*, 95-104.
[107] Liu, W. W., Todd, S., Coulson, D. T. R., Irvine, G. B., Passmore, A. P., McGuinness, B., McConville, M., Craig, D., and Johnston, J. A. (2009) A novel reciprocal and biphasic relationship between membrane cholesterol and beta-secretase activity in SH-SY5Y cells and in human platelets, *J. Neurochem. 108*, 341-349.
[108] Sidera, C., Parsons, R., and Austen, B. (2005) The regulation of beta-secretase by cholesterol and statins in Alzheimer's disease, *J. Neurol. Sci. 229-230*, 269-273.
[109] Kim, Y., Kim, C., Jang, H. Y., Mook-Jung, I., and Kim, B. (2016) Inhibition of Cholesterol Biosynthesis Reduces gamma-Secretase Activity and Amyloid-beta Generation, *J. Alzheimers Dis. 51*, 1057-1068.
[110] Runz, H., Rietdorf, J., Tomic, I., de Bernard, M., Beyreuther, K., Pepperkok, R., and Hartmann, T. (2002) Inhibition of intracellular cholesterol transport alters presenilin localization and amyloid precursor protein processing in neuronal cells, *J. Neurosci. 22*, 1679-1689.
[111] Grimm, M. O. W., Grimm, H. S., Tomic, I., Beyreuther, K., Hartmann, T., and Bergmann, C. (2008) Independent Inhibition of Alzheimer Disease beta- and gamma-Secretase Cleavage by Lowered Cholesterol Levels, *J. Biol. Chem. 283*, 11302-11311.
[112] McGleenon, B. M., Dynan, K. B., and Passmore, A. P. (1999) Acetylcholinesterase inhibitors in Alzheimer's disease, *Br. J. Clin. Pharmacol. 48*, 471-480.
[113] Schneider, L. S., Dagerman, K. S., Higgins, J. T., and McShane, R. (2011) Lack of evidence for the efficacy of memantine in mild alzheimer disease, *Arch. Neurol. 68*, 991-998.
[114] Johnson, J. W., and Kotermanski, S. E. (2006) Mechanism of action of memantine, *Curr. Opin. Pharm. 6*, 61-67.

[115] Olazarán, J., Reisberg, B., Clare, L., Cruz, I., Peña-Casanova, J., del Ser, T., Woods, B., Beck, C., Auer, S., Lai, C., Spector, A., Fazio, S., Bond, J., Kivipelto, M., Brodaty, H., Rojo, J. M., Collins, H., Teri, L., Mittelman, M., Orrell, M., Feldman, H. H., and Muñiz, R. (2010) Nonpharmacological Therapies in Alzheimer's Disease: A Systematic Review of Efficacy, *Dement. Geriatr. Cogn. Disord. 30*, 161-178.
[116] Davies, P., and Maloney, A. J. (1976) Selective loss of central cholinergic neurons in Alzheimer's disease, *Lancet 2*, 1403.
[117] Summers, W. K., Majovski, L. V., Marsh, G. M., Tachiki, K., and Kling, A. (1986) Oral Tetrahydroaminoacridine in Long-Term Treatment of Senile Dementia, Alzheimer Type, *N. Engl. J. Med. 315*, 1241-1245.
[118] Sassin, I., Schultz, C., Thal, D. R., Rüb, U., Arai, K., Braak, E., and Braak, H. (2000) Evolution of Alzheimer's disease-related cytoskeletal changes in the basal nucleus of Meynert, *Acta Neuropathol. 100*, 259-269.
[119] Whitehouse, P. J., Price, D. L., Clark, A. W., Coyle, J. T., and DeLong, M. R. (1981) Alzheimer disease: Evidence for selective loss of cholinergic neurons in the nucleus basalis, *Ann. Neurol. 10*, 122-126.
[120] Hampel, H., Mesulam, M. M., Cuello, A. C., Farlow, M. R., Giacobini, E., Grossberg, G. T., Khachaturian, A. S., Vergallo, A., Cavedo, E., Snyder, P. J., and Khachaturian, Z. S. (2018) The cholinergic system in the pathophysiology and treatment of Alzheimer's disease, *Brain*.
[121] Gefen, T., Gasho, K., Rademaker, A., Lalehzari, M., Weintraub, S., Rogalski, E., Wieneke, C., Bigio, E., Geula, C., and Mesulam, M. M. (2012) Clinically concordant variations of Alzheimer pathology in aphasic versus amnestic dementia, *Brain 135*, 1554-1565.
[122] Gómez-Isla, T., Hollister, R., West, H., Mui, S., Growdon, J. H., Petersen, R. C., Parisi, J. E., and Hyman, B. T. (1997) Neuronal loss correlates with but exceeds neurofibrillary tangles in Alzheimer's disease, *Ann. Neurol. 41*, 17-24.
[123] Arendt, T., Bigl, V., Tennstedt, A., and Arendt, A. (1985) Neuronal loss in different parts of the nucleus basalis is related to neuritic plaque formation in cortical target areas in alzheimer's disease, *Neuroscience 14*, 1-14.
[124] M.-Marsel, M. (2013) Cholinergic circuitry of the human nucleus basalis and its fate in Alzheimer's disease, *J. Comp. Neurol. 521*, 4124-4144.
[125] Arriagada, P. V., Marzloff, K., and Hyman, B. T. (1992) Distribution of Alzheimer-type pathologic changes in nondemented elderly individuals matches the pattern in Alzheimer's disease, *Neurology 42*, 1681-1681.
[126] S., G. D., George, P., Thomas, M., Vera, M., and R., I. J. (2003) Donepezil Is Associated with Delayed Nursing Home Placement in Patients with Alzheimer's Disease, *J. Am. Geriatr. Soc. 51*, 937-944.
[127] Nitsch, R., Slack, B., Wurtman, R., and Growdon, J. (1992) Release of Alzheimer amyloid precursor derivatives stimulated by activation of muscarinic acetylcholine receptors, *Science 258*, 304-307.
[128] Mori, F., Lai, C.-C., Fusi, F., and Giacobini, E. (1995) Cholinesterase inhibitors increase secretion of APPs in rat brain cortex, *Neuroreport 6*, 633-636.
[129] C., T. A., M., A. H., Charlene, S., Patricia, R., Angeliki, V. A., S., H. J., D., I. J., A.,

K. P., Fatemeh, Y., Marco, G., Erik, B., M., H. J., H., N. C., Brenda, H., R., M. S., Laure, P., and E., S. S. (2018) Comparative Effectiveness and Safety of Cognitive Enhancers for Treating Alzheimer's Disease: Systematic Review and Network Metaanalysis, *J. Am. Geriatr. Soc. 66*, 170-178.

[130] Howard, R. J., Juszczak, E., Ballard, C. G., Bentham, P., Brown, R. G., Bullock, R., Burns, A. S., Holmes, C., Jacoby, R., Johnson, T., Knapp, M., Lindesay, J., O'Brien, J. T., Wilcock, G., Katona, C., Jones, R. W., DeCesare, J., and Rodger, M. (2007) Donepezil for the Treatment of Agitation in Alzheimer's Disease, *N. Engl. J. Med. 357*, 1382-1392.

[131] H., F. H., Tuula, P., François, D. J., Brian, E., Bart, V. B., Susanne, S., and Shane, K. (2009) Treatment with galantamine and time to nursing home placement in Alzheimer's disease patients with and without cerebrovascular disease, *Int. J. Geriatr. Psychiatry 24*, 479-488.

[132] Maneno, M. K., Lee, E., Wutoh, A. K., Zuckerman, I. H., Jackson, P., Lombardo, F. A., Scott, K. R., and Xue, Z. (2006) National patterns of dementia treatment among elderly ambulatory patients, *J. Natl. Med. Assoc. 98*, 430-435.

[133] Brady, R., and Weinman, J. (2013) Adherence to Cholinesterase Inhibitors in Alzheimer's Disease: A Review, *Dement. Geriatr. Cogn. Disord. 35*, 351-363.

[134] Maxwell, C. J., Stock, K., Seitz, D., and Herrmann, N. (2014) Persistence and Adherence With Dementia Pharmacotherapy: Relevance of Patient, Provider, and System Factors, *Can. J. Psychiatry. 59*, 624-631.

[135] Hsieh, H., Boehm, J., Sato, C., Iwatsubo, T., Tomita, T., Sisodia, S., and Malinow, R. (2006) AMPAR removal underlies Abeta-induced synaptic depression and dendritic spine loss, *Neuron 52*, 831-843.

[136] Marcello, E., Epis, R., Saraceno, C., and Di Luca, M. (2012) Synaptic dysfunction in Alzheimer's disease, *Adv. Exp. Med. Biol. 970*, 573-601.

[137] Paula-Lima, A. C., Brito-Moreira, J., and Ferreira, S. T. (2013) Deregulation of excitatory neurotransmission underlying synapse failure in Alzheimer's disease, *J. Neurochem. 126*, 191-202.

[138] Selkoe, D. J. (2002) Alzheimer's Disease Is a Synaptic Failure, *Science 298*, 789-791.

[139] Palop, J. J., and Mucke, L. (2010) Amyloid-beta-induced neuronal dysfunction in Alzheimer's disease: from synapses toward neural networks, *Nat. Neurosci. 13*, 812-818.

[140] Ito, K., Tatebe, T., Suzuki, K., Hirayama, T., Hayakawa, M., Kubo, H., Tomita, T., and Makino, M. (2017) Memantine reduces the production of amyloid-beta peptides through modulation of amyloid precursor protein trafficking, *Eur. J. Pharmacol. 798*, 16-25.

[141] Decker, H., Lo, K. Y., Unger, S. M., Ferreira, S. T., and Silverman, M. A. (2010) Amyloid-β Peptide Oligomers Disrupt Axonal Transport through an NMDA Receptor-Dependent Mechanism That Is Mediated by Glycogen Synthase Kinase 3β in Primary Cultured Hippocampal Neurons, *J. Neurosci. 30*, 9166-9171.

[142] Mota, S. I., Ferreira, I. L., and Rego, A. C. (2014) Dysfunctional synapse in Alzheimer's disease – A focus on NMDA receptors, *Neuropharmacology 76*, 16-26.

[143] Ye, X., Tai, W., and Zhang, D. (2012) The early events of Alzheimer's disease pathology: from mitochondrial dysfunction to BDNF axonal transport deficits,

Neurobiol. Aging 33, 1122.e1121-1122.e1110.
[144] Grimm, A., Friedland, K., and Eckert, A. (2016) Mitochondrial dysfunction: the missing link between aging and sporadic Alzheimer's disease, *Biogerontology 17*, 281-296.
[145] Ferreira, I. L., Resende, R., Ferreiro, E., Rego, A. C., and Pereira, C. F. (2010) Multiple Defects in Energy Metabolism in Alzheimers Disease, *Curr. Drug Targets 11*, 1193-1206.
[146] Boehm, J. (2013) A 'danse macabre': tau and Fyn in STEP with amyloid beta to facilitate induction of synaptic depression and excitotoxicity, *Eur. J. Neurosci. 37*, 1925-1930.
[147] David, W. (2012) A review of the effects of memantine on clinical progression in Alzheimer's disease, *Int. J. Geriatr. Psychiatry 27*, 769-776.
[148] Reisberg, B., Doody, R., Stoffler, A., Schmitt, F., Ferris, S., Mobius, H. J., and Memantine Study, G. (2003) Memantine in moderate-to-severe Alzheimer's disease, *N. Engl. J. Med. 348*, 1333-1341.
[149] Rainer, H., Yvonne, W., Wolfgang, J., and Susanne, H. (2012) Efficacy of memantine in delaying clinical worsening in Alzheimer's disease (AD): responder analyses of nine clinical trials with patients with moderate to severe AD, *Int. J. Geriatr. Psychiatry 27*, 651-656.
[150] van Marum, R. J. (2009) Update on the use of memantine in Alzheimer's disease, *Neuropsychiatr. Dis. Treat. 5*, 237-247.
[151] Giacobini, E., and Gold, G. (2013) Alzheimer disease therapy—moving from amyloid-β to tau, *Nat. Rev. Neurol. 9*, 677.
[152] Sperling, R. A., Jack, C. R., and Aisen, P. S. (2011) Testing the Right Target and Right Drug at the Right Stage, *Sci. Transl. Med. 3*, 111cm133-111cm133.
[153] Tomaszewski, S., Gauthier, S., Wimo, A., and Rosa-Neto, P. (2016) Combination Therapy of Anti-Tau and Anti-Amyloid Drugs for Disease Modification in Early-stage Alzheimer's Disease: Socio-economic Considerations Modeled on Treatments for Tuberculosis, HIV/AIDS and Breast Cancer, *J. Prev. Alzheimers Dis. 3*, 164-172.
[154] Libeu, C. A. P., Descamps, O., Zhang, Q., John, V., and Bredesen, D. E. (2012) Altering APP Proteolysis: Increasing sAPPalpha Production by Targeting Dimerization of the APP Ectodomain, *PLoS One 7*.
[155] Chen, A. C., Kim, S., Shepardson, N., Patel, S., Hong, S., and Selkoe, D. J. (2015) Physical and functional interaction between the alpha- and gamma-secretases: A new model of regulated intramembrane proteolysis, *J. Cell Biol. 211*, 1157-1176.
[156] Sun, J., and Roy, S. (2017) The physical approximation of APP and BACE-1 - a key event in Alzheimer's disease pathogenesis, *Dev. Neurobiol.*
[157] Refolo, L. M., Sambamurti, K., Efthimiopoulos, S., Pappolla, M. A., and Robakis, N. K. (1995) Evidence that secretase cleavage of cell surface Alzheimer amyloid precursor occurs after normal endocytic internalization, *J. Neurosci. Res. 40*, 694-706.
[158] Parvathy, S., Hussain, I., Karran, E. H., Turner, A. J., and Hooper, N. M. (1999) Cleavage of Alzheimer's Amyloid Precursor Protein by alpha-Secretase Occurs at the Surface of Neuronal Cells, *Biochemistry 38*, 9728-9734.

[159] Vingtdeux, V., Hamdane, M., Begard, S., Loyens, A., Delacourte, A., Beauvillain, J. C., Buee, L., Marambaud, P., and Sergeant, N. (2007) Intracellular pH regulates amyloid precursor protein intracellular domain accumulation, *Neurobiol. Dis. 25*, 686-696.
[160] Matsumura, N., Takami, M., Okochi, M., Wada-Kakuda, S., Fujiwara, H., Tagami, S., Funamoto, S., Ihara, Y., and Morishima-Kawashima, M. (2014) gamma Secretase Associated with Lipid Rafts, *J. Biol. Chem. 289*, 5109-5121.
[161] Hur, J.-Y., Welander, H., Behbahani, H., Aoki, M., Frånberg, J., Winblad, B., Frykman, S., and Tjernberg, L. O. (2008) Active gamma-secretase is localized to detergent-resistant membranes in human brain, *FEBS J. 275*, 1174-1187.
[162] Vetrivel, K. S., Cheng, H., Lin, W., Sakurai, T., Li, T., Nukina, N., Wong, P. C., Xu, H., and Thinakaran, G. (2004) Association of gamma-secretase with lipid rafts in post-Golgi and endosome membranes, *J. Biol. Chem. 279*, 44945-44954.
[163] Schedin-Weiss, S., Caesar, I., Winblad, B., Blom, H., and Tjernberg, L. O. (2016) Super-resolution microscopy reveals gamma-secretase at both sides of the neuronal synapse, *Acta Neuropathol. Commun. 4*.
[164] Winblad, B., Caesar, I., Blom, H., Tjernberg, L. O., and Weiss, S. S. (2016) Gamma-Secretase Is Present at Both Sides of the Neuronal Synapse, *Alzheimer's & Dementia 12*, P1041-P1042.
[165] Barros, M., Houlihan, W., Gilchrist, L., and Li, Y. (2017) Partitioning of gamma-Secretase and its Substrates in Lipid Microdomains, *Biophys. J. 112*, 34a.
[166] Meckler, X., and Checler, F. (2016) Presenilin 1 and Presenilin 2 Target gamma-Secretase Complexes to Distinct Cellular Compartments, *J. Biol. Chem. 291*, 12821-12837.
[167] Linden, R., Frykman, S., Hur, J.-Y., Frånberg, J., Aoki, M., Winblad, B., Nahalkova, J., Behbahani, H., and Tjernberg, L. O. (2010) Synaptic and Endosomal Localization of Active gamma-Secretase in Rat Brain, *PLoS One 5*, e8948.
[168] Vetrivel, K. S., Cheng, H., Kim, S.-H., Chen, Y., Barnes, N. Y., Parent, A. T., Sisodia, S. S., and Thinakaran, G. (2005) Spatial Segregation of gamma-Secretase and Substrates in Distinct Membrane Domains, *J. Biol. Chem. 280*, 25892-25900.
[169] Chyung, J. H., Raper, D. M., and Selkoe, D. J. (2005) gamma-Secretase Exists on the Plasma Membrane as an Intact Complex That Accepts Substrates and Effects Intramembrane Cleavage, *J. Biol. Chem. 280*, 4383-4392.
[170] Sheng, J. G., Price, D. L., and Koliatsos, V. E. (2003) The beta-amyloid-related proteins presenilin 1 and BACE1 are axonally transported to nerve terminals in the brain, *Exp. Neurol. 184*, 1053-1057.
[171] Litterst, C., Georgakopoulos, A., Shioi, J., Ghersi, E., Wisniewski, T., Wang, R., Ludwig, A., and Robakis, N. K. (2007) Ligand binding and calcium influx induce distinct ectodomain/gamma-secretase-processing pathways of EphB2 receptor, *J. Biol. Chem. 282*, 16155-16163.
[172] Ray, W. J., Yao, M., Mumm, J., Schroeter, E. H., Saftig, P., Wolfe, M., Selkoe, D. J., Kopan, R., and Goate, A. M. (1999) Cell surface presenilin-1 participates in the gamma-secretase-like proteolysis of Notch, *J. Biol. Chem. 274*, 36801-36807.
[173] Sannerud, R., Esselens, C., Ejsmont, P., Mattera, R., Rochin, L., Tharkeshwar, Arun K., De Baets, G., De Wever, V., Habets, R., Baert, V., Vermeire, W.,

Michiels, C., Groot, Arjan J., Wouters, R., Dillen, K., Vints, K., Baatsen, P., Munck, S., Derua, R., Waelkens, E., Basi, Guriqbal S., Mercken, M., Vooijs, M., Bollen, M., Schymkowitz, J., Rousseau, F., Bonifacino, Juan S., Van Niel, G., De Strooper, B., and Annaert, W. (2016) Restricted Location of PSEN2/gamma-Secretase Determines Substrate Specificity and Generates an Intracellular Aβ Pool, *Cell*.

[174] Vetrivel, K. S., and Thinakaran, G. (2006) Amyloidogenic processing of beta-amyloid precursor protein in intracellular compartments, *Neurology 66*, S69-73.

[175] Tarassishin, L., Yin, Y. I., Bassit, B., and Li, Y. M. (2004) Processing of Notch and amyloid precursor protein by gamma-secretase is spatially distinct, *Proc. Natl. Acad. Sci. U. S. A. 101*, 17050-17055.

[176] Pasternak, S. H., Bagshaw, R. D., Guiral, M., Zhang, S., Ackerley, C. A., Pak, B. J., Callahan, J. W., and Mahuran, D. J. (2003) Presenilin-1, Nicastrin, Amyloid Precursor Protein, and γ-Secretase Activity Are Co-localized in the Lysosomal Membrane, *J. Biol. Chem. 278*, 26687-26694.

[177] Tam, J., Seah, C., and Pasternak, S. H. (2014) The Amyloid Precursor Protein is rapidly transported from the Golgi apparatus to the lysosome and where it is processed into beta-amyloid, *Mol. Brain 7*, 54.

[178] Tam, J. H. K., and Pasternak, S. H. (2015) Imaging the Intracellular Trafficking of APP with Photoactivatable GFP, *Journal of Visualized Experiments*.

[179] Hattori, C., Asai, M., Oma, Y., Kino, Y., Sasagawa, N., Saido, T. C., Maruyama, K., and Ishiura, S. (2002) BACE1 interacts with nicastrin, *Biochem. Biophys. Res. Commun. 293*, 1228-1232.

[180] Hébert, S. S., Bourdages, V., Godin, C., Ferland, M., Carreau, M., and Lévesque, G. (2003) Presenilin-1 interacts directly with the beta-site amyloid protein precursor cleaving enzyme (BACE1), *Neurobiol. Dis. 13*, 238-245.

[181] De Strooper, B. (2014) Lessons from a Failed gamma-Secretase Alzheimer Trial, *Cell 159*, 721-726.

[182] Doody, R. S., Raman, R., Farlow, M., Iwatsubo, T., Vellas, B., Joffe, S., Kieburtz, K., He, F., Sun, X., Thomas, R. G., Aisen, P. S., Siemers, E., Sethuraman, G., and Mohs, R. (2013) A Phase 3 Trial of Semagacestat for Treatment of Alzheimer's Disease, *N. Engl. J. Med. 369*, 341-350.

[183] Gijsen, H. J. M., and Mercken, M. (2012) gamma-Secretase Modulators: Can We Combine Potency with Safety?, *Int. J. Alzheimers Dis. 2012*, 1-10.

[184] Kimberly, W. T., Esler, W. P., Ye, W., Ostaszewski, B. L., Gao, J., Diehl, T., Selkoe, D. J., and Wolfe, M. S. (2003) Notch and the Amyloid Precursor Protein Are Cleaved by Similar gamma-Secretase(s), *Biochemistry 42*, 137-144.

[185] Tousseyn, T., Thathiah, A., Jorissen, E., Raemaekers, T., Konietzko, U., Reiss, K., Maes, E., Snellinx, A., Serneels, L., Nyabi, O., Annaert, W., Saftig, P., Hartmann, D., and De Strooper, B. (2009) ADAM10, the Rate-limiting Protease of Regulated Intramembrane Proteolysis of Notch and Other Proteins, Is Processed by ADAMS-9, ADAMS-15, and the gamma-Secretase, *J. Biol. Chem. 284*, 11738-11747.

[186] Sorensen, E. B., and Conner, S. D. (2010) gamma-Secretase-Dependent Cleavage Initiates Notch Signaling from the Plasma Membrane, *Traffic 11*, 1234-1245.

[187] Coric, V., van Dyck, C. H., Salloway, S., Andreasen, N., Brody, M., Richter, R. W.,

Soininen, H., Thein, S., Shiovitz, T., Pilcher, G., Colby, S., Rollin, L., Dockens, R., Pachai, C., Portelius, E., Andreasson, U., Blennow, K., Soares, H., Albright, C., Feldman, H. H., and Berman, R. M. (2012) Safety and Tolerability of the gamma-Secretase Inhibitor Avagacestat in a Phase 2 Study of Mild to Moderate Alzheimer Disease, *Arch. Neurol. 69*, 1430.

[188] Crump, C. J., Castro, S. V., Wang, F., Pozdnyakov, N., Ballard, T. E., Sisodia, S. S., Bales, K. R., Johnson, D. S., and Li, Y.-M. (2012) BMS-708,163 Targets Presenilin and Lacks Notch-Sparing Activity, *Biochemistry 51*, 7209-7211.

[189] Stenovec, M., Trkov, S., Lasič, E., Terzieva, S., Kreft, M., Rodríguez Arellano, J. J., Parpura, V., Verkhratsky, A., and Zorec, R. (2016) Expression of familial Alzheimer disease presenilin 1 gene attenuates vesicle traffic and reduces peptide secretion in cultured astrocytes devoid of pathologic tissue environment, *Glia 64*, 317-329.

[190] Kuzuya, A., Zoltowska, K. M., Post, K. L., Arimon, M., Li, X., Svirsky, S., Maesako, M., Muzikansky, A., Gautam, V., Kovacs, D., Hyman, B. T., and Berezovska, O. (2016) Identification of the novel activity-driven interaction between synaptotagmin 1 and presenilin 1 links calcium, synapse, and amyloid beta, *BMC Biol. 14*.

[191] Zoltowska, K. M., Maesako, M., Lushnikova, I., Takeda, S., Keller, L. J., Skibo, G., Hyman, B. T., and Berezovska, O. (2017) Dynamic presenilin 1 and synaptotagmin 1 interaction modulates exocytosis and amyloid beta production, *Mol. Neurodegener. 12*.

[192] Zoltowska, K. M., and Berezovska, O. (2017) Dynamic Nature of presenilin1/gamma-Secretase: Implication for Alzheimer's Disease Pathogenesis, *Mol. Neurobiol.*

[193] Wu, B., Yamaguchi, H., Lai, F. A., and Shen, J. (2013) Presenilins regulate calcium homeostasis and presynaptic function via ryanodine receptors in hippocampal neurons, *Proc. Natl. Acad. Sci. U.S.A.*

[194] Zhang, C., Wu, B., Beglopoulos, V., Wines-Samuelson, M., Zhang, D., Dragatsis, I., Sudhof, T. C., and Shen, J. (2009) Presenilins are essential for regulating neurotransmitter release, *Nature 460*, 632-636.

[195] Sharples, R. A., Vella, L. J., Nisbet, R. M., Naylor, R., Perez, K., Barnham, K. J., Masters, C. L., and Hill, A. F. (2007) Inhibition of gamma-secretase causes increased secretion of amyloid precursor protein C-terminal fragments in association with exosomes, *FASEB J. 22*, 1469-1478.

[196] Wang, H., Luo, W.-j., Zhang, Y.-w., Li, Y.-M., Thinakaran, G., Greengard, P., and Xu, H. (2004) Presenilins and gamma-Secretase Inhibitors Affect Intracellular Trafficking and Cell Surface Localization of the gamma-Secretase Complex Components, *J. Biol. Chem. 279*, 40560-40566.

[197] Kim, S. H., Leem, J. Y., Lah, J. J., Slunt, H. H., Levey, A. I., Thinakaran, G., and Sisodia, S. S. (2001) Multiple effects of aspartate mutant presenilin 1 on the processing and trafficking of amyloid precursor protein, *J. Biol. Chem. 276*, 43343-43350.

[198] Leem, J. Y., Saura, C. A., Pietrzik, C., Christianson, J., Wanamaker, C., King, L. T., Veselits, M. L., Tomita, T., Gasparini, L., Iwatsubo, T., Xu, H., Green, W. N., Koo,

E. H., and Thinakaran, G. (2002) A role for presenilin 1 in regulating the delivery of amyloid precursor protein to the cell surface, *Neurobiol. Dis. 11*, 64-82.
[199] Cai, D., Leem, J. Y., Greenfield, J. P., Wang, P., Kim, B. S., Wang, R., Lopes, K. O., Kim, S. H., Zheng, H., Greengard, P., Sisodia, S. S., Thinakaran, G., and Xu, H. (2003) Presenilin-1 regulates intracellular trafficking and cell surface delivery of beta-amyloid precursor protein, *J. Biol. Chem. 278*, 3446-3454.
[200] Kaether, C., Lammich, S., Edbauer, D., Ertl, M., Rietdorf, J., Capell, A., Steiner, H., and Haass, C. (2002) Presenilin-1 affects trafficking and processing of betaAPP and is targeted in a complex with nicastrin to the plasma membrane, *J. Cell Biol. 158*, 551-561.
[201] Gunawardena, S., Yang, G., and Goldstein, L. S. B. (2013) Presenilin controls kinesin-1 and dynein function during APP-vesicle transport in vivo, *Hum. Mol. Genet. 22*, 3828-3843.
[202] Farfara, D., Trudler, D., Segev-Amzaleg, N., Galron, R., Stein, R., and Frenkel, D. (2011) gamma-Secretase component presenilin is important for microglia beta-amyloid clearance, *Ann. Neurol. 69*, 170-180.
[203] Audagnotto, M., Kengo Lorkowski, A., and Dal Peraro, M. (2017) Recruitment of the amyloid precursor protein by gamma-secretase at the synaptic plasma membrane, *Biochem. Biophys. Res. Commun.*
[204] Barthet, G., Shioi, J., Shao, Z., Ren, Y., Georgakopoulos, A., and Robakis, N. K. (2011) Inhibitors of gamma-secretase stabilize the complex and differentially affect processing of amyloid precursor protein and other substrates, *FASEB J. 25*, 2937-2946.
[205] Bittner, T., Fuhrmann, M., Burgold, S., Jung, C. K. E., Volbracht, C., Steiner, H., Mitteregger, G., Kretzschmar, H. A., Haass, C., and Herms, J. (2009) gamma-Secretase Inhibition Reduces Spine Density In Vivo via an Amyloid Precursor Protein-Dependent Pathway, *J. Neurosci. 29*, 10405-10409.
[206] Nizzari, M., Venezia, V., Repetto, E., Caorsi, V., Magrassi, R., Gagliani, M. C., Carlo, P., Florio, T., Schettini, G., Tacchetti, C., Russo, T., Diaspro, A., and Russo, C. (2007) Amyloid Precursor Protein and Presenilin1 Interact with the Adaptor GRB2 and Modulate ERK 1,2 Signaling, *J. Biol. Chem. 282*, 13833-13844.
[207] Greenough, M. A. (2016) The Role of Presenilin in Protein Trafficking and Degradation-Implications for Metal Homeostasis, *J. Mol. Neurosci. 60*, 289-297.
[208] Wang, R., Tang, P., Wang, P., Boissy, R. E., and Zheng, H. (2006) Regulation of tyrosinase trafficking and processing by presenilins: partial loss of function by familial Alzheimer's disease mutation, *Proc. Natl. Acad. Sci. U. S. A. 103*, 353-358.
[209] Esselens, C., Oorschot, V., Baert, V., Raemaekers, T., Spittaels, K., Serneels, L., Zheng, H., Saftig, P., De Strooper, B., Klumperman, J., and Annaert, W. (2004) Presenilin 1 mediates the turnover of telencephalin in hippocampal neurons via an autophagic degradative pathway, *J. Cell Biol. 166*, 1041-1054.
[210] Bali, J., Siegenthaler, B., and Rajendran, L. (2016) gamma-Secretase regulates the alpha-secretase cleavage of the Alzheimer's disease, amyloid precursor protein, *Matters (Zürich)*.
[211] Ortega, F., Stott, J., Visser, S. A., and Bendtsen, C. (2013) Interplay between alpha-, beta-, and gamma-secretases determines biphasic amyloid-beta protein level in the

presence of a gamma-secretase inhibitor, *J. Biol. Chem. 288*, 785-792.
[212] Müller, U. C., Deller, T., and Korte, M. (2017) Not just amyloid: physiological functions of the amyloid precursor protein family, *Nat. Rev. Neurosci. 18*, 281-298.
[213] van der Kant, R., and Goldstein, Lawrence S. B. (2015) Cellular Functions of the Amyloid Precursor Protein from Development to Dementia, *Dev. Cell 32*, 502-515.
[214] Allinquant, B., Hantraye, P., Mailleux, P., Moya, K., Bouillot, C., and Prochiantz, A. (1995) Downregulation of amyloid precursor protein inhibits neurite outgrowth in vitro, *J. Cell Biol. 128*, 919-927.
[215] Milward, E. A., Papadopoulos, R., Fuller, S. J., Moir, R. D., Small, D., Beyreuther, K., and Masters, C. L. (1992) The amyloid protein precursor of Alzheimer's disease is a mediator of the effects of nerve growth factor on neurite outgrowth, *Neuron 9*, 129-137.
[216] Wang, S., Bolós, M., Clark, R., Cullen, C. L., Southam, K. A., Foa, L., Dickson, T. C., and Young, K. M. (2016) Amyloid β precursor protein regulates neuron survival and maturation in the adult mouse brain, *Mol. Cell. Neurosci. 77*, 21-33.
[217] Chasseigneaux, S., and Allinquant, B. (2012) Functions of Abeta, sAPPalpha and sAPPbeta : similarities and differences, *J. Neurochem. 120 Suppl 1*, 99-108.
[218] Southam, K. A., Stennard, F., Pavez, C., and Small, D. H. (2018) Knockout of Amyloid β Protein Precursor (APP) Expression Alters Synaptogenesis, Neurite Branching and Axonal Morphology of Hippocampal Neurons, *Neurochem. Res.*
[219] Hick, M., Herrmann, U., Weyer, S. W., Mallm, J. P., Tschape, J. A., Borgers, M., Mercken, M., Roth, F. C., Draguhn, A., Slomianka, L., Wolfer, D. P., Korte, M., and Muller, U. C. (2015) Acute function of secreted amyloid precursor protein fragment APPsalpha in synaptic plasticity, *Acta Neuropathol. 129*, 21-37.
[220] Heber, S., Herms, J., Gajic, V., Hainfellner, J., Aguzzi, A., Rulicke, T., Kretzschmar, H., von Koch, C., Sisodia, S., Tremml, P., Lipp, H. P., Wolfer, D. P., and Muller, U. (2000) Mice with combined gene knock-outs reveal essential and partially redundant functions of amyloid precursor protein family members, *J. Neurosci. 20*, 7951-7963.
[221] Torroja, L., Chu, H., Kotovsky, I., and White, K. (1999) Neuronal overexpression of APPL, the Drosophila homologue of the amyloid precursor protein (APP), disrupts axonal transport, *Curr. Biol. 9*, 489-493.
[222] Gunawardena, S., and Goldstein, L. S. B. (2001) Disruption of Axonal Transport and Neuronal Viability by Amyloid Precursor Protein Mutations in Drosophila, *Neuron 32*, 389-401.
[223] Xu, W., Weissmiller, A. M., White, J. A., Fang, F., Wang, X., Wu, Y., Pearn, M. L., Zhao, X., Sawa, M., Chen, S., Gunawardena, S., Ding, J., Mobley, W. C., and Wu, C. (2016) Amyloid precursor protein–mediated endocytic pathway disruption induces axonal dysfunction and neurodegeneration, *J. Clin. Invest. 126*, 1815-1833.
[224] Kimberly, W. T., Zheng, J. B., Guenette, S. Y., and Selkoe, D. J. (2001) The intracellular domain of the beta-amyloid precursor protein is stabilized by Fe65 and translocates to the nucleus in a notch-like manner, *J. Biol. Chem. 276*, 40288-40292.
[225] Ozaki, T., Li, Y., Kikuchi, H., Tomita, T., Iwatsubo, T., and Nakagawara, A. (2006) The intracellular domain of the amyloid precursor protein (AICD) enhances the

p53-mediated apoptosis, *Biochem. Biophys. Res. Commun. 351*, 57-63.
[226] Zhou, F., Gong, K., Song, B., Ma, T., van Laar, T., Gong, Y., and Zhang, L. (2012) The APP intracellular domain (AICD) inhibits Wnt signalling and promotes neurite outgrowth, *Biochim. Biophys. Acta 1823*, 1233-1241.
[227] Gongol, B., Marin, T. L., Jeppson, J. D., Mayagoitia, K., Shin, S., Sanchez, N., Kirsch, W. M., Vinters, H. V., Wilson, C. G., Ghribi, O., and Soriano, S. (2017) Cellular hormetic response to 27-hydroxycholesterol promotes neuroprotection through AICD induction of MAST4 abundance and kinase activity, *Sci. Rep. 7*.
[228] Kogel, D., Concannon, C. G., Muller, T., Konig, H., Bonner, C., Poeschel, S., Chang, S., Egensperger, R., and Prehn, J. H. M. (2012) The APP intracellular domain (AICD) potentiates ER stress-induced apoptosis, *Neurobiol. Aging 33*, 2200-2209.
[229] Konietzko, U. (2012) AICD Nuclear Signaling and Its Possible Contribution to Alzheimer's Disease, *Curr. Alzheimer Res. 9*, 200-216.
[230] Dawson, G. R., Seabrook, G. R., Zheng, H., Smith, D. W., Graham, S., O'Dowd, G., Bowery, B. J., Boyce, S., Trumbauer, M. E., Chen, H. Y., Van der Ploeg, L. H., and Sirinathsinghji, D. J. (1999) Age-related cognitive deficits, impaired long-term potentiation and reduction in synaptic marker density in mice lacking the beta-amyloid precursor protein, *Neuroscience 90*, 1-13.
[231] Palmeri, A., Ricciarelli, R., Gulisano, W., Rivera, D., Rebosio, C., Calcagno, E., Tropea, M. R., Conti, S., Das, U., Roy, S., Pronzato, M. A., Arancio, O., Fedele, E., and Puzzo, D. (2017) Amyloid-β Peptide Is Needed for cGMP-Induced Long-Term Potentiation and Memory, *J. Neurosci. 37*, 6926-6937.
[232] Almeida, C. G., Tampellini, D., Takahashi, R. H., Greengard, P., Lin, M. T., Snyder, E. M., and Gouras, G. K. (2005) Beta-amyloid accumulation in APP mutant neurons reduces PSD-95 and GluR1 in synapses, *Neurobiol. Dis. 20*, 187-198.
[233] Kamenetz, F., Tomita, T., Hsieh, H., Seabrook, G., Borchelt, D., Iwatsubo, T., Sisodia, S., and Malinow, R. (2003) APP processing and synaptic function, *Neuron 37*, 925-937.
[234] Li, S., Hong, S., Shepardson, N. E., Walsh, D. M., Shankar, G. M., and Selkoe, D. (2009) Soluble oligomers of amyloid Beta protein facilitate hippocampal long-term depression by disrupting neuronal glutamate uptake, *Neuron 62*, 788-801.
[235] Walsh, D. M., Klyubin, I., Fadeeva, J. V., Cullen, W. K., Anwyl, R., Wolfe, M. S., Rowan, M. J., and Selkoe, D. J. (2002) Naturally secreted oligomers of amyloid beta protein potently inhibit hippocampal long-term potentiation in vivo, *Nature 416*, 535-539.
[236] Palop, J. J., and Mucke, L. (2009) Epilepsy and cognitive impairments in Alzheimer disease, *Arch. Neurol. 66*, 435-440.
[237] Mucke, L., Masliah, E., Yu, G. Q., Mallory, M., Rockenstein, E. M., Tatsuno, G., Hu, K., Kholodenko, D., Johnson-Wood, K., and McConlogue, L. (2000) High-level neuronal expression of abeta 1-42 in wild-type human amyloid protein precursor transgenic mice: synaptotoxicity without plaque formation, *J. Neurosci. 20*, 4050-4058.
[238] Born, H. A., Kim, J. Y., Savjani, R. R., Das, P., Dabaghian, Y. A., Guo, Q., Yoo, J. W., Schuler, D. R., Cirrito, J. R., Zheng, H., Golde, T. E., Noebels, J. L., and Jankowsky, J. L. (2014) Genetic Suppression of Transgenic APP Rescues

Hypersynchronous Network Activity in a Mouse Model of Alzeimer's Disease, *J. Neurosci. 34*, 3826-3840.
[239] Bush, A. I., Hoey, S. E., Buonocore, F., Cox, C. J., Hammond, V. J., Perkinton, M. S., and Williams, R. J. (2013) AMPA Receptor Activation Promotes Non-Amyloidogenic Amyloid Precursor Protein Processing and Suppresses Neuronal Amyloid-Î² Production, *PLoS One 8*, e78155.
[240] Tampellini, D., Rahman, N., Gallo, E. F., Huang, Z., Dumont, M., Capetillo-Zarate, E., Ma, T., Zheng, R., Lu, B., Nanus, D. M., Lin, M. T., and Gouras, G. K. (2009) Synaptic activity reduces intraneuronal Abeta, promotes APP transport to synapses, and protects against Abeta-related synaptic alterations., *J. Neurosci. 29*, 9704-9713.
[241] Turrigiano, G. G. (2008) The Self-Tuning Neuron: Synaptic Scaling of Excitatory Synapses, *Cell 135*, 422-435.
[242] Thiagarajan, T. C., Lindskog, M., and Tsien, R. W. (2005) Adaptation to synaptic inactivity in hippocampal neurons, *Neuron 47*, 725-737.
[243] Groemer, T. W., Thiel, C. S., Holt, M., Riedel, D., Hua, Y., Huve, J., Wilhelm, B. G., and Klingauf, J. (2011) Amyloid precursor protein is trafficked and secreted via synaptic vesicles, *PLoS One 6*, e18754.
[244] Tononi, G., and Cirelli, C. (2003) Sleep and synaptic homeostasis: a hypothesis, *Brain Res. Bull. 62*, 143-150.
[245] Tononi, G., and Cirelli, C. (2006) Sleep function and synaptic homeostasis, *Sleep Med. Rev. 10*, 49-62.
[246] Vyazovskiy, V. V., Cirelli, C., Pfister-Genskow, M., Faraguna, U., and Tononi, G. (2008) Molecular and electrophysiological evidence for net synaptic potentiation in wake and depression in sleep, *Nat. Neurosci. 11*, 200-208.
[247] Frank, M. G. (2013) Why I am not shy: a reply to Tononi and Cirelli, *Neural Plast. 2013*, 394946.
[248] Kang, J. E., Lim, M. M., Bateman, R. J., Lee, J. J., Smyth, L. P., Cirrito, J. R., Fujiki, N., Nishino, S., and Holtzman, D. M. (2009) Amyloid-β Dynamics Are Regulated by Orexin and the Sleep-Wake Cycle, *Science 326*, 1005-1007.
[249] Venkitaramani, D. V., Chin, J., Netzer, W. J., Gouras, G. K., Lesne, S., Malinow, R., and Lombroso, P. J. (2007) Beta-amyloid modulation of synaptic transmission and plasticity, *J. Neurosci. 27*, 11832-11837.
[250] Roh, J. H., Huang, Y., Bero, A. W., Kasten, T., Stewart, F. R., Bateman, R. J., and Holtzman, D. M. (2012) Disruption of the sleep-wake cycle and diurnal fluctuation of beta-amyloid in mice with Alzheimer's disease pathology, *Sci. Transl. Med. 4*, 150ra122.
[251] R., M. A., and W., L. J. (2013) Sleep Facilitates Clearance of Metabolites from the Brain: Glymphatic Function in Aging and Neurodegenerative Diseases, *Rejuvenation Research 16*, 518-523.
[252] Igbavboa, U., Sun, G. Y., Weisman, G. A., He, Y., and Wood, W. G. (2009) Amyloid beta-protein stimulates trafficking of cholesterol and caveolin-1 from the plasma membrane to the Golgi complex in mouse primary astrocytes, *Neuroscience 162*, 328-338.
[253] Liu, Q., Zerbinatti, C. V., Zhang, J., Hoe, H. S., Wang, B., Cole, S. L., Herz, J., Muglia, L., and Bu, G. (2007) Amyloid precursor protein regulates brain

apolipoprotein E and cholesterol metabolism through lipoprotein receptor LRP1, *Neuron 56*, 66-78.
[254] Pierrot, N., Tyteca, D., D'Auria, L., Dewachter, I., Gailly, P., Hendrickx, A., Tasiaux, B., Haylani, L. E., Muls, N., N'Kuli, F., Laquerrière, A., Demoulin, J.-B., Campion, D., Brion, J.-P., Courtoy, P. J., Kienlen-Campard, P., and Octave, J.-N. (2013) Amyloid precursor protein controls cholesterol turnover needed for neuronal activity, *EMBO Mol. Med. 5*, 608-625.
[255] Wang, W., Mutka, A. L., Zmrzljak, U. P., Rozman, D., Tanila, H., Gylling, H., Remes, A. M., Huttunen, H. J., and Ikonen, E. (2014) Amyloid precursor protein alpha- and beta-cleaved ectodomains exert opposing control of cholesterol homeostasis via SREBP2, *FASEB J. 28*, 849-860.
[256] Grösgen, S., Grimm, M. O. W., Frieß, P., and Hartmann, T. (2010) Role of amyloid beta in lipid homeostasis, *Biochim. Biophys. Acta 1801*, 966-974.
[257] Grimm, M. O. W., Mett, J., Grimm, H. S., and Hartmann, T. (2017) APP Function and Lipids: A Bidirectional Link, *Front. Mol. Neurosci. 10*.
[258] Liu, Y., Zhang, Y. W., Wang, X., Zhang, H., You, X., Liao, F. F., and Xu, H. (2009) Intracellular trafficking of presenilin 1 is regulated by beta-amyloid precursor protein and phospholipase D1, *J. Biol. Chem. 284*, 12145-12152.
[259] Kamal, A., Almenar-Queralt, A., LeBlanc, J. F., Roberts, E. A., and Goldstein, L. S. B. (2001) Kinesin-mediated axonal transport of a membrane compartment containing beta-secretase and presenilin-1 requires APP, *Nature 414*, 643-648.
[260] Wahrle, S., Das, P., Nyborg, A. C., McLendon, C., Shoji, M., Kawarabayashi, T., Younkin, L. H., Younkin, S. G., and Golde, T. E. (2002) Cholesterol-Dependent gamma-Secretase Activity in Buoyant Cholesterol-Rich Membrane Microdomains, *Neurobiol. Dis. 9*, 11-23.
[261] Wada, S., Morishima-Kawashima, M., Qi, Y., Misono, H., Shimada, Y., Ohno-Iwashita, Y., and Ihara, Y. (2003) gamma-Secretase Activity Is Present in Rafts but Is Not Cholesterol-Dependent, *Biochemistry 42*, 13977-13986.
[262] Burns, M., Gaynor, K., Olm, V., Mercken, M., LaFrancois, J., Wang, L., Mathews, P. M., Noble, W., Matsuoka, Y., and Duff, K. (2003) Presenilin redistribution associated with aberrant cholesterol transport enhances beta-amyloid production in vivo, *J. Neurosci. 23*, 5645-5649.
[263] Alzheimer, A. (1907) Über eine eigenartige Erkrankung der Hirnrinde., *Allgemeine Zeitschrift für Psychiatrie und psychisch-gerichtliche Medizin. 64*.
[264] Strassnig, M., and Ganguli, M. (2005) About a Peculiar Disease of the Cerebral Cortex: Alzheimer's Original Case Revisited, *Psychiatry (Edgmont) 2*, 30-33.
[265] Haass, C., Lemere, C. A., Capell, A., Citron, M., Seubert, P., Schenk, D., Lannfelt, L., and Selkoe, D. J. (1995) The Swedish mutation causes early-onset Alzheimer's disease by beta-secretase cleavage within the secretory pathway, *Nat. Med. 1*, 1291-1296.
[266] Cossec, J.-C., Marquer, C., Panchal, M., Lazar, A. N., Duyckaerts, C., and Potier, M.-C. (2010) Cholesterol changes in Alzheimer's disease: methods of analysis and impact on the formation of enlarged endosomes, *Biochim. Biophys. Acta 1801*, 839-845.
[267] Li, Y., and Tsien, R. (2012) pHTomato, a red, genetically encoded indicator that

enables multiplex interrogation of synaptic activity., *Nat. Neurosci. 15*, 1047-1053.
[268] Gibson, D. G., Young, L., Chuang, R.-Y., Venter, J. C., Hutchison, C. A., and Smith, H. O. (2009) Enzymatic assembly of DNA molecules up to several hundred kilobases, *Nat. Methods 6*, 343-345.
[269] Liu, G., and Tsien, R. W. (1995) Synaptic transmission at single visualized hippocampal boutons, *Neuropharmacology 34*, 1407-1421.
[270] Edelstein, A., Amodaj, N., Hoover, K., Vale, R., and Stuurman, N. (2010) Computer Control of Microscopes Using μManager, *Curr. Protoc. Mol. Biol.*
[271] Schindelin, J., Arganda-Carreras, I., Frise, E., Kaynig, V., Longair, M., Pietzsch, T., Preibisch, S., Rueden, C., Saalfeld, S., Schmid, B., Tinevez, J.-Y., White, D. J., Hartenstein, V., Eliceiri, K., Tomancak, P., and Cardona, A. (2012) Fiji: an open-source platform for biological-image analysis, *Nat. Methods 9*, 676-682.
[272] Schneider, C. A., Rasband, W. S., and Eliceiri, K. W. (2012) NIH Image to ImageJ: 25 years of image analysis, *Nat. Methods 9*, 671-675.
[273] Thevenaz, P., Ruttimann, U. E., and Unser, M. (1998) A pyramid approach to subpixel registration based on intensity, *IEEE Transactions on Image Processing 7*, 27-41.
[274] Darbon, J., Cunha, A., Chan, T. F., Osher, S., and Jensen, G. J. (2008) Fast nonlocal filtering applied to electron cryomicroscopy, In *2008 5th IEEE International Symposium on Biomedical Imaging: From Nano to Macro*, pp 1331-1334.
[275] Buades, A., Coll, B., and Morel, J.-M. (2011) Non-Local Means Denoising, *Image Processing On Line 1*.
[276] Fridman, J. S., Caulder, E., Hansbury, M., Liu, X., Yang, G., Wang, Q., Lo, Y., Zhou, B. B., Pan, M., Thomas, S. M., Grandis, J. R., Zhuo, J., Yao, W., Newton, R. C., Friedman, S. M., Scherle, P. A., and Vaddi, K. (2007) Selective Inhibition of ADAM Metalloproteases as a Novel Approach for Modulating ErbB Pathways in Cancer, *Clin. Cancer Res. 13*, 1892-1902.
[277] Floyd, D. H., Kefas, B., Seleverstov, O., Mykhaylyk, O., Dominguez, C., Comeau, L., Plank, C., and Purow, B. (2012) Alpha-secretase inhibition reduces human glioblastoma stem cell growth in vitro and in vivo by inhibiting Notch, *Neuro Oncol. 14*, 1215-1226.
[278] Han, K., Müller, U. C., and Hülsmann, S. (2017) Amyloid-precursor Like Proteins APLP1 and APLP2 Are Dispensable for Normal Development of the Neonatal Respiratory Network, *Front. Mol. Neurosci. 10*.
[279] Thinakaran, G., and Koo, E. H. (2008) Amyloid Precursor Protein Trafficking, Processing, and Function, *J. Biol. Chem. 283*, 29615-29619.
[280] Plácido, A. I., Pereira, C. M. F., Duarte, A. I., Candeias, E., Correia, S. C., Santos, R. X., Carvalho, C., Cardoso, S., Oliveira, C. R., and Moreira, P. I. (2014) The role of endoplasmic reticulum in amyloid precursor protein processing and trafficking: Implications for Alzheimer's disease, *Biochimica et Biophysica Acta (BBA) - Molecular Basis of Disease 1842*, 1444-1453.
[281] Yamazaki, T., Selkoe, D. J., and Koo, E. H. (1995) Trafficking of cell surface beta-amyloid precursor protein: retrograde and transcytotic transport in cultured neurons, *J. Cell Biol. 129*, 431-442.
[282] Niederst, E. D., Reyna, S. M., and Goldstein, L. S. B. (2014) Axonal amyloid

precursor protein and its fragments undergo somatodendritic endocytosis and processing, *Mol. Biol. Cell 26*, 205-217.
[283] Muresan, V., and Ladescu Muresan, Z. (2015) Amyloid-beta precursor protein: Multiple fragments, numerous transport routes and mechanisms, *Exp. Cell Res.*
[284] Lammich, S., Kojro, E., Postina, R., Gilbert, S., Pfeiffer, R., Jasionowski, M., Haass, C., and Fahrenholz, F. (1999) Constitutive and regulated alpha-secretase cleavage of Alzheimer's amyloid precursor protein by a disintegrin metalloprotease, *Proc. Natl. Acad. Sci. U.S.A. 96*, 3922-3927.
[285] Choy, R. W. Y., Cheng, Z. L., and Schekman, R. (2012) Amyloid precursor protein (APP) traffics from the cell surface via endosomes for amyloid beta (A beta) production in the trans-Golgi network, *Proc. Natl. Acad. Sci. U. S. A. 109*, E2077-E2082.
[286] Das, U., Scott, David A., Ganguly, A., Koo, Edward H., Tang, Y., and Roy, S. (2013) Activity-Induced Convergence of APP and BACE-1 in Acidic Microdomains via an Endocytosis-Dependent Pathway, *Neuron 79*, 447-460.
[287] Das, U., Wang, L., Ganguly, A., Saikia, J. M., Wagner, S. L., Koo, E. H., and Roy, S. (2015) Visualizing APP and BACE-1 approximation in neurons yields insight into the amyloidogenic pathway, *Nat. Neurosci. 19*, 55-64.
[288] Bauereiss, A., Welzel, O., Jung, J., Grosse-Holz, S., Lelental, N., Lewczuk, P., Wenzel, E. M., Kornhuber, J., and Groemer, T. W. (2015) Surface Trafficking of APP and BACE in Live Cells, *Traffic 16*, 655-675.
[289] Kügler, S., Meyn, L., Holzmüller, H., Gerhardt, E., Isenmann, S., Schulz, J. B., and Bähr, M. (2001) Neuron-Specific Expression of Therapeutic Proteins: Evaluation of Different Cellular Promoters in Recombinant Adenoviral Vectors, *Mol. Cell. Neurosci. 17*, 78-96.
[290] Miesenbock, G., De Angelis, D. A., and Rothman, J. E. (1998) Visualizing secretion and synaptic transmission with pH-sensitive green fluorescent proteins, *Nature 394*, 192-195.
[291] Lazarenko, R. M., DelBove, C. E., Strothman, C. E., and Zhang, Q. (2017) Ammonium chloride alters neuronal excitability and synaptic vesicle release, *Sci. Rep. 7*, 5061.
[292] Villegas, C., Muresan, V., and Ladescu Muresan, Z. (2014) Dual-tagged amyloid-beta precursor protein reveals distinct transport pathways of its N- and C-terminal fragments, *Hum. Mol. Genet. 23*, 1631-1643.
[293] Osborn, M. J., Panoskaltsis-Mortari, A., McElmurry, R. T., Bell, S. K., Vignali, D. A. A., Ryan, M. D., Wilber, A. C., McIvor, R. S., Tolar, J., and Blazar, B. R. (2005) A picornaviral 2A-like sequence-based tricistronic vector allowing for high-level therapeutic gene expression coupled to a dual-reporter system, *Mol. Ther. 12*, 569-574.
[294] Jiang, M., and Chen, G. (2006) High Ca2+-phosphate transfection efficiency in low-density neuronal cultures, *Nat. Protoc. 1*, 695.
[295] Dzyubenko, E., Rozenberg, A., Hermann, D. M., and Faissner, A. (2016) Colocalization of synapse marker proteins evaluated by STED-microscopy reveals patterns of neuronal synapse distribution in vitro, *J. Neurosci. Methods 273*, 149-159.

[296] Krämer, A., Mentrup, T., Kleizen, B., Rivera-Milla, E., Reichenbach, D., Enzensperger, C., Nohl, R., Täuscher, E., Görls, H., Ploubidou, A., Englert, C., Werz, O., Arndt, H.-D., and Kaether, C. (2013) Small molecules intercept Notch signaling and the early secretory pathway, *Nat. Chem. Biol. 9*, 731-738.
[297] Burns, M. P., Igbavboa, U., Wang, L., Wood, W. G., and Duff, K. (2006) Cholesterol distribution, not total levels, correlate with altered amyloid precursor, protein processing in statin-treated mice, *Neuromolecular Med. 8*, 319-328.
[298] Willnow, T. E., and Andersen, O. M. (2013) Sorting receptor SORLA - a trafficking path to avoid Alzheimer disease, *J. Cell Sci. 126*, 2751-2760.
[299] DelBove, C. E., Deng, X., and Zhang, Q. (2018) The fate of nascent APP in hippocampal neurons: a live cell imaging study, *ACS Chem. Neurosci.*
[300] Sankaranarayanan, S., De Angelis, D., Rothman, J. E., and Ryan, T. A. (2000) The Use of pHluorins for Optical Measurements of Presynaptic Activity, *Biophys. J. 79*, 2199-2208.
[301] Tsien, R. Y. (1998) The Green Fluorescent Protein, *Annu. Rev. Biochem 67*, 509-544.
[302] Piatkevich, K. D., and Verkhusha, V. V. (2011) Guide to Red Fluorescent Proteins and Biosensors for Flow Cytometry, *Methods Cell Biol. 102*, 431-461.
[303] McCluskey, A., Daniel, J. A., Hadzic, G., Chau, N., Clayton, E. L., Mariana, A., Whiting, A., Gorgani, N. N., Lloyd, J., Quan, A., Moshkanbaryans, L., Krishnan, S., Perera, S., Chircop, M., Kleist, L. v., McGeachie, A. B., Howes, M. T., Parton, R. G., Campbell, M., Sakoff, J. A., Wang, X., Sun, J. Y., Robertson, M. J., Deane, F. M., Nguyen, T. H., Meunier, F. A., Cousin, M. A., and Robinson, P. J. (2013) Building a Better Dynasore: The Dyngo Compounds Potently Inhibit Dynamin and Endocytosis, *Traffic 14*, 1272-1289.
[304] Toh, W. H., and Gleeson, P. A. (2016) Dysregulation of intracellular trafficking and endosomal sorting in Alzheimer's disease: controversies and unanswered questions, *Biochem. J 473*, 1977-1993.
[305] Wei, W., Nguyen, L. N., Kessels, H. W., Hagiwara, H., Sisodia, S., and Malinow, R. (2010) Amyloid beta from axons and dendrites reduces local spine number and plasticity, *Nat. Neurosci. 13*, 190-196.
[306] Wilhelm, B. G., Mandad, S., Truckenbrodt, S., Krohnert, K., Schafer, C., Rammner, B., Koo, S. J., Classen, G. A., Krauss, M., Haucke, V., Urlaub, H., and Rizzoli, S. O. (2014) Composition of isolated synaptic boutons reveals the amounts of vesicle trafficking proteins, *Science 344*, 1023-1028.
[307] Fanutza, T., Del Prete, D., Ford, M. J., Castillo, P. E., and D'Adamio, L. (2015) APP and APLP2 interact with the synaptic release machinery and facilitate transmitter release at hippocampal synapses, *eLife 4*.
[308] Laßek, M., Weingarten, J., Einsfelder, U., Brendel, P., Müller, U., and Volknandt, W. (2013) Amyloid precursor proteins are constituents of the presynaptic active zone, *J. Neurochem. 127*, 48-56.
[309] Zhang, Q., Li, Y., and Tsien, R. W. (2009) The dynamic control of kiss-and-run and vesicular reuse probed with single nanoparticles, *Science 323*, 1448-1453.
[310] Dawkins, E., and Small, D. H. (2014) Insights into the physiological function of the beta-amyloid precursor protein: beyond Alzheimer's disease, *J. Neurochem. 129*, 756-769.

[311] Winckler, B., and Mellman, I. (2010) Trafficking Guidance Receptors, *Cold Spring Harb. Perspect. Biol. 2*, a001826-a001826.
[312] Nakata, T., and Hirokawa, N. (2003) Microtubules provide directional cues for polarized axonal transport through interaction with kinesin motor head, *J. Cell Biol. 162*, 1045-1055.
[313] O'Brien, R. J., and Wong, P. C. (2011) Amyloid Precursor Protein Processing and Alzheimer's Disease, In *Annual Review of Neuroscience, Vol 34* (Hyman, S. E., Jessell, T. M., Shatz, C. J., Stevens, C. F., and Zoghbi, H. Y., Eds.), pp 185-204.
[314] Muller, U. C., and Zheng, H. (2012) Physiological functions of APP family proteins, *Cold Spring Harb. Perspect. Med. 2*, a006288.
[315] Pfisterer, U., Kirkeby, A., Torper, O., Wood, J., Nelander, J., Dufour, A., Bjorklund, A., Lindvall, O., Jakobsson, J., and Parmar, M. (2011) Direct conversion of human fibroblasts to dopaminergic neurons, *Proc. Natl. Acad. Sci. U. S. A. 108*, 10343-10348.
[316] Mahley, R. W. (2016) Central Nervous System Lipoproteins: ApoE and Regulation of Cholesterol Metabolism, *Arterioscler. Thromb. Vasc. Biol. 36*, 1305-1315.
[317] Blanchette-Mackie, E. J. (2000) Intracellular cholesterol trafficking: role of the NPC1 protein, *Biochim. Biophys. Acta 1486*, 171-183.
[318] Harris, B., Pereira, I., and Parkin, E. (2009) Targeting ADAM10 to lipid rafts in neuroblastoma SH-SY5Y cells impairs amyloidogenic processing of the amyloid precursor protein, *Brain Res. 1296*, 203-215.
[319] Nhan, H. S., Chiang, K., and Koo, E. H. (2015) The multifaceted nature of amyloid precursor protein and its proteolytic fragments: friends and foes, *Acta Neuropathol. 129*, 1-19.
[320] Huang, Y.-W. A., Zhou, B., Wernig, M., and Südhof, T. C. (2017) ApoE2, ApoE3, and ApoE4 Differentially Stimulate APP Transcription and Aβ Secretion, *Cell*.
[321] Korade, Z., and Kenworthy, A. K. (2008) Lipid rafts, cholesterol, and the brain, *Neuropharmacology 55*, 1265-1273.
[322] Egawa, J., Pearn, M. L., Lemkuil, B. P., Patel, P. M., and Head, B. P. (2016) Membrane lipid rafts and neurobiology: age-related changes in membrane lipids and loss of neuronal function, *J. Physiol. 594*, 4565-4579.
[323] Xiu, J., Nordberg, A., Qi, X., and Guan, Z. Z. (2006) Influence of cholesterol and lovastatin on alpha-form of secreted amyloid precursor protein and expression of alpha 7 nicotinic receptor on astrocytes, *Neurochem. Int. 49*, 459-465.
[324] Simons, M., Keller, P., De Strooper, B., Beyreuther, K., Dotti, C. G., and Simons, K. (1998) Cholesterol depletion inhibits the generation of beta-amyloid in hippocampal neurons, *Proc. Natl. Acad. Sci. U. S. A. 95*, 6460-6464.
[325] Kalvodova, L., Kahya, N., Schwille, P., Ehehalt, R., Verkade, P., Drechsel, D., and Simons, K. (2005) Lipids as modulators of proteolytic activity of BACE: involvement of cholesterol, glycosphingolipids, and anionic phospholipids in vitro, *J. Biol. Chem. 280*, 36815-36823.
[326] Sebastião, A. M., Colino-Oliveira, M., Assaife-Lopes, N., Dias, R. B., and Ribeiro, J. A. (2013) Lipid rafts, synaptic transmission and plasticity: Impact in age-related neurodegenerative diseases, *Neuropharmacology 64*, 97-107.
[327] Dason, J. S., Smith, A. J., Marin, L., and Charlton, M. P. (2014) Cholesterol and F-

actin are required for clustering of recycling synaptic vesicle proteins in the presynaptic plasma membrane, *J. Physiol. 592*, 621-633.
[328] Pfrieger, F. W. (2003) Role of cholesterol in synapse formation and function, *Biochim. Biophys. Acta 1610*, 271-280.
[329] Wood, W. G., Igbavboa, U., Muller, W. E., and Eckert, G. P. (2011) Cholesterol asymmetry in synaptic plasma membranes, *J. Neurochem. 116*, 684-689.
[330] Wood, W. G., Schroeder, F., Igbavboa, U., Avdulov, N. A., and Chochina, S. V. (2002) Brain membrane cholesterol domains, aging and amyloid beta-peptides, *Neurobiol. Aging 23*, 685-694.
[331] Shinohara, M., Tachibana, M., Kanekiyo, T., and Bu, G. J. (2017) Thematic Review Series: ApoE and Lipid Homeostasis in Alzheimer's Disease Role of LRP1 in the pathogenesis of Alzheimer's disease: evidence from clinical and preclinical studies, *J. Lipid Res. 58*, 1267-1281.
[332] Cam, J. A., and Bu, G. (2006) Modulation of beta-amyloid precursor protein trafficking and processing by the low density lipoprotein receptor family, *Mol. Neurodegener. 1*, 8.
[333] Dason, J. S., Smith, A. J., Marin, L., and Charlton, M. P. (2010) Vesicular Sterols Are Essential for Synaptic Vesicle Cycling, *J. Neurosci. 30*, 15856-15865.
[334] Yue, H.-Y., and Xu, J. (2015) Cholesterol regulates multiple forms of vesicle endocytosis at a mammalian central synapse, *J. Neurochem. 134*, 247-260.
[335] Herr, U.-M., Strecker, P., Storck, S. E., Thomas, C., Rabiej, V., Junker, A., Schilling, S., Schmidt, N., Dowds, C. M., Eggert, S., Pietrzik, C. U., and Kins, S. (2017) LRP1 Modulates APP Intraneuronal Transport and Processing in Its Monomeric and Dimeric State, *Front. Mol. Neurosci. 10*.
[336] Schneider, A., Rajendran, L., Honsho, M., Gralle, M., Donnert, G., Wouters, F., Hell, S. W., and Simons, M. (2008) Flotillin-Dependent Clustering of the Amyloid Precursor Protein Regulates Its Endocytosis and Amyloidogenic Processing in Neurons, *J. Neurosci. 28*, 2874-2882.
[337] Gamba, P., Testa, G., Sottero, B., Gargiulo, S., Poli, G., and Leonarduzzi, G. (2012) The link between altered cholesterol metabolism and Alzheimer's disease, *Ann. N. Y. Acad. Sci. 1259*, 54-64.
[338] Simons, K., and Gerl, M. J. (2010) Revitalizing membrane rafts: new tools and insights, *Nat. Rev. Mol. Cell Biol. 11*, 688.
[339] Takamori, S., Holt, M., Stenius, K., Lemke, E. A., Gronborg, M., Riedel, D., Urlaub, H., Schenck, S., Brugger, B., Ringler, P., Muller, S. A., Rammner, B., Grater, F., Hub, J. S., De Groot, B. L., Mieskes, G., Moriyama, Y., Klingauf, J., Grubmuller, H., Heuser, J., Wieland, F., and Jahn, R. (2006) Molecular anatomy of a trafficking organelle, *Cell 127*, 831-846.
[340] Ebinu, J. O., and Yankner, B. A. (2002) A RIP Tide in Neuronal Signal Transduction, *Neuron 34*, 499-502.
[341] Cirrito, J. R., Kang, J.-E., Lee, J., Stewart, F. R., Verges, D. K., Silverio, L. M., Bu, G., Mennerick, S., and Holtzman, D. M. (2008) Endocytosis Is Required for Synaptic Activity-Dependent Release of Amyloid-beta In Vivo, *Neuron 58*, 42-51.
[342] Sannerud, R., Declerck, I., Peric, A., Raemaekers, T., Menendez, G., Zhou, L., Veerle, B., Coen, K., Munck, S., De Strooper, B., Schiavo, G., and Annaert, W.

(2011) ADP ribosylation factor 6 (ARF6) controls amyloid precursor protein (APP) processing by mediating the endosomal sorting of BACE1, *Proc. Natl. Acad. Sci. U. S. A. 108*, E559-568.
[343] Eggert, S., Thomas, C., Kins, S., and Hermey, G. (2017) Trafficking in Alzheimer's Disease: Modulation of APP Transport and Processing by the Transmembrane Proteins LRP1, SorLA, SorCS1c, Sortilin, and Calsyntenin, *Mol. Neurobiol.*
[344] Wagner, T., and Pietrzik, C. U. (2012) The role of lipoprotein receptors on the physiological function of APP, *Exp. Brain Res. 217*, 377-387.
[345] Yan, Y., Xu, T.-H., Harikumar, K. G., Miller, L. J., Melcher, K., and Xu, H. E. (2017) Dimerization of the transmembrane domain of amyloid precursor protein is determined by residues around the gamma-secretase cleavage sites, *J. Biol. Chem.*
[346] Eggert, S., Gonzalez, A. C., Thomas, C., Schilling, S., Schwarz, S. M., Tischer, C., Adam, V., Strecker, P., Schmidt, V., Willnow, T. E., Hermey, G., Pietrzik, C. U., Koo, E. H., and Kins, S. (2017) Dimerization leads to changes in APP (amyloid precursor protein) trafficking mediated by LRP1 and SorLA, *Cell Mol Life Sci*.
[347] Andersen, O. M., Schmidt, V., Spoelgen, R., Gliemann, J., Behlke, J., Galatis, D., McKinstry, W. J., Parker, M. W., Masters, C. L., Hyman, B. T., Cappai, R., and Willnow, T. E. (2006) Molecular Dissection of the Interaction between Amyloid Precursor Protein and Its Neuronal Trafficking Receptor SorLA/LR11†, *Biochemistry 45*, 2618-2628.
[348] Pietrzik, C. U., Busse, T., Merriam, D. E., Weggen, S., and Koo, E. H. (2002) The cytoplasmic domain of the LDL receptor-related protein regulates multiple steps in APP processing, *EMBO J. 21*, 5691-5700.
[349] Pietrzik, C. U., Yoon, I. S., Jaeger, S., Busse, T., Weggen, S., and Koo, E. H. (2004) FE65 constitutes the functional link between the low-density lipoprotein receptor-related protein and the amyloid precursor protein, *J. Neurosci. 24*, 4259-4265.
[350] Ulery, P. G., Beers, J., Mikhailenko, I., Tanzi, R. E., Rebeck, G. W., Hyman, B. T., and Strickland, D. K. (2000) Modulation of beta-amyloid precursor protein processing by the low density lipoprotein receptor-related protein (LRP) - Evidence that LRP contributes to the pathogenesis of Alzheimer's disease, *J. Biol. Chem. 275*, 7410-7415.
[351] Hardy, J. (2017) Membrane damage is at the core of Alzheimer's disease, *Lancet N. 16*, 342.
[352] Leduc, V., Jasmin-Bélanger, S., and Poirier, J. (2010) APOE and cholesterol homeostasis in Alzheimer's disease, *Trends Mol. Med. 16*, 469-477.
[353] Burns, M. P., and Rebeck, G. W. (2010) Intracellular cholesterol homeostasis and amyloid precursor protein processing, *Biochimica Et Biophysica Acta-Molecular and Cell Biology of Lipids 1801*, 853-859.
[354] El Gaamouch, F., Jing, P., Xia, J. H., and Cai, D. M. (2016) Alzheimer's Disease Risk Genes and Lipid Regulators, *Journal of Alzheimers Disease 53*, 15-29.
[355] Cataldo, A. M., Peterhoff, C. M., Troncoso, J. C., Gomez-Isla, T., Hyman, B. T., and Nixon, R. A. (2000) Endocytic pathway abnormalities precede amyloid beta deposition in sporadic Alzheimer's disease and Down syndrome: differential effects of APOE genotype and presenilin mutations, *Am. J. Pathol. 157*, 277-286.
[356] Peric, A., and Annaert, W. (2015) Early etiology of Alzheimer's disease: tipping the

balance toward autophagy or endosomal dysfunction?, *Acta Neuropathol. 129*, 363-381.
[357] Fonseca, A. C., Resende, R., Oliveira, C. R., and Pereira, C. M. (2010) Cholesterol and statins in Alzheimer's disease: current controversies, *Exp. Neurol. 223*, 282-293.